A QUASI-RESONANT BIDIRECTIONAL CONVERTER WITH SOFT-SWITCHING OPERATION FOR ENERGY STORAGE APPLICATIONS

Devina Aggarwal

A thesis submitted to

the Faculty of Graduate Studies in partial fulfillment of the requirements

for the degree of Master's of Applied Science

Graduate Program in Electrical Engineering and Computer Science

York University

Toronto, Ontario

April 2018

ABSTRACT

The increased penetration of renewable energy power systems to produce clean and sustainable energy has led to the increased usage of various types of energy storage devices, such as high-power density battery technologies, flywheel energy storage and super-capacitors. Energy storage devices are essential in any renewable generation systems to ensure providing uninterruptible and reliable power. Typically, a power electronic converter is required to serve as the intermediary between the common grid in a renewable energy system and the energy storage device. To be specific, the power converter must be able to facilitate bidirectional power flow between the grid and the energy storage device. Since the voltage level of the energy storage device is often much lower than the grid voltage level, the bidirectional converter must ensure that the voltage level can be stepped up or down efficiently as per the system requirements depending on the direction of the power flow.

In this thesis, a unique quasi-resonant bidirectional converter topology is proposed for energy storage application. The proposed circuit only requires two switches to achieve bidirectional power flow. Hence, compared to the conventional dual-active bridge (DAB) based bidirectional converter topologies that require 8 switches, the total number of active switching devices required the proposed topology is greatly reduced. In addition, both switches in the proposed topology is able to achieve zero voltage switching (ZVS) turn-on and zero current switching (ZCS) turn-off to minimize the switching power losses without using additional auxiliary circuits. The operating principles and design equations of the proposed circuit will be discussed in detail in this thesis. An extended version of the proposed topology that employs a modular design structure for high power application is also presented and discussed. Simulation results and experimental works on a proof-of-concept hardware prototype are given to highlight the performance of the proposed bidirectional converter.

This one's for you, Dad

ACKNOWLEDGMENT

I would like to begin by expressing my sincerest gratitude to my supervisor, Dr. John Lam. His support and guidance gave my research efforts the direction, which was imperative to the successful completion of this thesis. Dr. Lam's expertise in Power Electronics helped me overcome the research roadblocks I faced during my Masters.

The technical advice I got from the student members of Dr. Lam's research group was instrumental in my achieving requisite results as a graduate student. I would like to extend a special vote of thanks to Mehdi Abasi who willingly shared his knowledge with me and took the time to help me out at every stage of my thesis. I would also like to thank Sanjida Moury and Kajanan Kanathipan for their support.

I thank Ms. Stefanie Lamonaca Caputo for sorting my financial issues, easing me into the master's program at York University and for all the insightful conversations, which helped me through periods of frustration. I thank Dr. Franck Van Breugel for being incredibly understanding and his faith in my capabilities. I am thankful to Dr. Ali Hooshyar for expanding my knowledge and urging me to pursue excellence. This thesis would not have been possible without the constant encouragement I got from Dr. Jit Sharma. His support through tough times kept me on track.

I would like to take this opportunity to thank my father for his unequivocal contribution in my journey as a master's student. His love, blessings and the technical advice he gave me were crucial to my being able to complete this work. Lastly, my mother's unconditional love, support and her confidence in me spurred me on even when I faced disappointment.

Table of Contents

LIST OF TABLES

LIST OF FIGURES

NOMENCLATURE

V_{in}	Input voltage
V_{out}	Output voltage
D	Duty ratio
$P_{s(on)}$	Switch power (on-state)
$V_{s(off)}$	Switch voltage (off-state)
I_s	Switch current
f_s	Switching frequency
V_{inmin}	Minimum input voltage
V_{inmax}	Maximum input voltage
V_o	Output voltage
P_{omin}	Minimum output power
P_{omax}	Maximum output power
f_{smin}	Minimum switching frequency
f_{smax}	Maximum switching frequency
f_o	Resonant frequency
I_{omin}	Minimum output current
I_{omax}	Maximum output current
ω_o	Angular resonant frequency
Z_R	Resistive impedance
DAB	Dual-active bridge converter

KVL	Kirchhoff’s voltage law
KCL	Kirchhoff’s current law
ZVS	Zero voltage switching
ZCS	Zero current switching
MOSFET	Metal oxide semiconductor field oxide transistor

CHAPTER 1

INTRODUCTION

At present, fossil fuels are used to meet 80% of global energy needs and supply 66% of the global electricity demand. They also contribute 60% of the greenhouse gas emissions, which cause climate change [1]. Figure 1-1 shows the steady increase in CO_2 emissions from 1990 to 2016 due to fuel combustion worldwide.

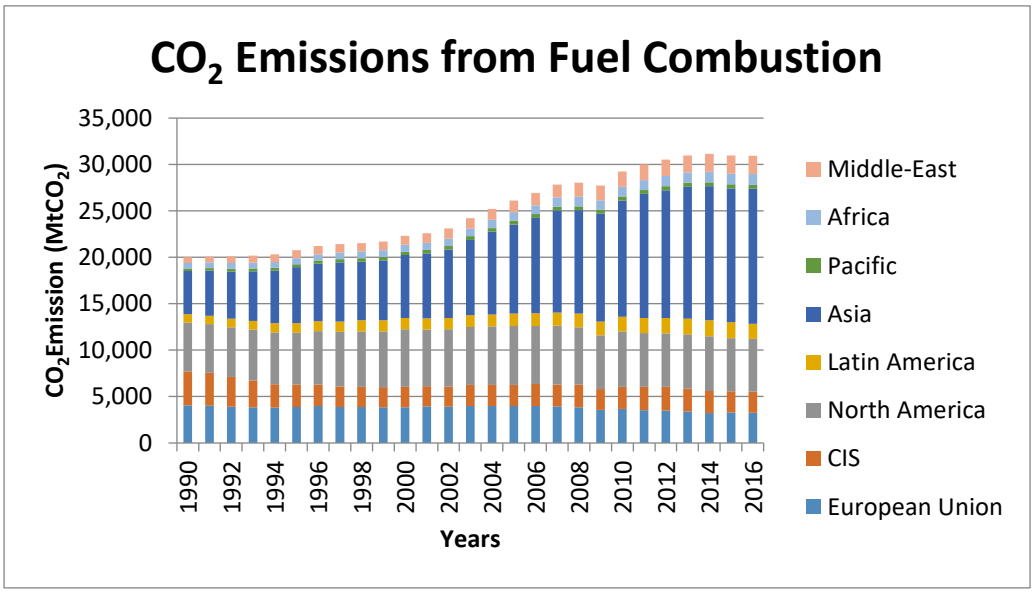

Figure 1-1 Worldwide carbon dioxide emissions [2]

In addition to fossil fuels being major sources of pollution, it has been predicted that oil supplies will be completely consumed by 2052 [3]. Recognizing that the unsustainability of fossil fuels and

our dependability on them jeopardizes our future energy needs, renewable energy resources are the way of the future.

Renewable energy is generated from inexhaustible or renewable resources on earth. Some of these examples are: solar energy, wind energy, hydropower, biomass and biofuels. These resources are found in abundance on this planet. They are feasible substitutes for conventional energy resources. Therefore, the energy generated from them is also known as alternative energy.

There are several reasons, which make using renewable energy favorable. They are:

1. Fossil fuel depletion is becoming a pressing concern.
2. Extraction of fossil fuels is becoming more difficult and costly as they become less abundant.
3. Renewable energy generation has a lower carbon footprint.
4. Renewable energy resources are dependable energy sources for the future as they are inexhaustible.
5. Using renewable energy increases energy security for countries and reduces their dependence on imported fossil fuels.

Statistical data provided by the International Energy Outlook (IEO) shows that the usage of renewable energy resources has been continuously rising since 2005. Figure 1-2 shows the projections provided by the IEO till 2035 for power generation capacity increase with various renewable energy sources [4]. Table 1-1 shows the percentage increase in the installed capacity of renewable energy power plants by 2035.

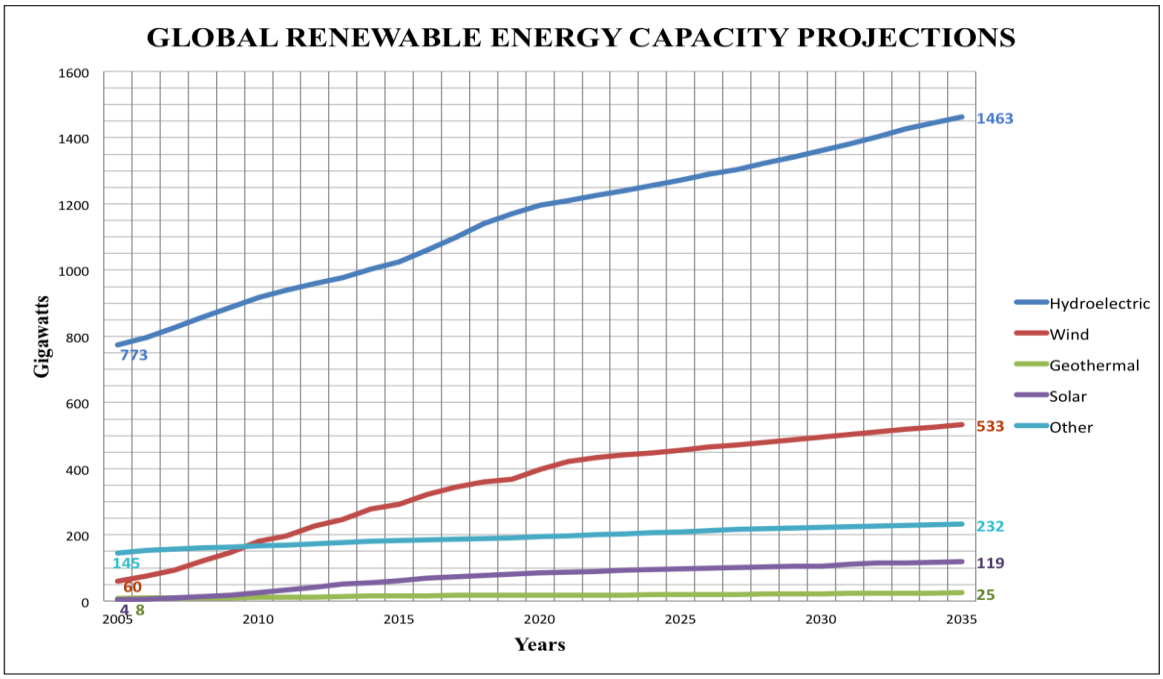

Figure 1-2 Global renewable energy capacity projections

Table 1-1 Percentage increase in renewable energy resources installations

Energy source	Growth in capacity
Solar	8.3%
Wind	5.7%
Geothermal	3.7%
Hydropower	2.0%
Other (biofuel, biomass)	1.4%

In Canada, a large part of Ontario's energy needs are already being met using renewable energy. Figure 1-3 shows the distribution of Ontario's power generation in 2016. The statistics show that

renewable energy has already been an integral part of our present energy supply, and they will continue to play a crucial role in the nation's energy supply in the future. For example, the Canadian Wind Energy Association is targeting by 2025 that onshore and offshore wind power will be able to supply 20% of the nation's electricity demand.

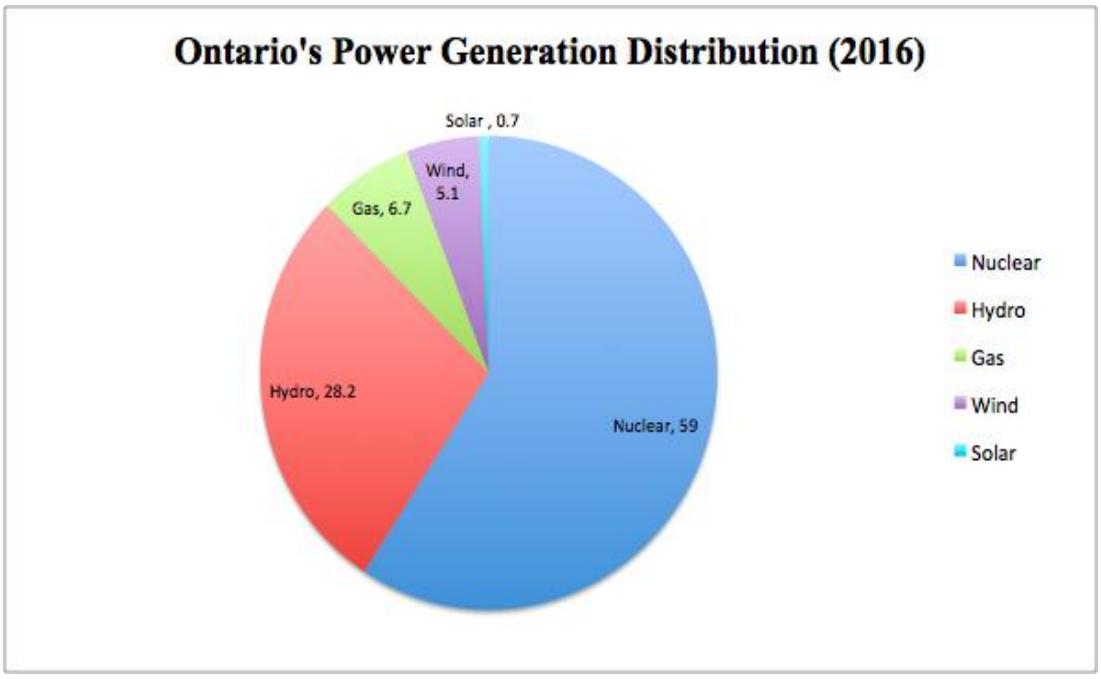

Figure 1-3 Ontario's power generation distribution in 2016 (in percentages)

1.1 Energy Storage Systems

The increased penetration of renewable energy technology has popularized microgrids. Distribution generation such as wind turbines, photovoltaic and other renewable energy technologies are connected to microgrids to provide electricity. However, the fluctuations in the power generated by distributed generation are a serious concern.

An essential part of the operation of any utility grid is to ensure that the power supply is steady. The utility grid should maintain power flow efficiently even in conditions of peak demand. This implies that the power supplied to load needs to be reliable. The grid's reliability is compromised when the grid has deficient power. An implicit solution is to store power when the grid has surplus power. However, energy storage is a very expensive proposition. Owing to the cost involved, most utility grids do not employ energy storage devices [5].

The energy storage devices make the power supply from the microgrid more robust. They create the required balance between the energy available in the microgrid for supply and the demand [6]. In addition to catering to peak energy demands, energy storage systems also reduce the requirement to keep upgrading or installing new supply lines and make power plants more efficient. Voltage sags can be mitigated by incorporating energy storage systems in microgrids [7].

The need for energy storage systems is made evident by the productivity losses suffered in their absence owing to poor power quality. An estimated $400 billion is lost annually in the US economy due to this reason [8]. Table 1-2 shows the various uses of energy storage systems, the power level specific to the application and the duration of time for which the power can be stored [9].

Table 1-2 Applications of energy storage systems on utility scale

Application	Power level (mw)	Storage time (hours)
Increase the **integration of renewable energy systems**	1-100	1-24

while ensuring reliability, stability and quality of power.		
Frequency regulation required to ensure balance between the generated power and peak demand.	1-30	<1
Load leveling to reduce fluctuation.	1-100	4-8
Peak shaving in order to reduce electricity consumption during peak demands.	0.1-10	0.5-2
Arbitrage is the method used to store energy and then sell it during peak demand hours when it is expensive.	50-500	1-10
Black start to restore electricity power station.	1-10	0.25

There are various types of energy storage systems. They are as follows [10]-[17]:

1. Battery Energy Storage Systems
2. Redox Flow Batteries
3. Super Capacitors
4. Fuel Cells

5. Superconducting Magnetic Energy Storage
6. Flywheels
7. Compressed Air Energy Storage Systems
8. Pumped Hydro

Approximately, 127,000 MW of energy storage has been installed worldwide. According to National Research Council of Canada, the energy storage market will grow to $200 billion over the next years. A major driving force for this market is storing surplus energy at night when demand is low. In Ontario, the Beck project at Niagara Falls is an example of pumped hydro. Batteries and flywheels are being used to stabilize base load demands from the grid in Minto, Ontario. In particular lithium ion batteries are being used. An example of such a project can be found in Strathroy, Ontario. Energy storage of 50 MW was procured by Ontario. Its cost was less than the cost of generating power to compensate for the 50 MW power using conventional methods. Therefore, energy storage devices are cost effective in the long run.

1.2 Battery Energy Storage Systems

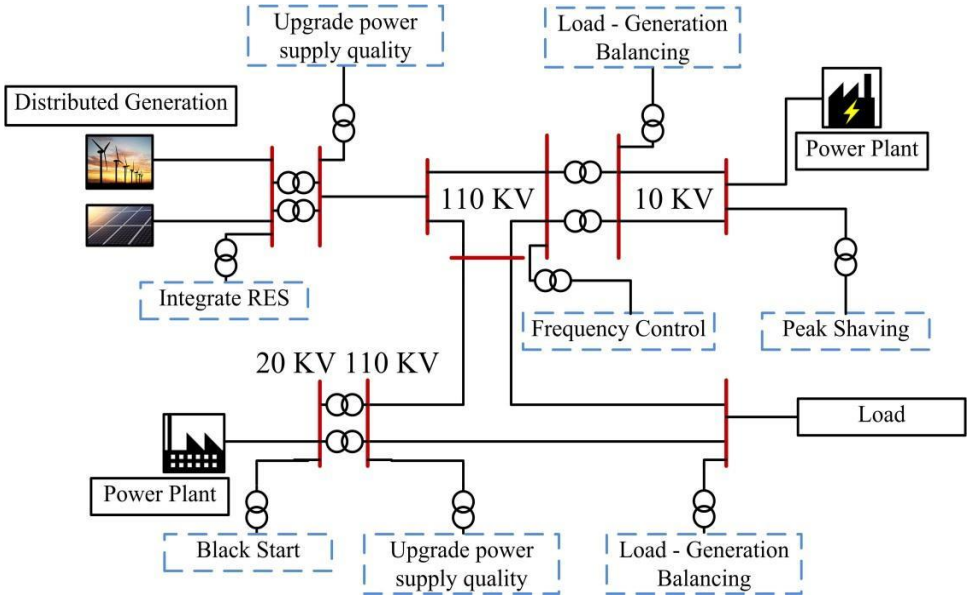

Figure 1-4 Application of battery energy storage systems [18]

Figure 1-4 shows various applications of a battery energy storage system when distributed generation is integrated with a power grid. Currently there are six main types of batteries which are being utilized.

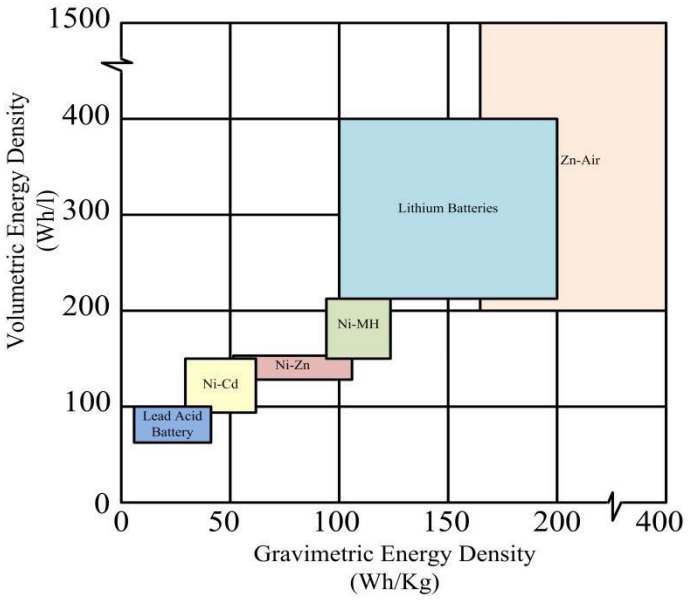

Figure 1-5 Comparison of different batteries based on energy density [19]

Figure 1-5 illustrates the various battery technologies which we currently employ. The battery technologies have been compared based on their power density and specific energy. Lithium batteries have higher gravimetric energy density and volumetric energy density than Nickel based batteries as well as Lead Acid batteries. Hence, they are considered superior to their counterparts.

1.2.1 Lithium Ion Battery

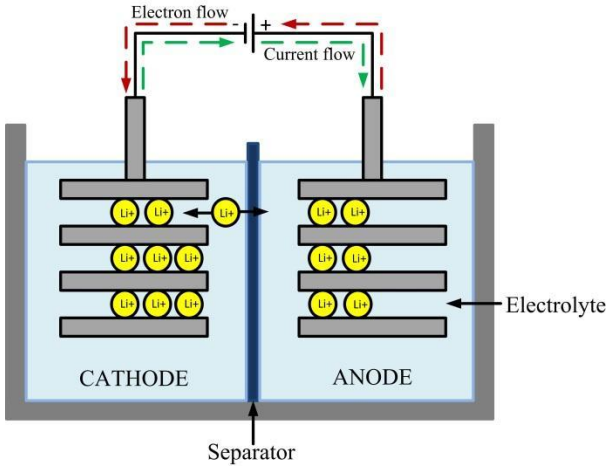

Fig 1-6 Lithium ion battery

Lithium Ion batteries have several advantages which make them suitable for renewable energy storage applications. The advantages are as follows [20]:

- High energy density (upto 200 Wh/kg)
- High cell voltages (3.6V)
- Low probability of self-discharge
- Long lifetimes owing to absence of memory effect in charge and discharge cycles (6,000 to 15,000 cycles).
- High efficiency (85%-95%)

Based on the various electro-chemical configurations of lithium ion batteries, they can store energy for up to one hour or for more than one day. The battery is charged by surplus energy produced by the distributed generation during the day. The battery then supplies power to the grid when there is deficiency of power [21]. For example, the battery may be connected to a microgrid in conjunction

with a photovoltaic panel. The panel generates power during the day time. However, at night time due to lack of irradiation, there is no power generation. This may cause a power deficit in the grid which is compensated for by the battery. The relatively high cost of the lithium ion batteries lead is a hindrance in their usage. However, they are considered a viable technology for grid applications.

1.2.2 Nickel Cadmium Battery

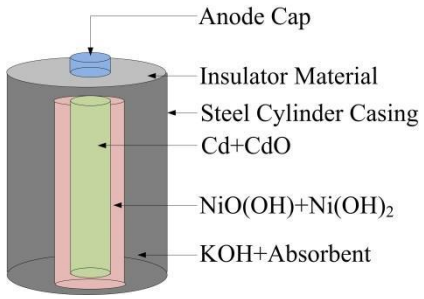

Figure 1-7 Basic nickel cadmium battery

Nickel cadmium batteries shown in Figure 1-7 are also used as energy storage systems for grid applications. These batteries have a significantly lower energy density in comparison to lithium ion batteries. However, they have several advantages which are as follows [8], [22]:

- Long lifetime (20-25 years)
- High reliability even after 20 years.
- Does not require frequent specific gravity assessments or internal resistance measurements
- Not prone to corrosion of the thin plate structure which extends lifetime
- High initial installation cost is compensated by low life cycle cost
- Low equivalent series resistance

There are two main disadvantages of Nickel Cadmium batteries [23]. The batteries have severe self-discharge and memory issues which may affect their lifetime. However, they have the advantage of being able to sustain periods of deep discharge. The second disadvantage is that these batteries contain around 16% cadmium. Cadmium is a highly toxic substance. The high cost of disposal of these batteries, negatively impacts their initial cost.

1.2.3 Nickel Zinc Battery

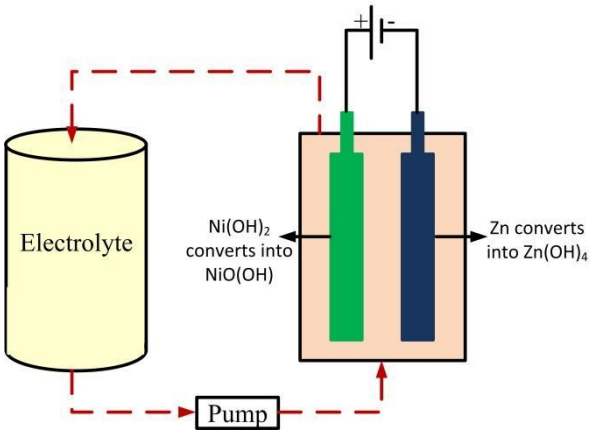

Figure 1-8 Nickel zinc battery [24]

The nickel-zinc battery has been shown in Figure 1-8. This battery has lower efficiency than lithium ion battery and lead acid battery [25]. The lithium ion battery can achieve an efficiency of 85%-95%. The efficiency of lead acid battery is in the range of 72%-90%. However, the Ni-Zn battery only has an efficiency of 65%-85%. The key advantage of the Ni-Zn battery is its ability to support 5,000-10,000 charge-discharge cycles before its capacity falls below 80% of the original capacity.

As opposed to the Ni-Zn battery the cycle life of lead acid battery is only in the range of 500-1000 and that of lithium ion battery is less than 1000. The Ni-Zn battery also has the advantage of being less expensive than lithium ion battery. Its cost is comparable to lead acid batteries.

1.2.4 Nickel Metal Hydride Battery

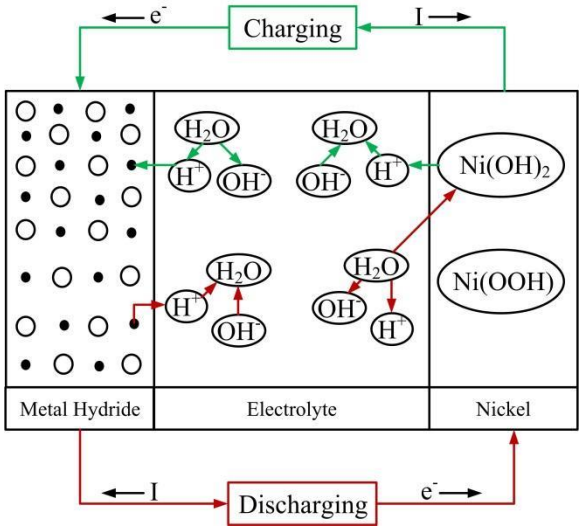

Figure 1-9 Nickel metal hydride battery [26]

Nickel Metal Hydride batteries are conventionally not used as energy storage devices for grid applications. However, these batteries have low toxicity making them environment friendly options for future use for renewable energy storage applications. In addition to this the nickel metal hydride batteries have several advantages. The advantages are listed below [27]:

- High energy density
- Excellent voltage stability
- Abuse resistance
- Safe
- 3-5 years lifetime

- 500-1000 charge-discharge cycles
- High efficiency over a wide temperature range from 0-50°C

1.2.5 Lead Acid Battery

Lead acid battery has been shown in Figure 1-10. Lead Acid batteries are widely used for domestic applications. This is primarily due to their low cost especially in comparison to lithium ion batteries. However, their low energy density and short lifetime makes them poor candidates for energy storage applications. Typical lead acid batteries only last 1000-2000 charge-discharge cycles [28]. On the contrary, lithium ion batteries can have a lifetime which can last up to 10,000 charge-discharge cycles. The consequence of this short lifetime is that the battery has to be replaced very often which raises the maintenance cost.

Lead acid batteries cannot sustain deep discharges. They need to be operated at a high state of charge in order to ensure they can have an optimum lifetime [29]. Since, lead acid can operate within a relatively small temperature range, high temperatures negatively impact the battery lifetime [30].

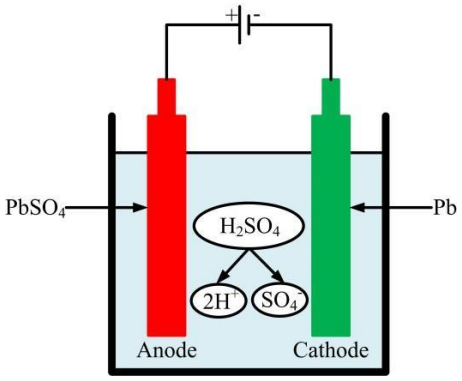

Figure 1-10 Lead acid battery

1.2.6 Zinc Air Battery

Zinc Air batteries are being touted as the battery energy storage systems of the future. It has been projected that these batteries shown in Figure 1-11 will come into large scale use from 2020-2030. Zinc Air batteries can be designed to have gravimetric (specific) energy density in the range of 350-500 Wh/kg. One of the key advantages of using zinc is that it is not as easily corroded by electrolytes as aluminum which is used conventionally. This makes the battery's lifetime longer. In addition to this zinc air batteries can be designed with an inbuilt regenerator system [31]. A reversible reaction takes place in the batteries to convert zinc oxide back to zinc using the power from the grid. Therefore, these batteries present a very environment friendly solution with almost no wastage.

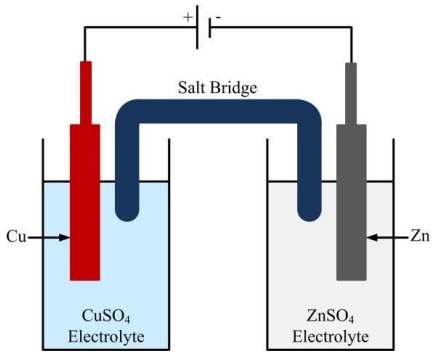

Figure 1-11 Zinc air battery

1.3 Power Converters in a Power Grid

Power converters find multiple uses in a power grid system. Some of the common uses are:

- To ensure proper voltage conversion
- To improve power quality
- To achieve maximum power point tracking
- To interface energy storage systems with the power grid

Figure 1-12 shows a typical power grid system. The system depicted in the figure is a hybrid system which contains a DC bus [32]. The salient points of the system are as follows:

1. The DC bus depicts the DC microgrid with which the various distributed generation systems are integrated. Some of the common distributed generation systems are solar photovoltaic panels and wind turbines.
2. Power converters act as interfaces between distributed generation systems and the power grid. Figure 1-13 shows a buck converter. Buck converters are used to step-down voltage levels. Figure 1-14 shows a boost converter. Boost converters are used to step-up voltage levels. Both these converters can be used to implement maximum power point tracking and increase efficiency of the distributed generation system by upgrading the quality of power delivered. In case of wind turbines, an additional AC-DC converter has to be used. This is because wind turbines generate AC electricity. In order to match the supply to the demand, rectification is necessary. Therefore, the AC-DC converter shown in Figure 1-15 has to be added.
3. In order to smooth the power supply which is negatively impacted by the intermittency of distributed generation systems, energy storage systems are integrated with the power grid.
4. Bidirectional converters are necessary to integrate ESS to the power grid. DC-DC bidirectional converters are required for this application.
5. The bidirectional converters are also utilized to connect the DC bus to the AC Power Grid which has been shown as the AC subsystem. A DC-AC bidirectional converter is required for this application.
6. Proper voltage conversion between the DC bus voltage and DC loads is ensured by using DC-DC converters such as buck converter and boost converter.

7. The AC loads are supplied directly supplied by the AC grid via a bypass in the grid connected mode. However, in the isolated mode or when there is a fault, the AC loads have to be supplied from the inverter shown in Figure 1-16.

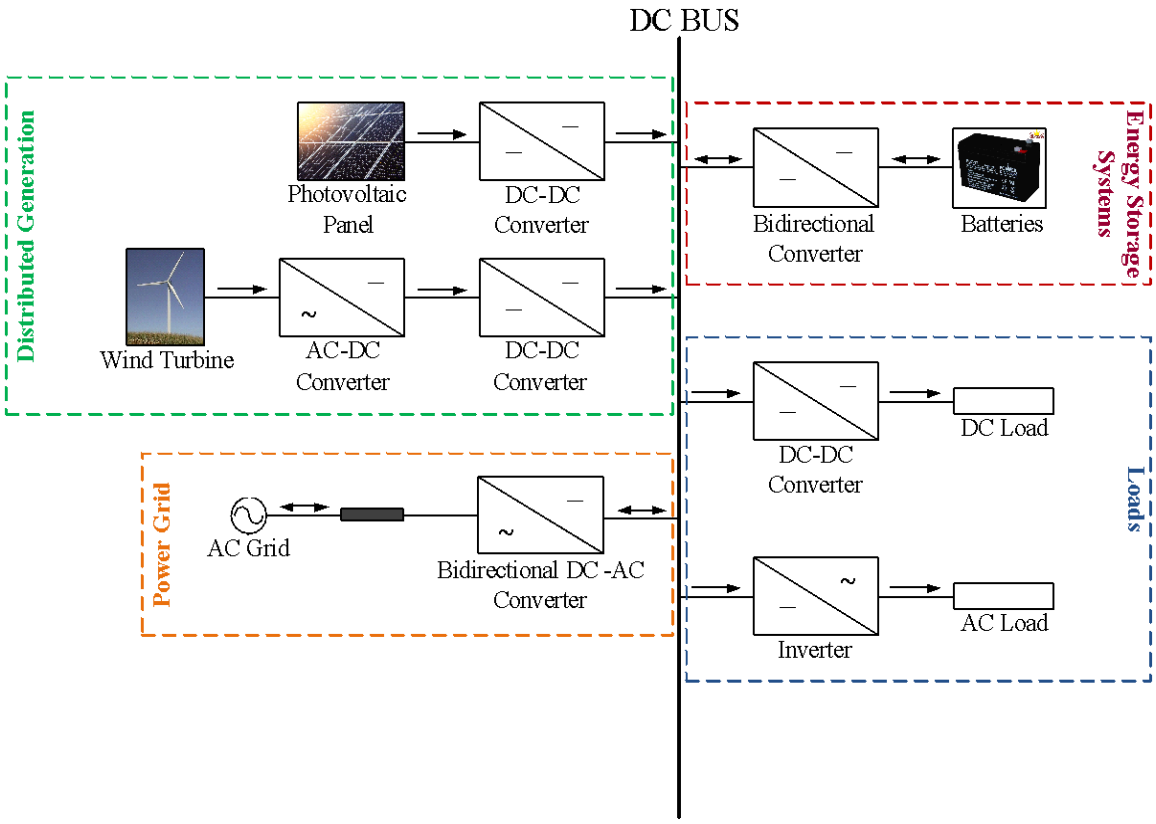

Figure 1-12 Typical power grid system

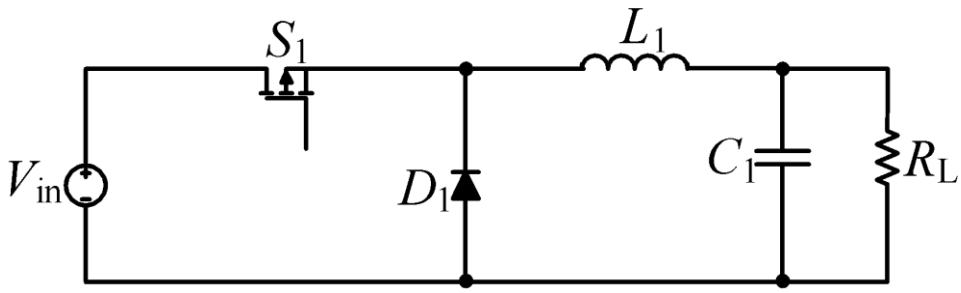

Figure 1-13 Buck converter

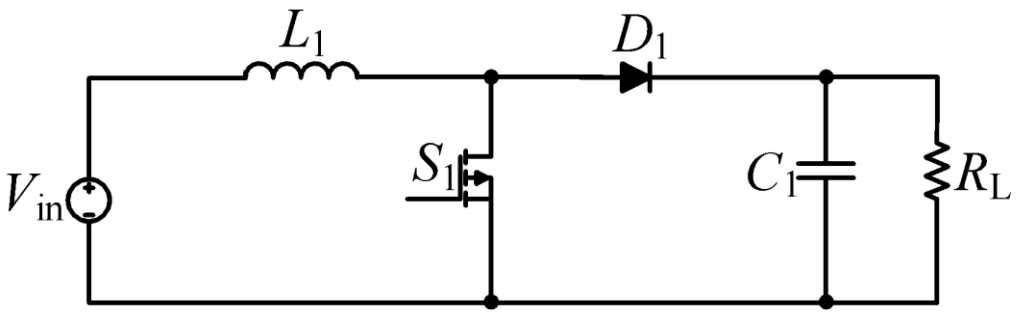

Figure 1-14 Boost converter

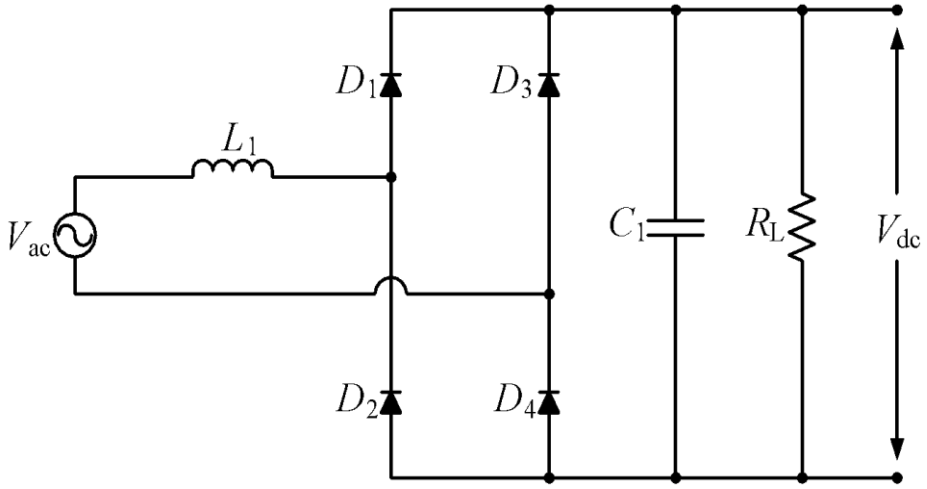

Figure 1-15 AC-DC converter

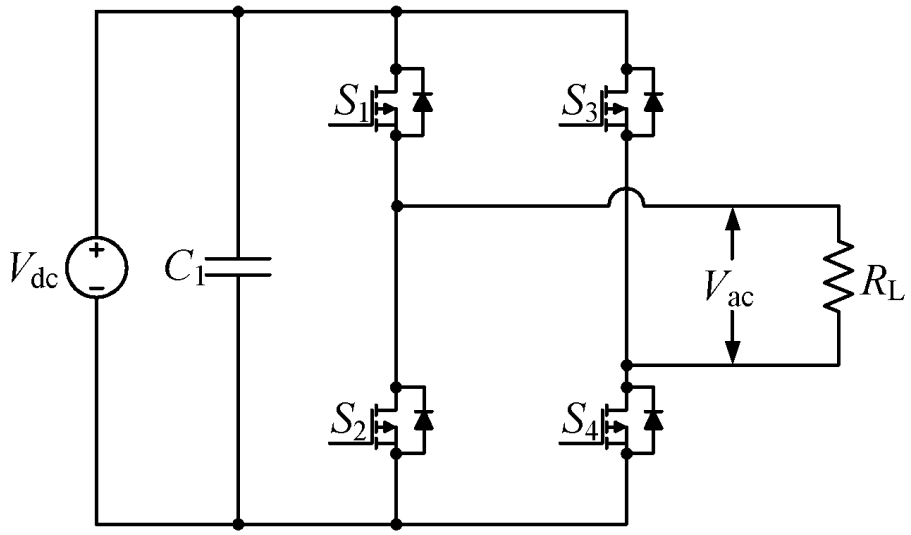

Figure 1-16 Inverter

While effectively extracting energy is paramount in a renewable energy system, energy storage mechanisms are essential in a renewable energy power system for managing the power flow within the system to reliably and consistently deliver the demanded energy to the load. Power electronics plays a critical role in an energy storage system to ensure that the required voltage conversion is provided between the energy storage device and the distributed voltage. It is projected that by 2030, power electronic devices will be used as intermediary devices for 80% of grid to load supplies [33].

This thesis focuses on bidirectional converter technology. As mentioned earlier, bidirectional converter (BDC) is used as the power interface between the energy storage device and the common voltage bus. The bidirectional converter is required to:

1. To correctly step up or step down voltage levels.
2. To store power in the energy storage device when the grid has surplus power.
3. To supply power to the grid from the storage device when it has deficiency of power.
4. To achieve proper voltage conversion with very high power circuit efficiency.

1.4 Significance of Switching Power Losses

Switching power loss as shown in Figure 1-17 is a common type of power loss in power electronics converters. It is the power loss that occurs in the switching transistors inside the circuit during the turn-on and turn-off instant of the transistor. This phenomenon is called Hard Switching. The turn-on switching power loss is given by Eq. 1-1.

$$P_{s(on)} = \frac{1}{2} \times V_{s(off)} \times I_s \times f_s \times t_{c(on)} \quad \text{(Eq. 1-1)}$$

where the turn-on crossover interval($t_{c(on)}$) is given by Eq. 1-2. The turn-on crossover time is the interval which starts from the initial rise of the switch current and ends when the switch voltage falls to zero.

$$t_{c(on)} = t_{ri} + t_{fv} \quad \text{(Eq. 1-2)}$$

In Eq. 1-2, the switch current rise time is given by t_{ri} and t_{fv} is the time taken by the switch voltage to fall to zero. Therefore, Eq. 1-1 can be written as Eq. 1-3. The switching frequency is given by f_s.

$$P_{s(on)} = \frac{1}{2} \times V_{s(off)} \times I_s \times f_s \times (t_{ri} + t_{fv}) \quad \text{(Eq. 1-3)}$$

Similarly the turn-off crossover interval is given by Eq. 1-4.

$$t_{c(off)} = t_{rv} + t_{fi} \quad \text{(Eq. 1-4)}$$

Hence, the turn-off switching power loss is given by Eq. 1-6.

$$P_{s(off)} = \frac{1}{2} \times V_{s(off)} \times I_s \times f_s \times t_{c(off)} \quad \text{(Eq. 1-5)}$$

$$P_{s(off)} = \frac{1}{2} \times V_{s(off)} \times I_s \times f_s \times (t_{rv} + t_{fi}) \quad \text{(Eq. 1-6)}$$

Where t_{rv} is the switch voltage rise time and t_{fi} is the switch current fall time.

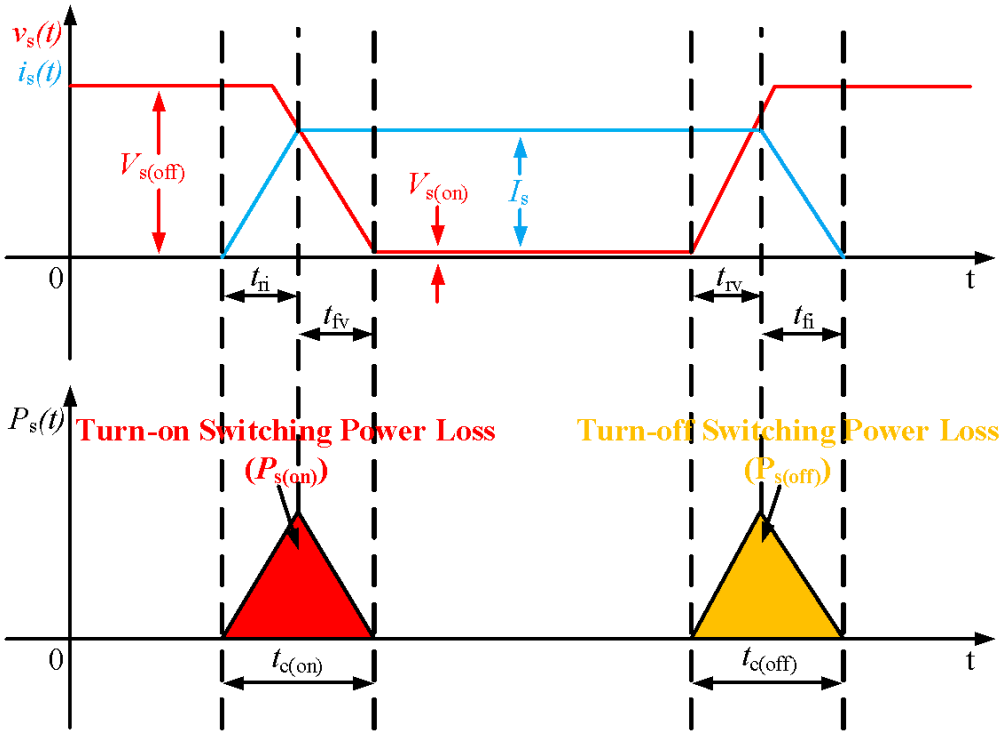

Figure 1-17 Hard switching

To reduce switching power losses, a mechanism called soft-switching technique is used in the power converter to reduce the turn-on and turn-off loss of the transistor to almost zero. Zero voltage switching (ZVS) and zero current switching (ZCS) are the two basic soft-switching techniques that are used to reduce the switching power loss. They are shown in Figure 1-19. To achieve soft-switching operation, a unique circuit configuration called resonant circuit is commonly used, which consists of different combinations of inductors and capacitors as shown in Figure 1-18. Depending on the employed power converter structure, a suitable type of resonant circuit is then used to achieve soft-switching.

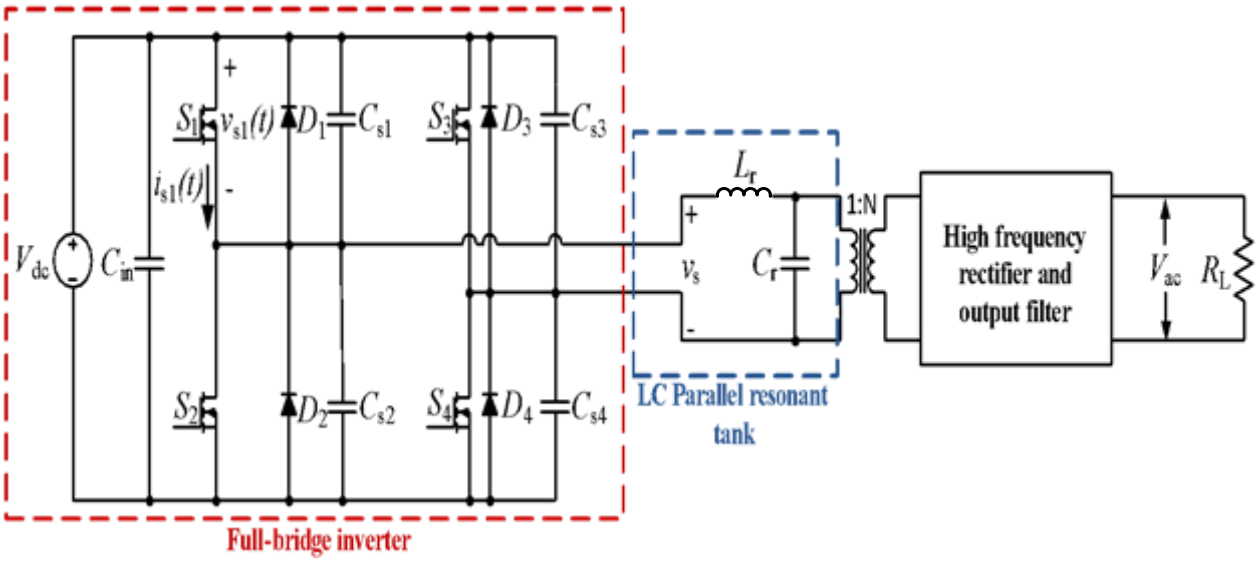

Figure 1-18 Full-bridge LC parallel resonant converter

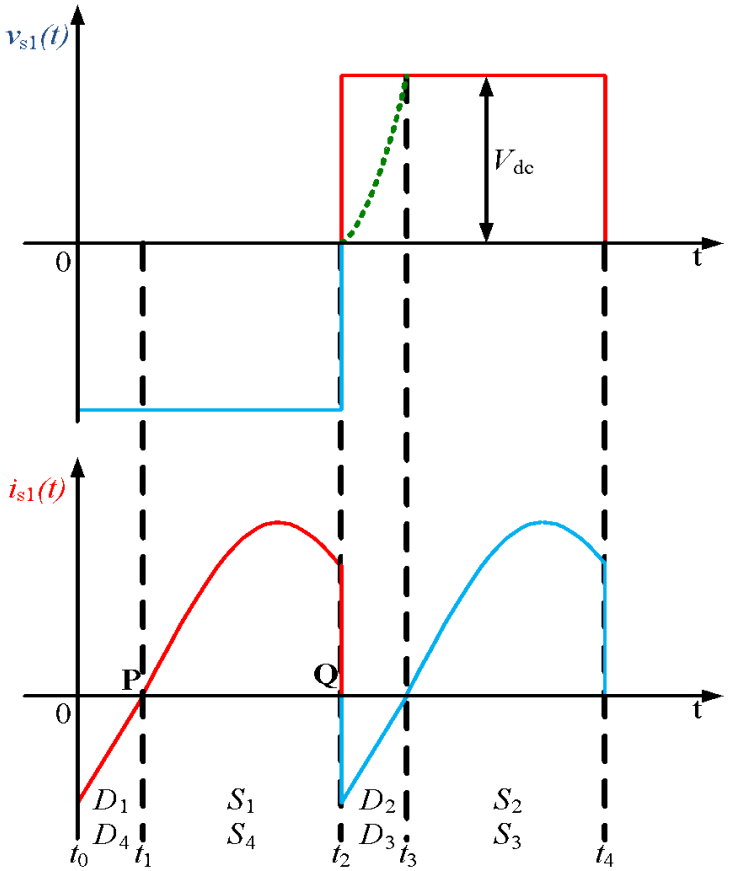

Figure 1-19 Soft-switching (zero voltage switching and zero current switching)

Figure 1-19 shows soft-switching. From $t_0 - t_1$, the anti-parallel diodes, $D_1$and D_4 are conducting. At t_1, the MOSFETs, S_1 and S_4 are turned on without any turn-on switching loss. Therefore, at point P, the MOSFETs, S_1 and S_4 are turned on with Zero Voltage Switching as the switch voltage is zero before the switch starts conducting forward current. The turn-off time of the diodes, $D_1$and D_4, is equal to the interval, $t_1 - t_2$. This time is equal to the forward conduction time of the MOSFETs, S_1 and S_4. At t_2, S_1 and S_4 are turned off. When these switches are turned off, the current across them is maintained due to the presence of the resonant inductor. The inductive action of the resonant inductor L_r causes the direction of the current to reverse. This current then flows through the anti-parallel diodes, $D_2$and $D_3$to facilitate the soft-switching turn-on of MOSFETs, S_2 and S_3. In order to reduce turn-off switching losses to almost zero, snubber capacitors, C_{s1}, C_{s2}, C_{s3} and C_{s4} are placed in parallel to the switches S_1, S_2, S_3 and S_4 respectively. The snubber capacitors cause the voltage to rise slowly as shown in the interval, $t_2 - t_3$. Since the voltage rises slowly, the drain-source voltage across the switch is almost zero when the switch turns-off. In the presence of snubber capacitors, the turn-off mechanism is close to Zero Current Switching. From $t_3 - t_4$, MOSFETs S_2 and S_3 are turned on.

1.5 Existing Bidirectional Converter Technology

The need for an interface between an energy storage element and the grid made the growth of interest in bidirectional converter technology inevitable. Bidirectional converters are a unique type of power converters that allow power to flow in both directions. These converters maintain the voltage polarity on both ends. This means that the output can be taken on either end of the bidirectional converter however; the voltage polarity will not be inverted. These converters have the capability of providing

the proper voltage conversion between the energy storage unit and the common distribution voltage level and vice versa [34].

Currently, bidirectional converters are commonly used in the following applications [35]-[40]:

1. Hybrid electrical vehicles
2. Fuel cell power systems and photovoltaic systems
3. Uninterruptable power systems
4. Battery and super capacitor balancer
5. Power management for dual voltage automotive systems

Currently, there are several different types of bidirectional converters available. They can be classified into two major categories:

1. Isolated bidirectional converters
2. Non-isolated bidirectional converters

Isolated converters derive their name from the high frequency isolation transformer in the topologies. Isolated converters can achieve large voltage gains due to the presence of the transformer. The voltage can easily be stepped up or stepped down by changing the transformer's turn ratio. Soft-switching can be easily achieved in these topologies by using a resonant tank circuit. Several isolated BDC topologies are based on flyback and forward flyback converters. The other common topologies include half-bridge and full-bridge topologies [41].

Many non-isolated converter topologies have been developed. They are less bulky than their isolated bidirectional converter counterparts. Transformer losses are also avoided in these topologies. Basic buck/boost BDC, sepic/zeta BDC, coupled inductor BDC and magnetic-less BDC topologies have been discussed in the following sections.

1.5.1 Flyback and Forward Flyback Bidirectional Converter

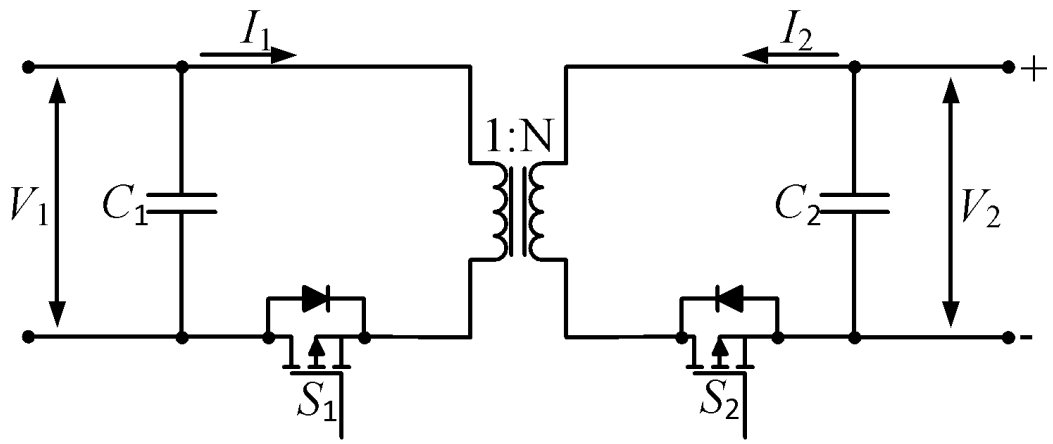

Figure 1-20 Flyback bidirectional converter

Flyback BDCs as shown in Figure 1-20 are often used due to their low cost and good transient response. They have galvanic isolation. These BDCs have a very simple structure which is easy to control [42]. However, flyback converters have many disadvantages. In the absence of the snubber capacitors in the flyback converter topology shown in Figure 1-21, the leakage inductance is discharged through the MOSFETs which results in high voltage stress across the switches. RC and RCD snubbers on the low voltage side and the high voltage side respectively, can be used in order to eliminate this problem [43]. The RC snubber is used to damp high frequency oscillations which cause voltage spikes across switch S_1in the off-state Figure 1-21. The RCD snubber shown on the high voltage side of the flyback converter topology prevents voltage spikes across switch S_2.

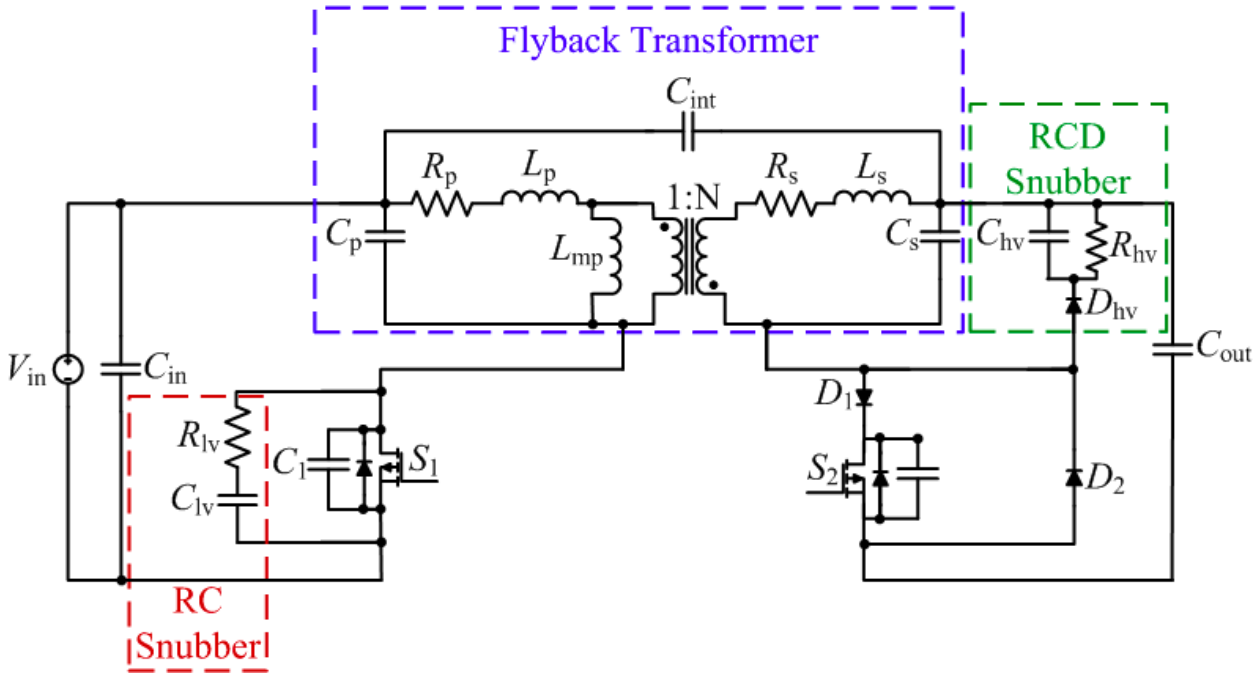

Figure 1-21 Flyback converter with RC and RCD snubber

Forward flyback converters as shown in Figure 1-22 offer several advantages over conventional forward converters. The forward flyback converters have lower secondary transformer copper losses than conventional forward converters. Owing to this at full load condition, the forward flyback converters have higher efficiency. The secondary transformer loss is given by Eq. 1-7.

$$P_{loss,Cu} = R_{dc} I_{dc}^2 + \sum_{k=1}^{\infty} R_{ac,k} I_{ac,k}^2 \quad \text{(Eq. 1-7)}$$

where, R_{dc} is the DC resistance of the secondary transformer copper winding. I_{dc} is the DC component of the current flowing through the secondary transformer copper winding. $R_{ac,k}$ and $I_{ac,k}$ are the AC resistance and AC current component of the secondary transformer copper winding respectively at the k^{th}fundamental harmonic of the switching frequency. One of the biggest advantages of this topology is the low voltage ripple due to the cancellation of the current ripple of the two output inductances because of the presence of the diodes on the secondary side.

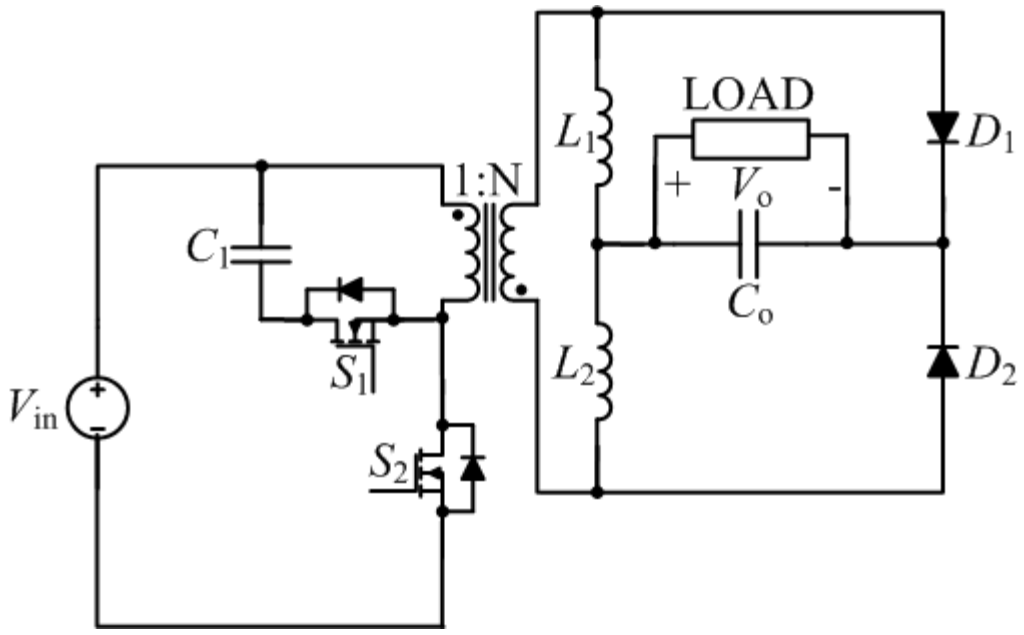

Figure 1-22 Forward flyback converter

These converters are very suitable for high voltage applications. However, these topologies suffer from a lot of transformer losses. Losses occur in the primary winding as well as in the core [44]. Although these converters require smaller output capacitors than flyback converters, the transformer inductor is much larger making these converters less attractive for high power applications. In the absence of a resonant tank, these converters cannot be used for high power applications. A LC resonant tank has been employed in order to reduce switching losses in [45]. This enables the proposed forward flyback converter to be used for photovoltaic power application at a power level of 400W. Quasi-resonant topologies enhance the efficiency of these converters. Efficiencies up to 94% can be achieved. Active voltage clamping techniques also reduce the voltage and current stresses as shown in Figure 1-23 [46]. L_1which acts as the leakage inductance of the transformer is used to achieve zero voltage switching and to turn-off the anti-parallel diode of the switch on the output side. This reduces the output noise and switching loss. The capacitors $C_1$and $C_2$are used to facilitate the zero current switching to reduce turn-off losses. The key operating waveforms of the

circuit topology are illustrated in Figure 1-24. As can be seen from Figure 1-24, MOSFETs $S_1$and $S_2$are complementary. S_3 and S_2 are turned off at the same time. Similarly, $S_4$and S_1also turn off at the same time. $C_{cl}$and C_{ch}clamp the voltage to $v_{Ccl}$and v_{Cch}respectively. The voltage is clamped to $v_{Ccl}$when $S_2$and $S_3$are on and to$v_{Cch}$when $S_1$and $S_4$are on.

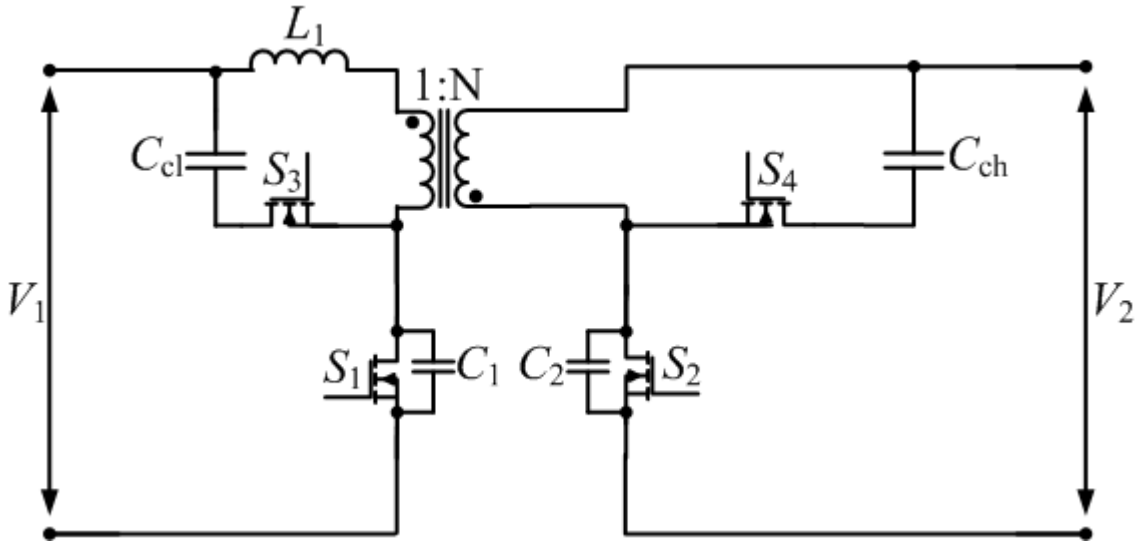

Figure 1-23 Forward flyback converter with active voltage clamp

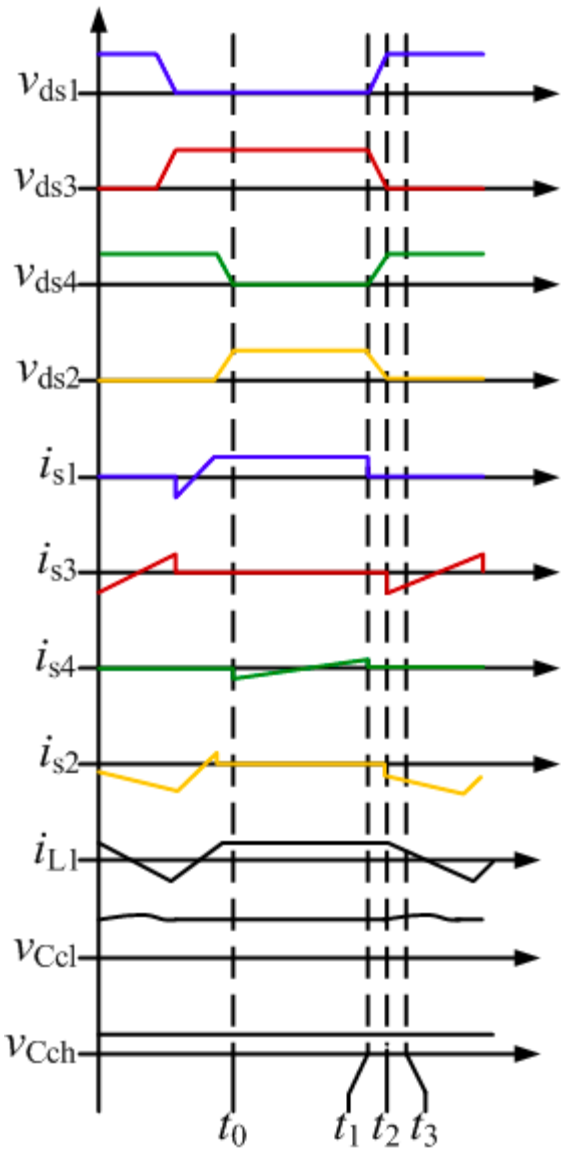

Figure 1-24 Operating waveforms of forward flyback converter with active voltage clamp

1.5.2 Half Bridge Bidirectional Converter

Conventional bidirectional have several drawbacks. The absence of galvanic isolation, more noise and reverse recovery losses in the rectifier diode due to which the switching speed is restrained are some of the major drawbacks. It is also difficult to realize soft-switching in conventional bidirectional converters.

Half bridge BDCs can easily meet all the aforementioned requirements. Zero voltage switching can be achieved in this topology and only four switches are used. Conventional half bridge bidirectional converters with hard-switching work in continuous conduction mode. Lack of soft-switching causes switching losses. Despite the presence of an isolation transformer, these converters are less bulky and are easier to control than the full bridge bidirectional converter topologies. Soft-switching can be achieved for a wide load range which is a drawback of conventional bidirectional converters [47]. The soft-switched bidirectional half bridge dc-dc converter shown in Figure 1-25 is based on the dual half bridge converter topology. This topology has several distinct advantages. The topology has half the number of switches in comparison to the dual full bridge converter topology. The total component count for the same power rating is halved too in this topology as opposed to the dual full bridge topology. Zero voltage switching can be achieved in both directions without the addition of any extra components in this topology. The controller is simple and the accessory power needs are low in this topology. A synchronized duty cycle control is used for the two half bridges i.e. the low voltage side and the high voltage side converter. In this type of control, the output voltage is basically modulated according to the duty cycle of switches S_2 andS_4. The low voltage side acts like a boost converter whereas the high voltage side acts as a buck converter. Phase shift control can also be used for this topology. When this type of control is used, all the switches operate at 50% duty cycle. The output current and voltage is determined by the phase-shift angle between the primary and secondary voltages. These factors render this topology low cost, highly efficient, easy to control, lightweight and compact. They are suitable for high power applications [48].

Figure 1-26 shows the voltage and current waveforms of the half bridge bidirectional converter. At t_0, the switch S_1 turns off with zero voltage switching. This is possible due to the presence of the capacitor, C_{s1} in parallel with the switch. The leakage inductance causes the transformer primary

current $I_{tp}$to keeping reducing from $t_0 - t_3$. From $t_0 - t_1$, C_{s1} is charged while C_{s2} is discharged. At t_1, the C_{s2} is completely discharged to zero. The antiparallel diode across switch S_2, D_{s2} is forward biased. Since the antiparallel diode starts conducting, the switch S_2can then turn on with zero voltage switching. Similarly, at t_2, S_3 turns off with zero voltage switching and the capacitor C_{s3} starts getting charged. C_{s4} gets discharged resulting in the antiparallel diode D_{s4} conducting at $t_3$so that switch S_4turns on with zero voltage switching. At t_4, switch S_2 is triggered. The operating stages from $t_6 - t_{11}$ are similar.

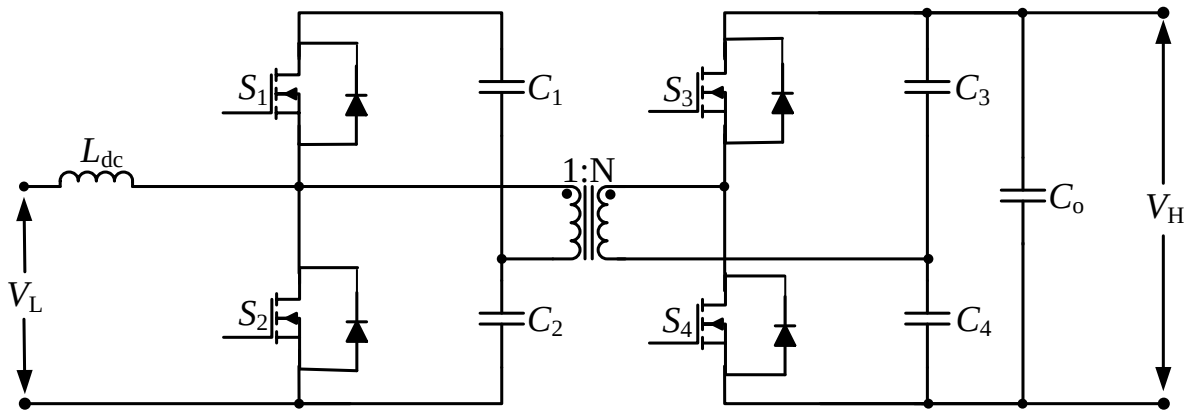

Figure 1-25 Half bridge bidirectional converter

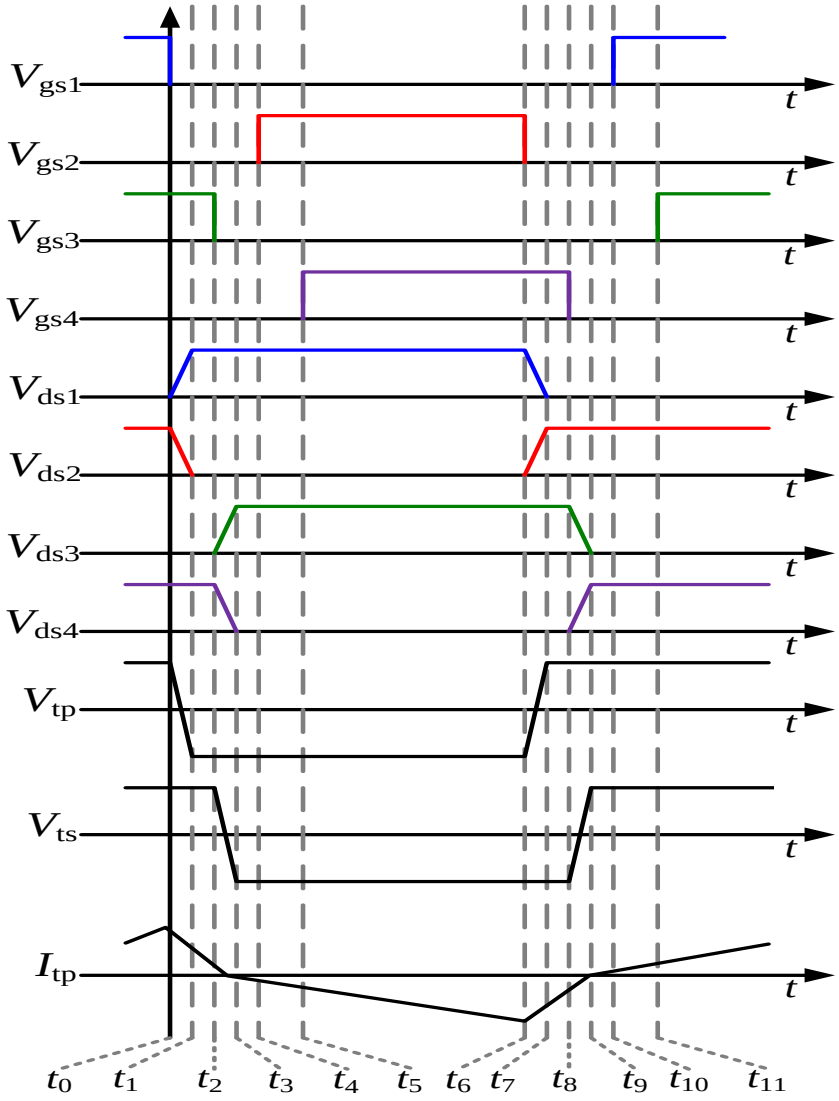

Figure 1-26 Voltage and current waveforms of the half bridge bidirectional converter

1.5.3 Full Bridge Bidirectional Converter

The most common type of the existing bidirectional converters is using a transformer that is located between two full bridge circuits [48]-[49], this bidirectional converter configuration is also called a dual-active bridge (DAB) converter. However, these topologies require eight switches as shown in Figure 1-21. In power electronics, increased number of switches implies that the number of driver

and control circuits for the switch will need to be increased as well. Consequently, bidirectional converter that employs two full bridge circuits will result in a large size and high cost converter. In addition, the leakage inductance and parasitic capacitance of the secondary winding of the transformer can result in large current and voltage spikes, which then lead to increased system losses and electrical noise.

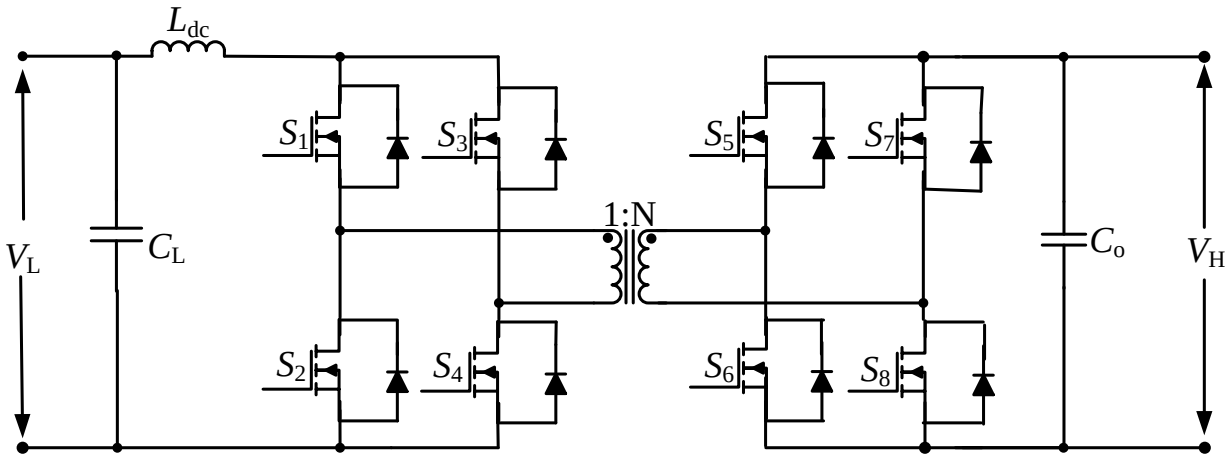

Figure 1-27 Dual-active bridge bidirectional converter

1.5.4 Bidirectional Converters with Auxiliary Switches

Bidirectional converters with soft switching capability are required to reduce switching losses and increase efficiency. One of the methods of achieving zero voltage and zero current switching in bidirectional converters is to utilize auxiliary switches in the topologies. The half bridge bidirectional converters mentioned in Section 1.5.3 are commonly used bidirectional converter topologies. Instead of zero voltage switching and zero current switching, conventionally zero voltage transition and zero current transition techniques have been used to achieve soft switching within this topology.

However, in order to compensate for the switch commutation problems in half bridge bidirectional converter topologies, two auxiliary switches have to be added. This gives rise to two problems. Firstly, the component count increases and secondly, the auxiliary switches have a different control timing from the main switches. This makes controlling the circuit more complex. Figure 1-28 shows a bidirectional converter with two auxiliary switches S_{a1} and S_{a2} [54].

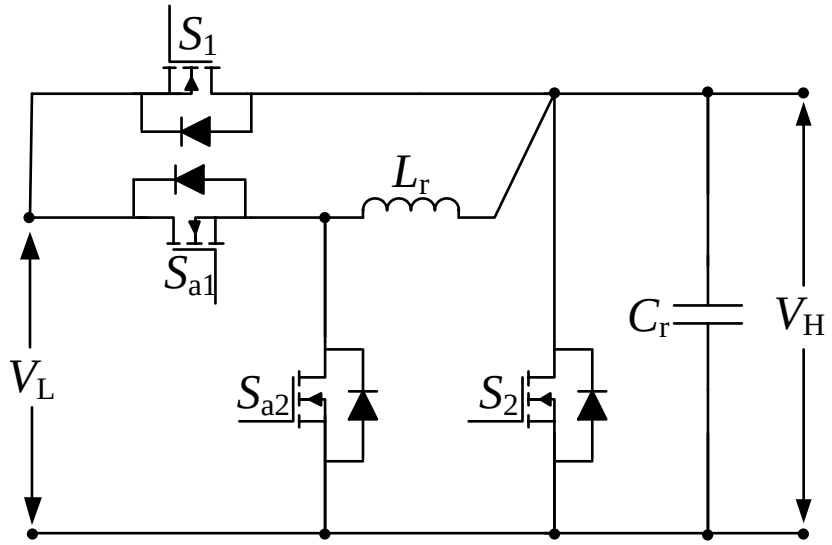

Figure 1-28 Bidirectional converter with two auxiliary switches

In order to reduce the component count and complexity of the controller, some topologies with only one auxiliary switch have been introduced. Figure 1-29 shows a bidirectional converter topology with one auxiliary switch and a coupled inductor. Topologies with coupled inductors are very popular because of high conversion ratio and lesser switching losses. However, the topology shown in Figure 1-29 has some disadvantages [55]. The two main switches, S_1 and S_2turn on and off with zero voltage switching. However, the auxiliary switch S_a operates under hard switching condition. The high turn ratio of the coupled inductor complicates the circuit design.

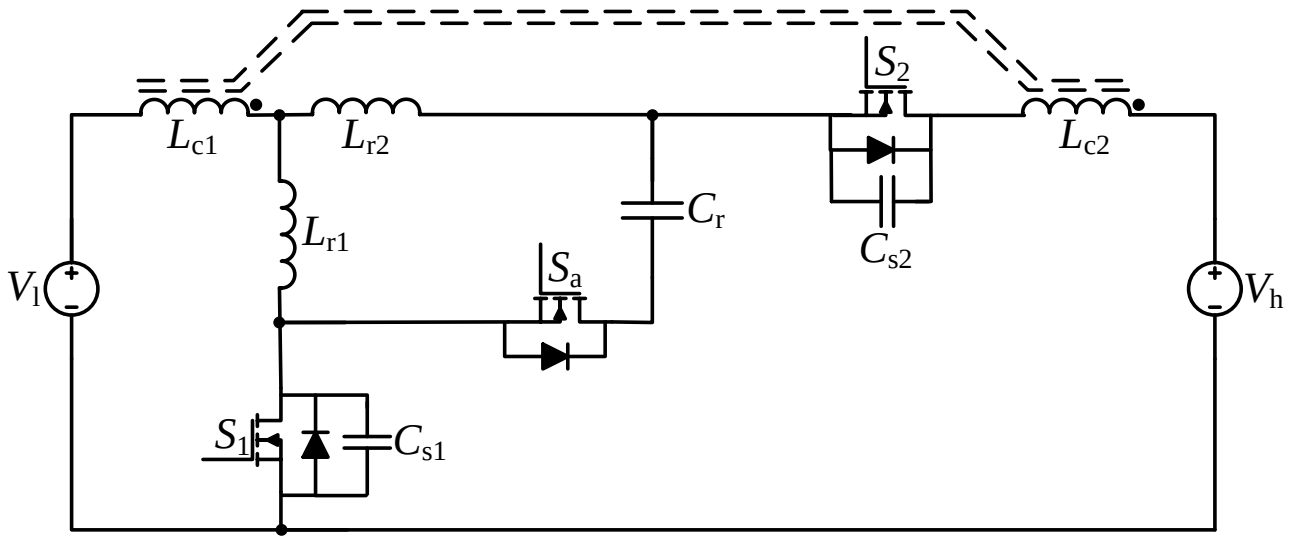

Figure 1-29 Bidirectional converter with one auxiliary switch

1.5.5 Buck/Boost Bidirectional Converter

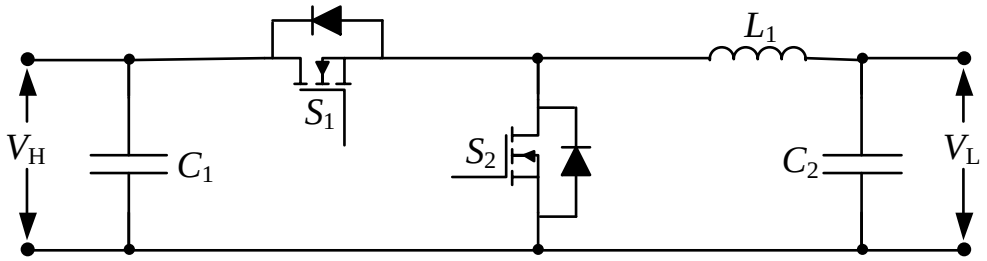

Figure 1-30 Buck/Boost Bidirectional converter

Buck/boost converters as shown in Figure 1-30 (also called step-down/up converters) are a more primitive way of achieving bidirectional power conversion. Unidirectional buck-boost converters can be converted into bidirectional converters by replacing the diodes with unidirectional switches. This topology is very simple. However, the parasitic elements limit the conversion ratio of voltage. In addition, switching power losses exist in these converters since soft switching techniques are not able to be achieved in this topology [51].

1.5.6 Sepic/Zeta Bidirectional Converter

Sepic/Zeta converters are relatively new BDC topologies. These converters have not been explored as much as other converter topologies mentioned in previous sections. Sepic/Zeta converters offer the advantage of having galvanic isolation. The device stress in this topology is the same as that encountered in full bridge and half bridge BDC topologies. However, these converters only require two switches which significantly reduces switching losses. Sepic/Zeta BDC topologies find use for low power applications [53]. Figure 1-31 shows a conventional bidirectional sepic/zeta converter. The converter operates in the sepic mode in the forward voltage conversion mode and in the zeta mode in the reverse voltage conversion mode. The converter has the same transfer function as that of the buck/boost converter given by Eq. 1-8.

$$\frac{V_{out}}{V_{in}} = \frac{D}{1-D} \qquad \text{(Eq. 1-8)}$$

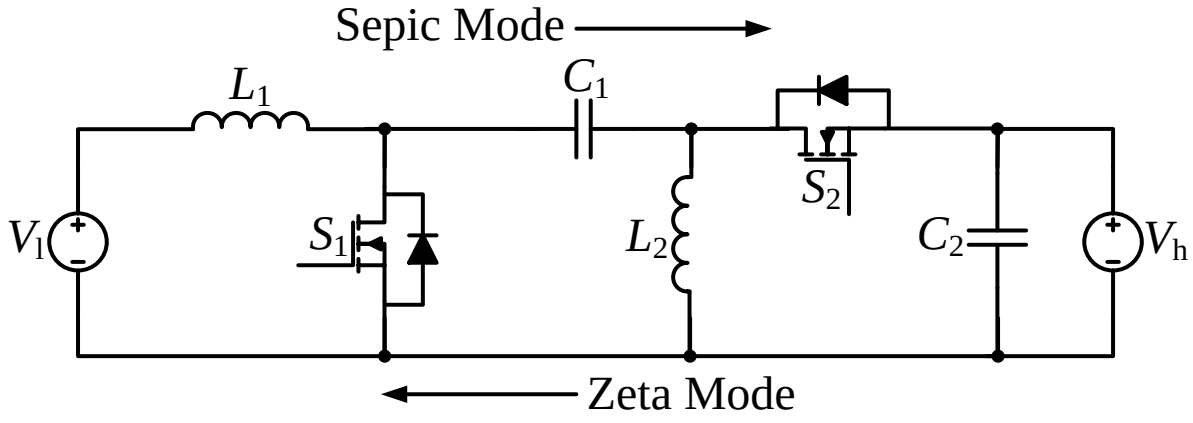

Figure 1-31 Bidirectional sepic/zeta converter

The bidirectional sepic/zeta converter shown in Figure 1-32 has a coupled inductor [56]. The topology shown in Figure 1-32 is a modified version of the conventional bidirectional sepic/zeta converter shown in Figure 1-31. This converter is more efficient than the conventional sepic/zeta

bidirectional converter and it has the advantage of having a low component count as it has only two switches. The output voltage of this topology is smoother than the conventional topology shown in Figure 1-30. This reduces the size and cost of the output filter. The coupling of the inductors improves the efficiency of the converter because it reduces switching stresses. However, the mean value of the output voltage of the modified topology is reduced in comparison to the conventional bidirectional sepic/zeta converter topology. The other disadvantage is that this topology requires the use of switches of high voltage and current ratings. When the topology is implemented for an operation which requires a large voltage range where, the initial turn on voltage and current across the switch becomes very high due to large variation in input voltages.

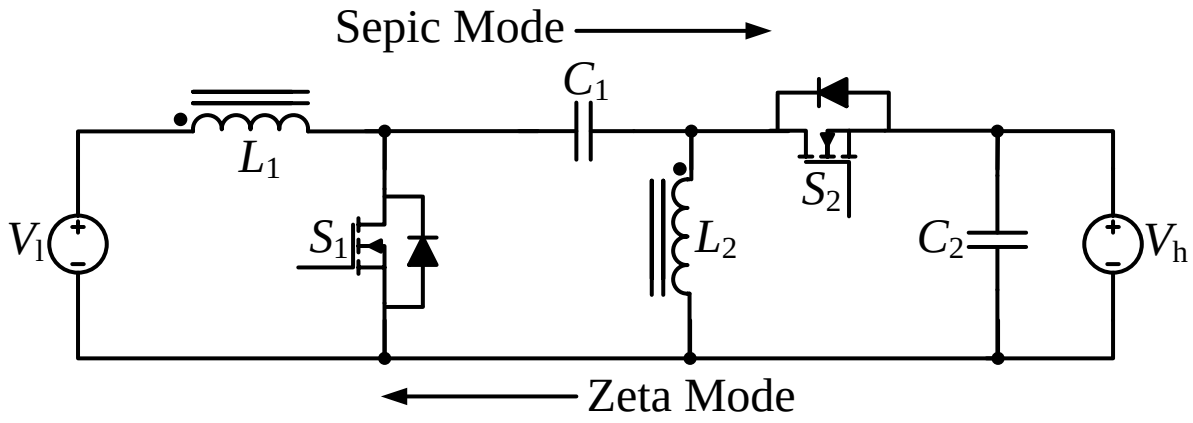

Figure 1-32 Bidirectional sepic/zeta converter with coupled inductor

1.6 Research Motivation

The increased integration of renewable energy technology and energy storage systems into power grids necessitates the development of efficient bidirectional converter technology. The existing converters suffer from several drawbacks. The research motivation for this thesis is to address the

problems in current bidirectional converters and devise an improved topology for energy storage applications.

1.7 Thesis Contributions

Summarizing the drawbacks seen in the bidirectional converters reported in literature, a new bidirectional converter topology that utilizes quasi-resonant (also called semi-resonant) circuit approach will be devised in this thesis research. The proposed converter will have the following features:

1. The devised circuit will only require two switches (i.e. MOSFET [metal–oxide–semiconductor field-effect transistor]). Therefore, compared to the commonly used DAB topologies, the total number of active switching devices required will be greatly reduced.
2. Switching power losses will be significantly reduced in the devised topology with the utilization of loss-less switching techniques such as ZVS or ZCS without using additional auxiliary circuits.
3. Due to loss-less switching techniques, the operating frequency of the devised converter will be at least two to three times higher than the frequency used in the DAB and buck-boost converter topologies.
4. As well, due to very high frequency operation, the sizes of all the passive circuit components such as inductors and capacitors will be substantially reduced in the devised converter, which will result in a truly compact yet highly power efficient bidirectional converter.
5. Since only two switches are employed in the proposed topology, the driver and control circuits for the switches will be greatly simplified compared to the DAB converter.

6. The proposed circuit will require a few more passive components than the buck-boost bidirectional converter topology. However, the proposed circuit will operate at switching frequencies which are two to three times higher than those used in the existing circuit. Hence, the size of the passive components will be minimized, and the overall circuit volume and weight will be reduced. Soft-switching will be achieved in the proposed circuit to minimize the switching losses in the existing circuit.

Chapter 2

Proposed Quasi-Resonant Bidirectional Converter with Soft Switching Operation

2.1 Introduction

Chapter 1 discusses several existing bidirectional converter topologies and their corresponding drawbacks. One of the drawbacks is the high number of switches being utilized in some of these topologies that leads to higher switching losses as well as cost. In addition to these topologies that do not exhibit soft-switching capability, which augments the switching losses, several topologies also utilize additional auxiliary switches which increase the complexity of the controller and the active component count. Hence, their efficiency is compromised.

In this research, a new topology of bidirectional converter is proposed to address the aforementioned drawbacks. The objective of this thesis is to design and present a highly efficient bidirectional converter, which is apt for energy storage applications. This chapter will discuss the characteristics of the proposed topology in details.

2.2 Proposed Two-Switch Bidirectional Converter Topology with Soft-Switching Capability

The proposed topology has been shown in Fig. 2-1.

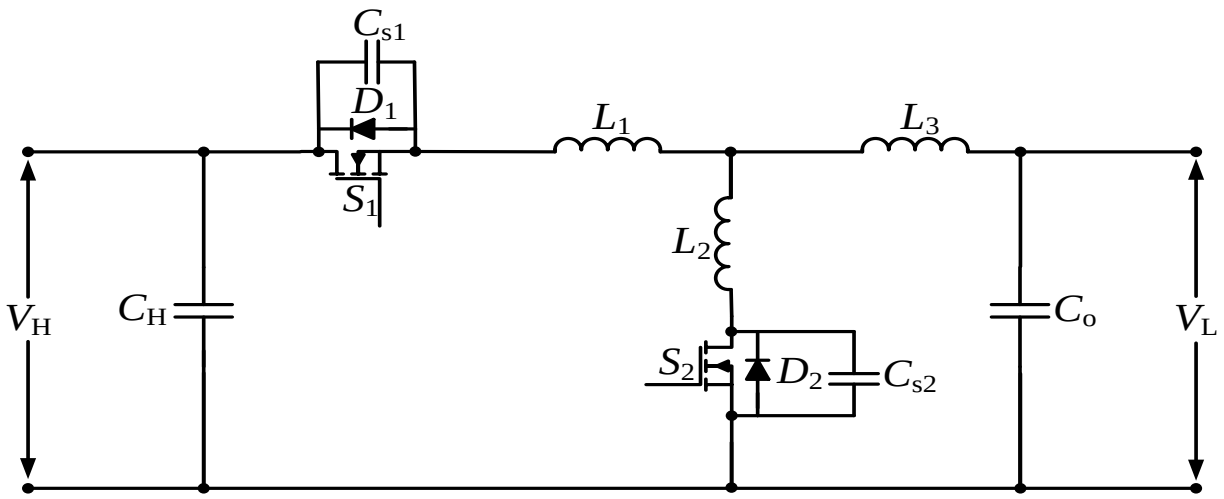

Figure 2-1 Proposed bidirectional converter

As can be observed from Fig. 2-1, the proposed topology utilizes only two MOSFETs as the active switching devices. The proposed topology is based on a resonant buck converter and boost converter concept. The two topologies are combined in order to devise a new soft-switched bidirectional topology. Fig. 2-2 shows a resonant buck converter.

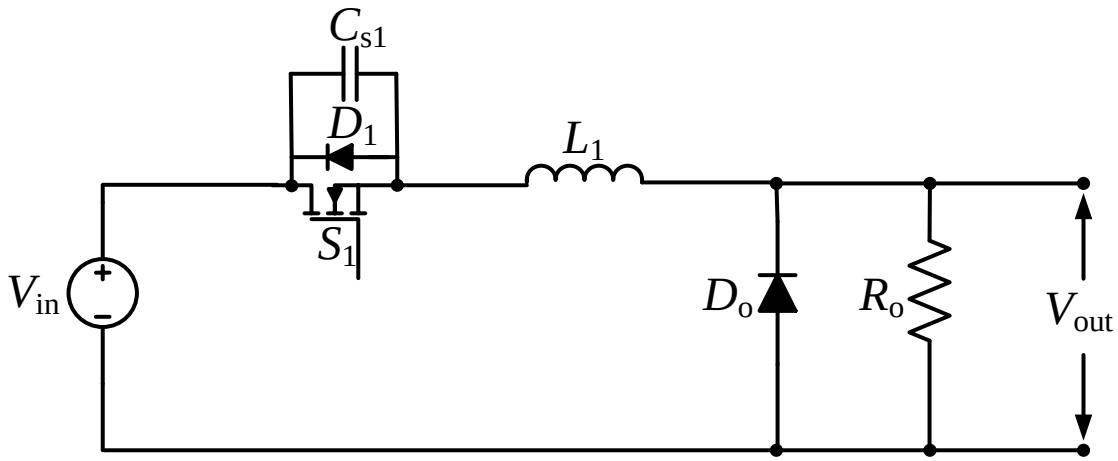

Figure 2-2 Resonant buck converter

Fig. 2-3 show the general waveforms [57] for the resonant buck converter shown in Fig. 2-2.

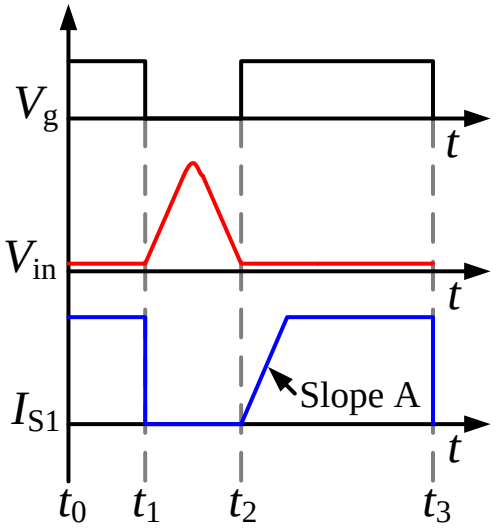

Figure 2-3 General waveforms for resonant buck converter

In Fig. 2-3, from $t_1 - t_2$, the switch S_1 shown in Fig. 2-2 is turned off. During this interval the resonant components C_{S1} and L_1resonate. At t_1, the voltage V_{in} across the switch S_1 becomes zero. Therefore, the switch can then turn on with zero voltage switching (ZVS). This is made possible due to the fact that the intrinsic capacitance, C_{oss} of the MOSFET switch, S_1 is discharged by the resonant tank formed by $C_{S1}$and L_1during the time interval, $t_1 - t_2$. The switch current, I_{S1} starts rising with Slope A at t_1. The slope is given by the Eq. (2-1).

$$Slope\ A = \frac{V_{in}}{L_1} \qquad \text{(Eq. 2-1)}$$

Fig. 2-4 shows a resonant boost converter. Fig. 2-5 shows the general waveforms of the resonant boost converter.

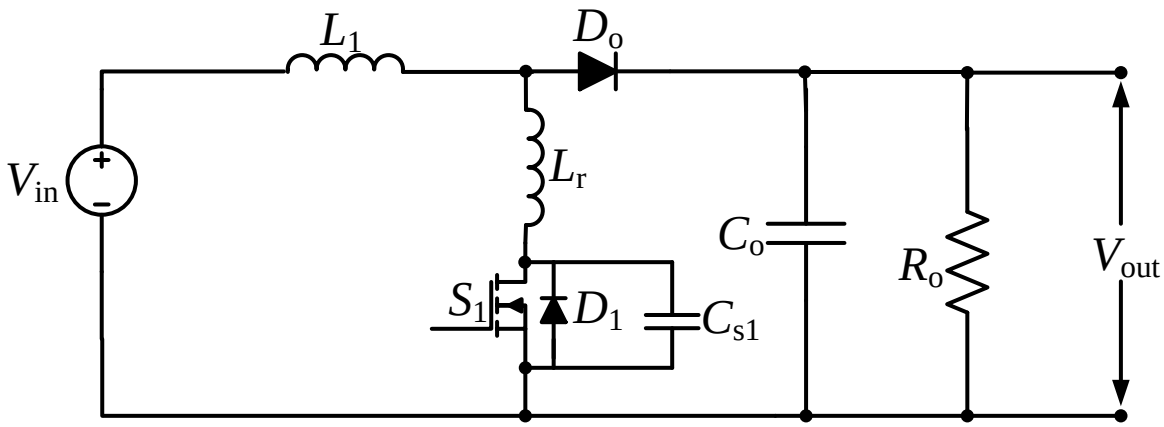

Figure 2-4 Resonant boost converter

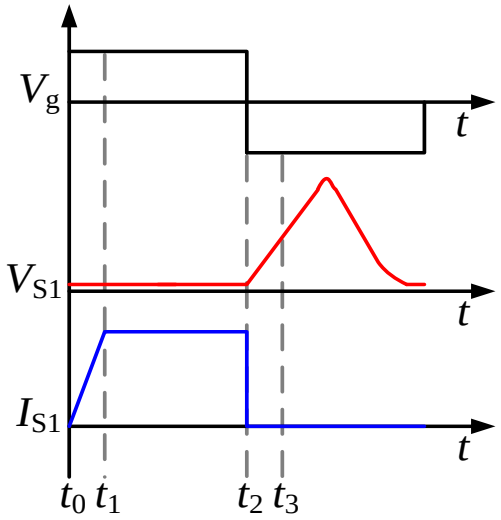

Figure 2-5 General waveforms for resonant boost converter

The waveforms [58] for the resonant boost converter are similar to that of the resonant buck converter. It is evident that due to the presence of the resonant tank formed by $L_r$and C_{s1}, the switch can turn on and turn off with zero switching voltage (ZVS). As in the previous case of the resonant buck converter, the resonant tank discharges the intrinsic capacitance of the MOSFET switch, S_1.

2.3 Advantages of Zero Voltage Switching

The devised topology presented in this thesis has several benefits [57]. The zero-voltage switching technique allows turn on and turn off of switches without any switching loss due to discharge of C_{oss}. Zero voltage switching reduces the electromagnetic induction losses during the turn on and turn off of switches. Topologies with zero voltage switching can also have a large input voltage and frequency range. At high frequencies, the size of the parasitic components which are the inductor and capacitor is reduced.

In the absence of zero voltage switching capability, the Miller Effect severely compromises the efficiency of the MOSFETs being used in the circuit. MOSFETs have three types of intrinsic capacitances. The gate to source capacitance is the input capacitance, the drain to source capacitance is the output capacitance and reverse transfer capacitance is the Miller capacitance. The Miller capacitance is the smallest of three capacitances. The Miller capacitance causes the switch to start turning off the switch as soon as it's turned on. This phenomenon is called negative feedback. Therefore, the switching time is not ideal causing greater switching losses. The Miller effect is substantially reduced by implementing zero voltage switching (ZVS).

2.4 Characteristics of Proposed Bidirectional Converter Topology

The proposed bidirectional converter has two switches as has been mentioned previously. The proposed topology is the result of the combination of the resonant buck converter shown in Fig. 2-2 and the resonant boost converter shown in Fig. 2-4. Fig. 2-6 shows the derivation of the devised topology. As can be seen from Fig. 2-6, the proposed topology operates in bidirectional modes. For

the buck mode of operation, the MOSFET, S_2 is turned off. MOSFET, $S_1$is switched with the required duty ratio. The anti-parallel diode of S_2 is used as the diode for the buck converter.

In boost operating mode, S_1 is turned off and its anti-parallel diode acts as the diode for the boost topology. Since the proposed circuit consists of two different sets of resonant components, soft-switching operation is achieved. Since the topology uses only two switches, the controller is simplified. A simple PWM controller can be utilized for the operation of the proposed topology. This greatly reduces the complexity of the circuit operation. The controller provides very high frequency operation which is an important characteristic of the converter presented.

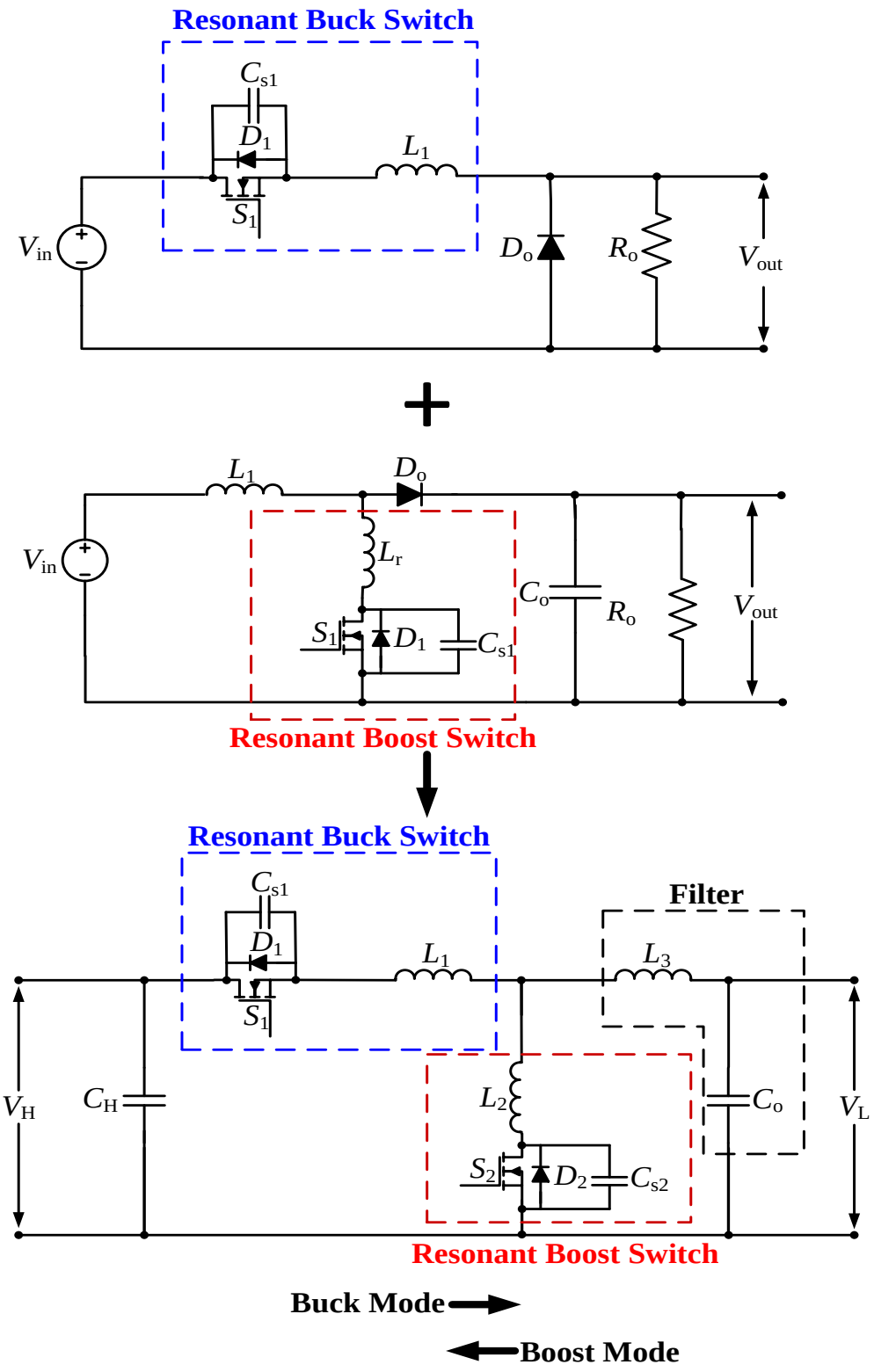

Figure 2-6 Derivation of the proposed topology

2.5 Design Equations for Proposed Topology

This section details the various design equations involved in the practical implementation of the proposed converter topology. Table 2-1 enumerates the parameters which are required in order to design the Bidirectional Converter topology described in this thesis work.

Table 2-1 Initial circuit parameters for circuit design

Initial circuit parameter	Full form
V_{inmin}	Minimum Input Voltage
V_{inmax}	Maximum Input Voltage
V_o	Output Voltage
P_{omin}	Minimum Output Power
P_{omax}	Maximum Output Power
f_{smin}	Minimum Switching Frequency
f_{smax}	Maximum Switching Frequency

The proposed circuit topology employs two switches. The first switch, S_1 is turned on during the buck mode of operation and the second switch, S_2 is turned on during the boost mode of operation. Owing to this topology the two switches working during the two modes have two corresponding LC resonant tanks.

Eq. 2-2 is used to calculate the minimum output current, I_{omin}.

$$I_{omin} = \frac{P_{omin}}{V_o} \quad \text{(Eq. 2-2)}$$

Similarly, Eq. 2-3 is used to calculate the maximum output current, I_{omax}.

$$I_{omax} = \frac{P_{omax}}{V_o} \quad \text{(Eq. 2-3)}$$

Using the maximum and minimum output current obtained from Eq. 2-2 and Eq. 2-3, Eq. 2-4 gives the maximum Drain to Source Voltage denoted by V_{DSmax} of switch S_1.

$$V_{DSmax} = V_{inmax} \times \left(1 + \frac{I_{omax}}{I_{omin}}\right) \quad \text{(Eq. 2-4)}$$

The maximum and minimum switching frequency denoted by f_{smax} and f_{smin} are determined based on the circuit application requirement. The resonant frequency, f_o has to be smaller than the selected switching frequency. Eq. 2-5 calculates the angular resonant frequency, ω_o.

$$\omega_o = 2 \times \pi \times f_o \quad \text{(Eq. 2-5)}$$

Next, the Minimum Drain to Source Voltage, V_{DSmin} is calculated by Eq. 2-6.

$$V_{DSmin} = R_{DSon} \times I_{omin} \quad \text{(Eq. 2-6)}$$

where, R_{DSon} is the on-state drain to source resistance of the MOSFET being utilized.

From Eq. 2-2 and Eq. 2-6, the resistive impedance, Z_R is calculated using the Eq. 2-7.

$$Z_R = \frac{(V_{inmax} - V_{DSmin})}{I_{omin}} \quad \text{(Eq. 2-7)}$$

Now, the resonant capacitance for switch S_2 which is used during the boost mode of operation of the bidirectional converter can be calculated based on the values obtained from Eq. 2-5 and Eq. 2-7. The resonant capacitance, C_{S2} is calculated using Eq. 2-8.

$$C_{S2} = \frac{1}{Z_R \times \omega_o} \quad \text{(Eq. 2-8)}$$

The capacitance obtained from Eq. 2-8 is then used to calculate the inductance, L_2 which corresponds to resonant tank of switch S_1. Switch S_2 is used during the buck mode of operation. Using the impedance obtained from Eq. 2-7 and the capacitance obtained from Eq. 2-8, Eq. 2-9 is used to determine the inductance, L_1.

$$L_1 = \frac{(Z_R)^2}{C_{S2}} \quad \text{(Eq. 2-9)}$$

The load resistance in the case of the buck mode of operation is calculated by using Eq. 2-10.

$$R_{Lbuck} = \frac{V_o}{I_{omax}} \quad \text{(Eq. 2-10)}$$

In case of the boost mode of operation, the input voltage now equals the output voltage of the buck mode of operation. Similarly, the output voltage of the boost mode is now equivalent to the input voltage of the buck mode of operation. However, the output power level is retained at the previously selected power level.

The minimum load resistance, $R_{Lboostmin}$ for the boost mode of operation is calculated by Eq. 2-11 based on the assumption that the efficiency of any given circuit topology is never 100% in practical implementation.

$$R_{Lboostmin} = \frac{V_o^2}{P_{omin}} \quad \text{(Eq. 2-11)}$$

where, V_o is equal to the initial value of V_{in} selected for the buck converter.

The maximum load resistance, $R_{Lboostmax}$ for the boost mode of operation is then given by Eq. 2-12.

$$R_{Lboostmax} = 2 \times R_{Lboostmin} \quad \text{(Eq. 2-12)}$$

We can now assume the Quality Factor, Q to be any value based standard values which conform to the circuit design requirements. The resonant frequency is again considered smaller than the switching frequency as previously selected.

Then, the inductance L_2 corresponding to resonant tank used in conjunction with switch S_2 can be calculated as shown in Eq. 2-13.

$$L_2 = \frac{Q \times R_{Lboostmin}}{\omega_0} \quad \text{(Eq. 2-13)}$$

Finally, the resonant capacitance, C_{S1} in parallel with the switch S_1 used in the buck mode of operation can be calculated in Eq. 2-14 [58].

$$C_{s1} = \left(\frac{1}{2 \times \omega_o \times R_{Lboostmin}}\right) \times 10^2 \quad \text{(Eq. 2-14)}$$

Figure 2-7 shows the proposed circuit in buck operating stage. Kirchhoff's Voltage Law is used to determine the voltage stress on switch S_1 for different frequencies when the switch is turned off.

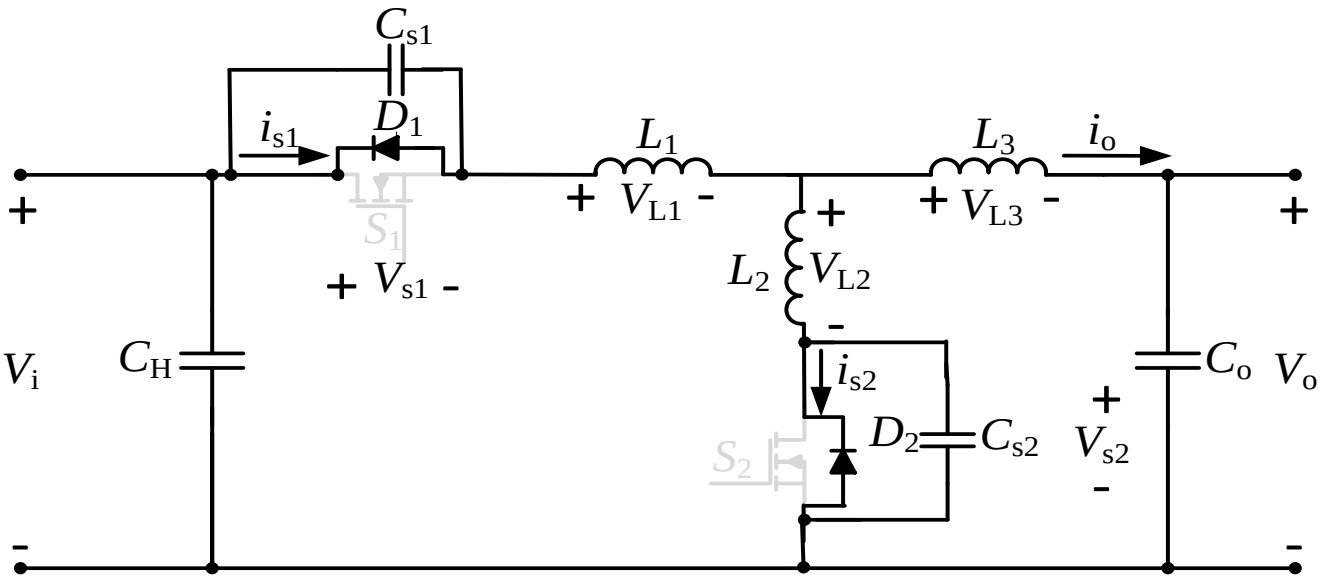

Figure 2-7 KVL for buck operating mode

Then, Eq. 2-15 gives the voltage stress on switch S_1. The voltage is determined using KVL loop.

$$V_{s1} = V_i - V_{L1} - V_{L2} - V_{s2} \quad \text{(Eq. 2-15)}$$

Since,

$$V_{L1} = L_1 \left(\frac{di_{s1}}{dt}\right) \quad \text{(Eq. 2-16)}$$

And

$$V_{L2} = L_2 \left(\frac{di_{s2}}{dt}\right) \quad \text{(Eq. 2-17)}$$

Eq. 2-15 can be written as Eq. 2-18 by substituting Eq. 2-16 and Eq. 2-17.

$$V_{s1} = V_i - L_1 \left(\frac{di_{s1}}{dt}\right) - L_2 \left(\frac{di_{s2}}{dt}\right) - V_{s2} \quad \text{(Eq. 2-18)}$$

Figure 2-8 shows the proposed circuit in boost operating stage. Kirchhoff's Voltage Law is used to determine the voltage stress on switch S_2 for different frequencies when the switch is turned off.

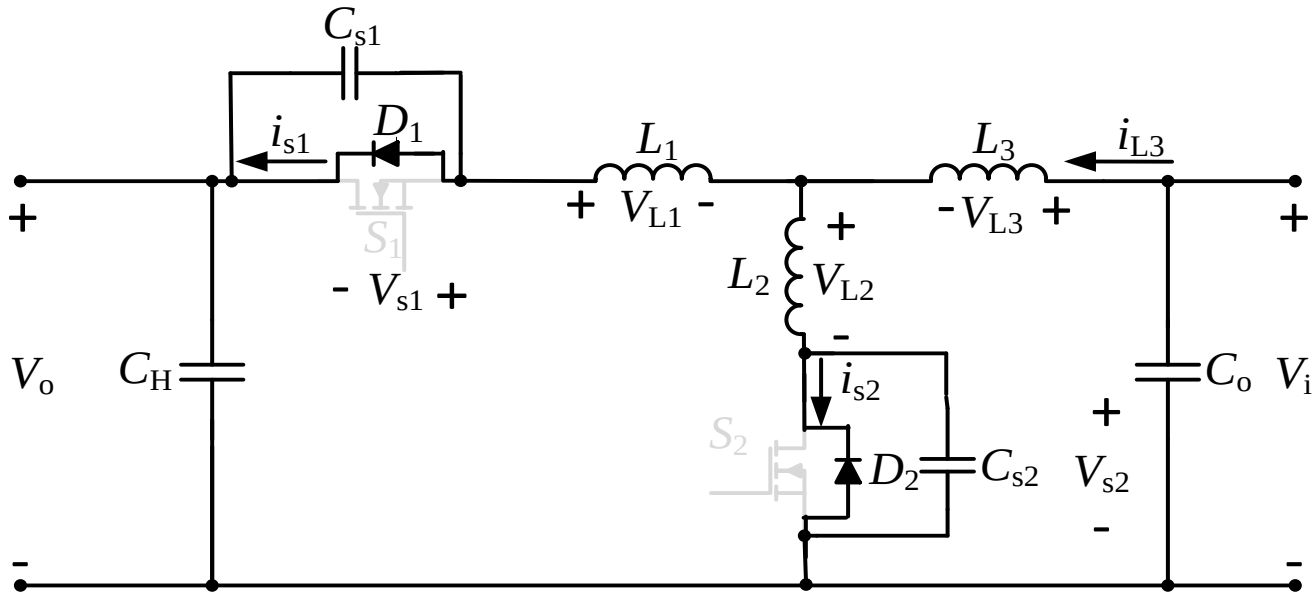

Figure 2-8 KVL for boost operating mode

Then, Eq. 2-19 gives the voltage stress on switch S_2. The voltage is determined using KVL loop.

$$V_{s2} = V_o + V_{L1} - V_{L2} + V_{s1} \quad \text{(Eq. 2-19)}$$

Eq. 2-19 can be written as Eq. 2-20 by substituting Eq. 2-16 and Eq. 2-17.

$$V_{s2} = V_i + L_1\left(\frac{di_{s1}}{dt}\right) - L_2\left(\frac{di_{s2}}{dt}\right) + V_{s2} \quad \text{(Eq. 2-20)}$$

Figure 2-10 shows the Voltage with respect to Frequency Graph for voltage across switch S_2 using Eq. 2-20.

2.6 Operating Stages

2.6.1 Buck Mode of Operation

Fig. 2-9 shows the waveforms of the proposed bidirectional converter during the buck mode of operation.

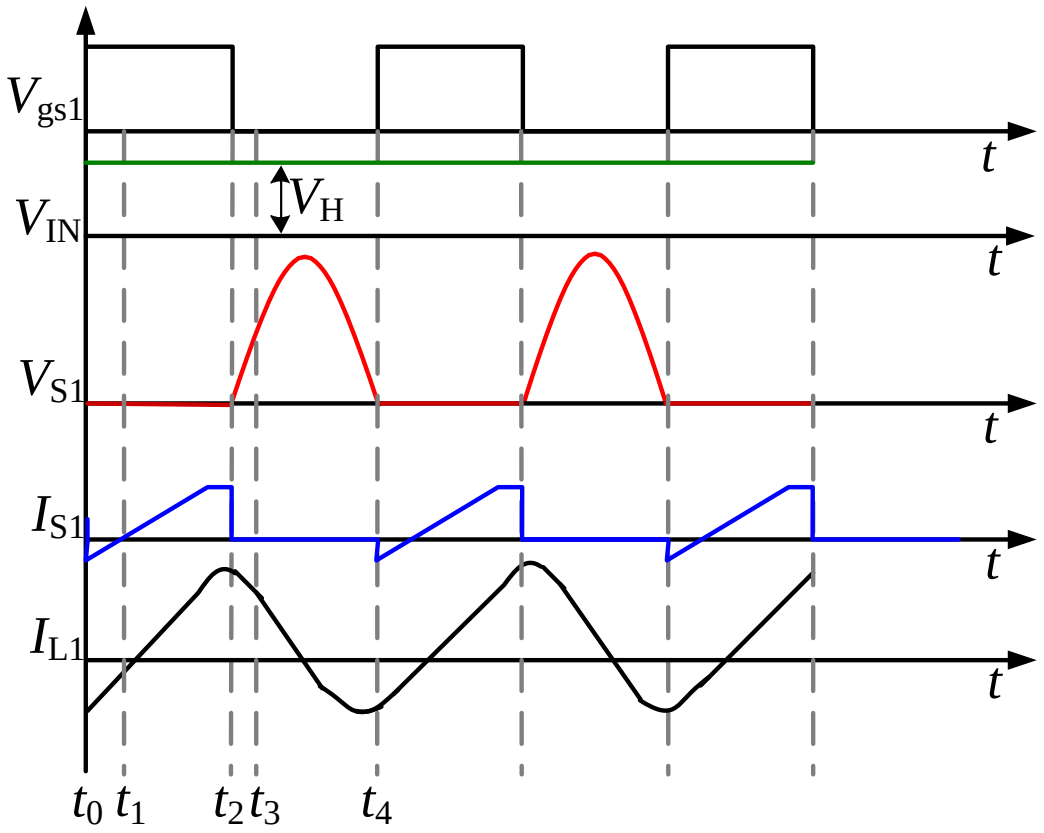

Figure 2-9 Operating stage waveforms for buck mode of operation

Interval 1 $(\boldsymbol{t_0 - t_1})$***:*** During the first interval the switch S_1 is turned on. In the buck mode of operation switch S_2 remains off. Initially the antiparallel diode of the switch S_1 is conducting. The diode discharges the intrinsic capacitance of the switch.

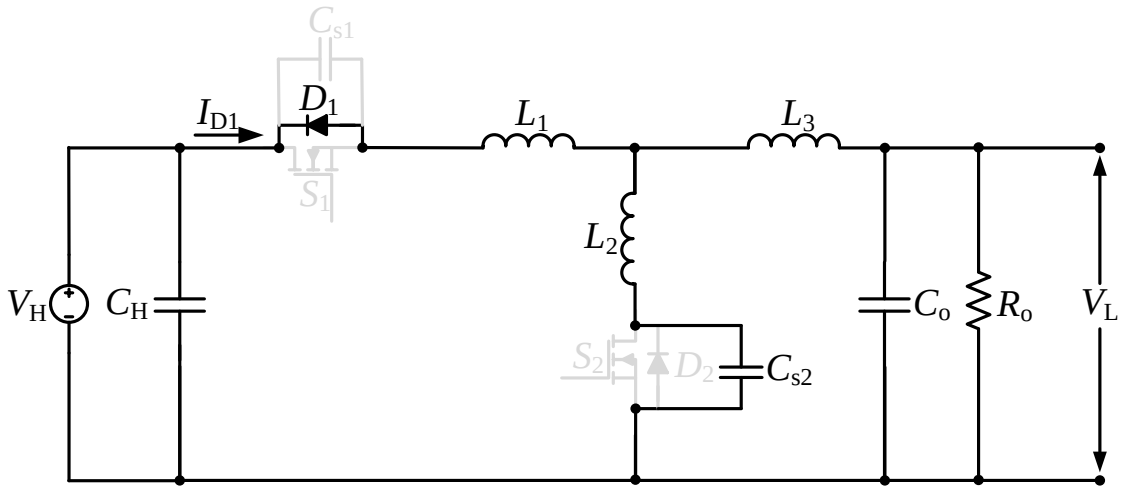

Figure 2-10 Equivalent circuit in the interval $(t_0 - t_1)$

Interval 2 **$(t_1 - t_2)$*:*** The switch S_1 is then turned on with Zero Voltage Switching (ZVS). Owing to this, there is no switching loss. The antiparallel diode, D_2 of switch S_2 is turned on and acts as a catch diode. At time, t_2 the switch current is reduced to zero and the switch turns off with zero current switching.

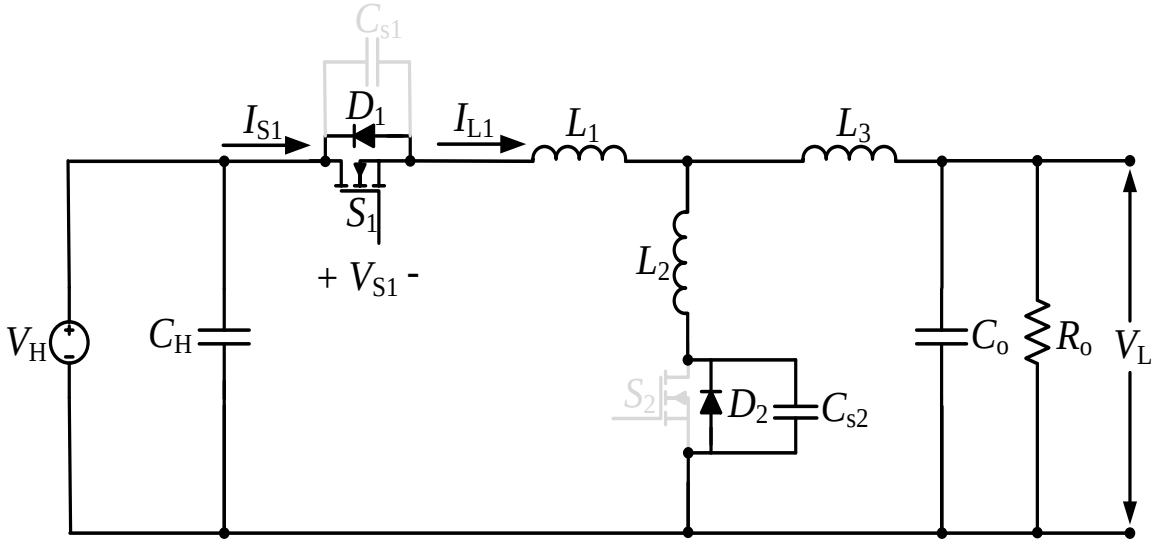

Figure 2-11 Equivalent circuit in the interval $(t_1 - t_2)$

Interval 3 $(\boldsymbol{t_2 - t_3})$***:*** During this interval both the switches, S_1 and S_2 are turned off. Since, no current flows through switch S_1 during this time interval and the current passing through the resonant inductor L_1 cannot change instantaneously, the current is diverted through the resonant capacitor C_{S1} parallel to the switch. The voltage across the capacitor C_{S1} then starts rising until it becomes equal to the input voltage, V_H. The voltage across the resonant inductor L_1 remains constant during this interval.

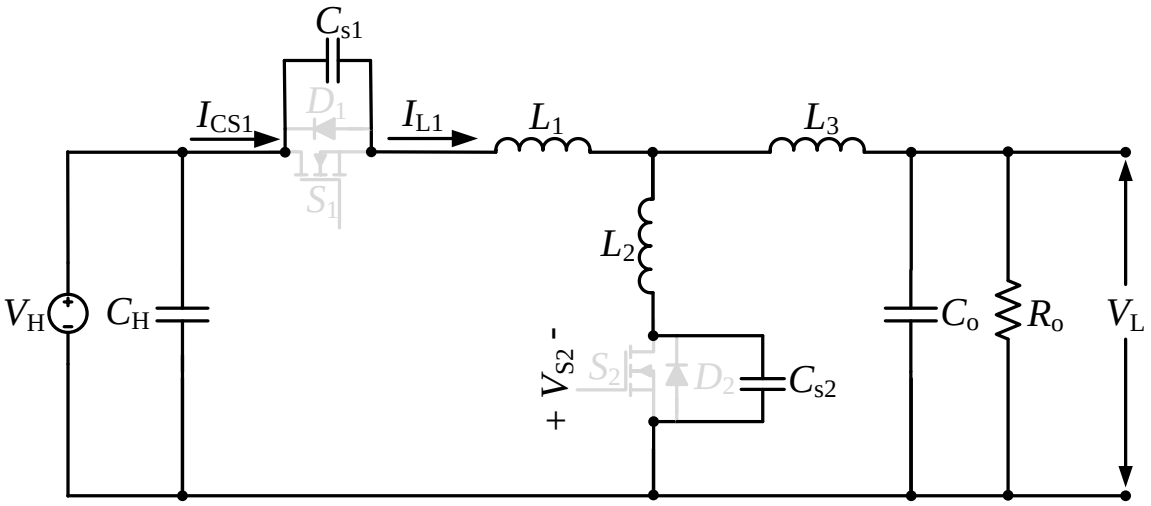

Figure 2-12 Equivalent circuit in the interval $(\boldsymbol{t_2 - t_3})$

Interval 4 $(\boldsymbol{t_3 - t_4})$***:*** During this interval, both switches, S_1 and S_2 are turned off. At time, t_1 the current passing through the resonant inductor and capacitor becomes equal to the output current. At this stage, the LC resonant tank comprising of L_1 and C_{S1} begins to resonate at the resonant frequency. At time t_4, the antiparallel diode, D_1 of the switch S_1 again starts conducting and discharges the intrinsic capacitance of the MOSFET, S_1 so that the switch can turn on again with ZVS.

2.6.2 Boost Mode of Operation

Fig. 2-13 shows the waveforms of the proposed bidirectional converter during the boost mode of operation.

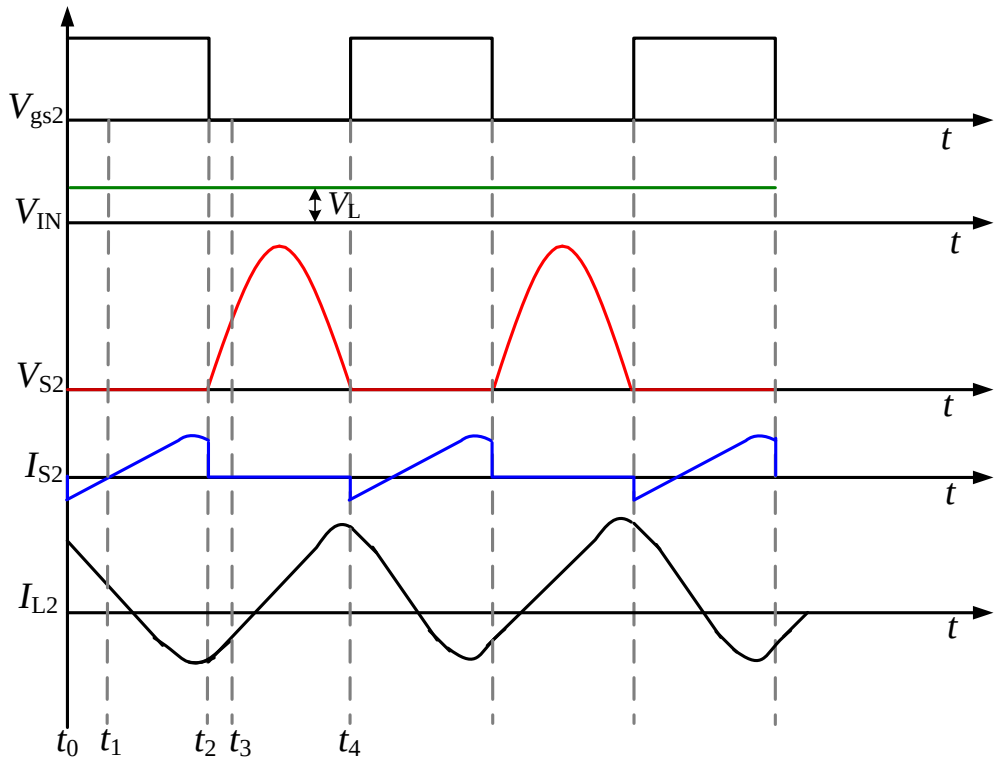

Figure 2-13 Operating stage waveforms for boost mode of operation

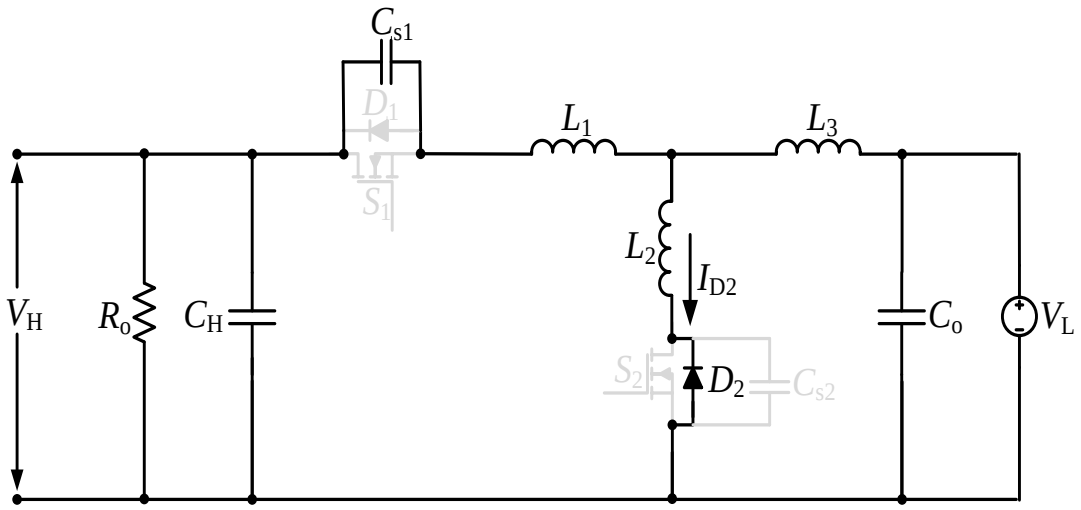

Figure 2-14 Equivalent circuit in the interval $(t_0 - t_1)$

Interval 1 **$(t_0 - t_1)$*:*** During the first interval the switch S_2 is turned on. In the boost mode of operation switch S_1 remains off. Initially the antiparallel diode, D_2 of the switch S_2 is conducting. The diode discharges the intrinsic capacitance of the switch.

Interval 2 **$(t_1 - t_2)$*:*** The switch S_2 is turned on with Zero Voltage Switching (ZVS). Owing to this, there is no switching loss. The antiparallel diode, D_1 of switch S_1 is turned on and acts as a catch diode. At time, t_2 the switch current is reduced to zero and the switch turns off with zero current switching.

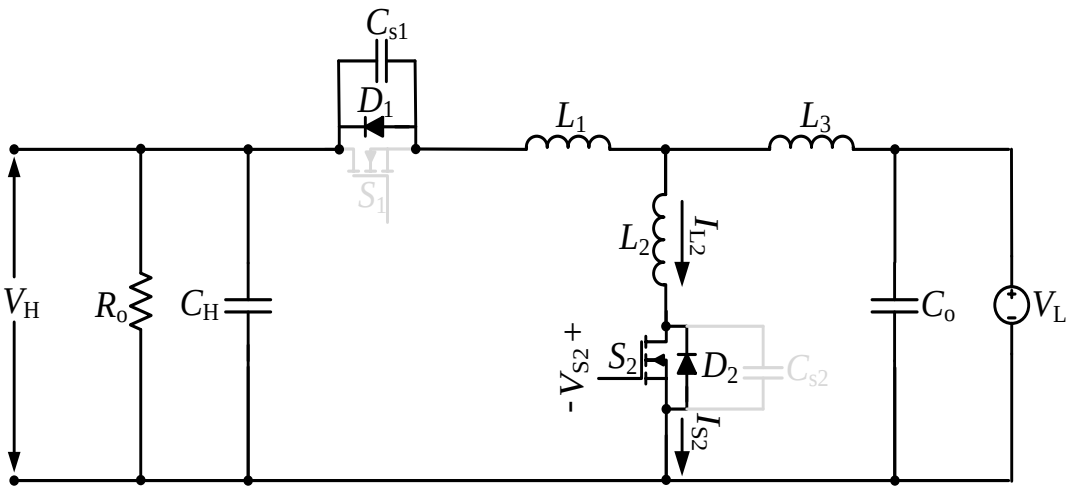

Figure 2-15 Equivalent circuit in the interval $(t_1 - t_2)$

Interval 3 **$(t_2 - t_3)$*:*** From $t_2 - t_3$ both the switches, S_1 and S_2 are turned off. As in the case of the buck mode, the current is diverted through the resonant capacitor, C_{S2} parallel to the switch because no drain current flows through the switch S_2 during this time interval and the current passing through the corresponding resonant inductor, L_2 cannot change instantaneously. The voltage across the capacitor C_{S2} then starts rising until it becomes equal to the input voltage, V_L. The voltage across the resonant inductor L_2 remains constant during this interval.

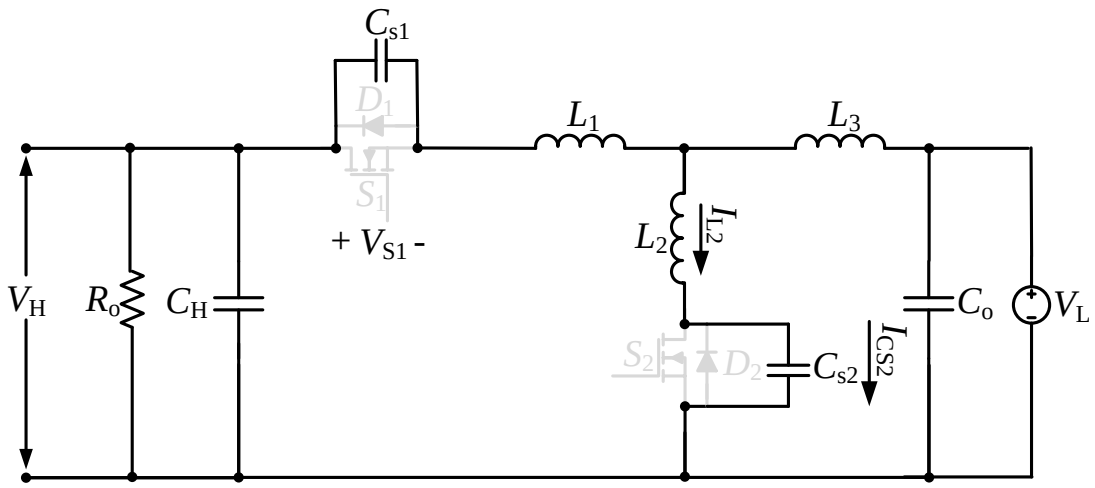

Figure 2-16 Equivalent circuit in the interval $(t_2 - t_3)$

Interval 4 **$(t_3 - t_4)$*:*** This is the resonant interval. During this interval too both the switches, S_1 and S_2 remain turned off. At time, t_2 the current passing through the resonant inductor and capacitor becomes equal to the output current. At this stage, the LC resonant tank comprising of L_2 and C_{S2} begins to resonate at the resonant frequency. At time t_4, the antiparallel diode D_2 starts conducting again and discharges the intrinsic capacitance of the MOSFET, S_2 so that the switch will turn on again with ZVS.

2.7 Chapter Summary

Chapter 2 elucidates the design equations for the proposed topology. The operating stages are discussed in detail. The equivalent circuits for each interval for the two different operating modes have been illustrated and explained. The soft-switching operation of the proposed circuit has been described in this chapter.

Chapter 3

Design Example and Performance of the Proposed Bidirectional Converter

3.1 Introduction

In this chapter, a 200 kHz design example for the proposed topology is presented. Simulation results are first given to highlight the soft-switching performance of the proposed circuit. The performance of the proposed circuit is then compared with a standard 200 kHz buck-boost type bidirectional converter topology with the same power condition. To confirm the feasibility of the proposed circuit at very high frequency operation, results are then given on a 2 MHz design with the same power level.

Then this chapter will present the experimental results on a laboratory-scale 70W proof-of-concept hardware prototype which operates at a switching frequency of around 100 kHz. All the switching waveforms will be provided to highlight the features of the proposed bidirectional converter.

3.2 Design Example

A design example is given in this section to validate the theoretical analysis of the proposed bidirectional converter topology. Table 3-1 gives the design specifications. The circuit components parameters are then designed according to the design equations provided in Chapter 2.

Table 3-1 Design specifications

Maximum Input Voltage (V_{inmax}) for buck operating stage and Maximum Output Voltage (V_{omax}) for boost operating stage	400V
Minimum Input Voltage (V_{inmin}) for buck operating stage and Minimum Output Voltage (V_{omax}) for boost operating stage	300V
Output Voltage (V_o) for buck operating stage and Input Voltage (V_{in}) for boost operating stage.	96V
Minimum Switching Frequency (f_{smin})	200kHz

Eq. 2-2 from chapter 2 can be used to determine the minimum output current. Eq. 3-1 shows the derived value of the minimum output current, I_{omin}.

$$I_{omin} = \frac{500\ W}{96\ V} = 5.2\ A \qquad \text{(Eq. 3-1)}$$

Similarly, the maximum output current can also be calculated from Eq. 2-3. Eq. 3-2 calculates the value of the maximum output current, I_{omax}.

$$I_{omax} = \frac{1000\ W}{96\ V} = 10.4\ A \qquad \text{(Eq. 3-2)}$$

Using the maximum and minimum output current obtained from Eq. 3-1 and Eq. 3-2, Eq. 2-4 gives the maximum voltage across the switch denoted by V_{DSmax} of switch S_1. S_1 is the switch which turns on during the buck mode of operation.

$$V_{DSmax} = 400 \times \left(1 + \frac{10.4}{5.2}\right) = 1200\ V \qquad \text{(Eq. 3-3)}$$

The resonant frequency, f_o is smaller than the maximum switching frequency, f_{smax}. The resonant frequency is calculated in Eq. 3-4.

$$f_o = 300 - \left(\frac{1}{100} \times 300\right) = 297\ kHz \quad \text{(Eq. 3-4)}$$

Using the result from Eq. 3-4, the angular frequency was determined using Eq. 2-5 in Eq. 3-5.

$$\omega_o = 2 \times \pi \times 297 \times 10^3 = 1866 \times 10^3\ rad/sec \quad \text{(Eq. 3-5)}$$

Then, the Minimum Drain to Source Voltage, V_{DSmin} is determined in Eq. 3-6 using Eq. 2-6. Using standard datasheet values, R_{DSon} is 0.8 Ω.

$$V_{DSmin} = 0.8 \times 5.2 = 4.16\ V \quad \text{(Eq. 3-6)}$$

The resistive impedance, Z_R is calculated using the Eq. 2-7 in Eq. 3-7.

$$Z_R = \frac{(400-4.16)}{5.2} = 76.12\Omega \quad \text{(Eq. 3-7)}$$

Switch, S_2 is turned on during the boost operating stage. Capacitor, C_{s2} is the resonant capacitance in the LC resonant tank for switch, S_2. The capacitance, C_{s2} is determined using Eq. 2-8.

$$C_{S2} = \frac{1}{76.12 \times 1866 \times 10^3} = 7.04\ nF \quad \text{(Eq. 3-8)}$$

The obtained capacitance, C_{S2} in Eq. 3-8 is used to calculate the inductance, L_1 which is the resonant inductor for switch, S_1. Eq. 2-9 is used to calculate L_1 in Eq. 3-9.

$$L_1 = \frac{76.12}{1866 \times 10^3} = 40.7\ \mu H \quad \text{(Eq. 3-9)}$$

The load resistance in the case of the buck mode of operation is determined using Eq. 2-10 in Eq. 3-10.

$$R_{Lbuck} = \frac{96}{10.4} = 9.2\ \Omega \quad \text{(Eq. 3-10)}$$

Eq. 2-11 is used to determine the minimum load resistance, $R_{Lboostmin}$ for the boost mode of operation in Eq. 3-11.

$$R_{Lboostmin} = \frac{400^2}{500} = 320\ \Omega \quad \text{(Eq. 3-11)}$$

Similarly, Eq. 2-12 gives the maximum load resistance, $R_{Lboostmax}$ for the boost mode of operation.

$$R_{Lboostmax} = 2 \times 320 = 680\ \Omega \quad \text{(Eq. 3-12)}$$

Using the chosen Quality Factor, Q, we can calculate the inductance, L_2 which is the resonant inductance in the resonant tank of the switch, S_2 in Eq. 3-13. To calculate the resonant frequency is normalized to the switching frequency with a factor of 0.08.

$$L_2 = \frac{320}{2\pi \times 2500 \times 10^3 \times 1} = 20.3\ \mu H \quad \text{(Eq. 3-13)}$$

Finally, the resonant capacitance of switch, S_1 is determined using Eq. 3-14.

$$C_{s1} = \left(\frac{1}{2 \times 2\pi \times 2500 \times 10^3 \times 320}\right) \times 10^2 = 10\ nF \quad \text{(Eq. 3-14)}$$

3.3 Results and Analysis

To verify the validity of the proposed topology, the circuit was first simulated in the Powersim (PSIM) software. The presented results are then compared to the results of a conventional buck-boost bidirectional converter without any soft-switching capability.

3.3.1 Results of 500 W, 200 kHz Simulation of Proposed Converter

The circuit parameters listed in Table 3-2 are used to simulate the 200 kHz design of the proposed bidirectional converter circuit.

Table 3-2 Circuit parameters for 500 W, 200 kHz simulation of proposed circuit

Circuit parameter	Value
Switch On-State Resistance	390 mΩ
Switch Diode Forward Voltage	0.8 V
Resonant Inductor (L_1)	40.7 μH
Resonant Capacitor (C_{S1})	10.4 nF
Resonant Inductor (L_2)	20 μH
Resonant Capacitor (C_{S2})	7.4 nF

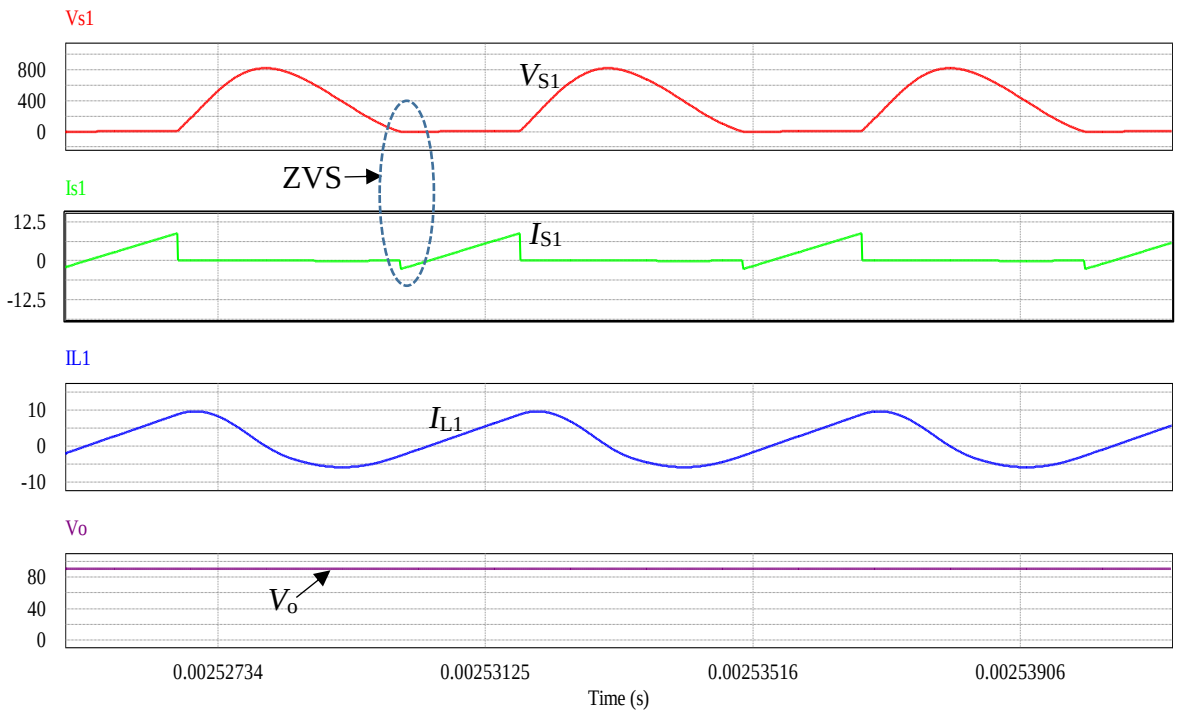

Figure 3-1 Simulation results for buck operating stage for 500 W, 200 kHz topology

Figure 3-1 shows the results obtained for the buck operating stage when the power rating is 500W and the switching frequency is 200 kHz. The input voltage during this mode of operation was 400 V. Switch S_1, is turned on during the boost mode of operation. In Fig. 3-1, the voltage (V_{S1}) and current (I_{s1}) across the switch showed that zero voltage switching during turn on and zero current switching during turn off are achieved. This is due to the presence of the LC resonant tank. The resonant inductor current (I_{L1}) is shown in Fig. 3-1. The current is in continuous conduction mode as per requirement. The output voltage when the duty cycle was 0.35 is then 96 V. The output voltage level was selected to be 96 V considering four 24 V lithium-ion batteries placed in series. When lithium ion batteries are compared with valve regulated lead acid batteries, it is found that the lithium ion batteries perform better in warmer climates as their lifetime is 3 times the lifetime of valve regulated lead acid batteries. Even though valve regulated lead acid batteries have been very popular

for off-grid energy storage applications, lithium ion batteries are now being favored as they have 3.5 times the energy density of the valve regulated lead acid batteries [59].

The efficiency of the proposed converter during the buck operating stage was determined to be 96.9%.

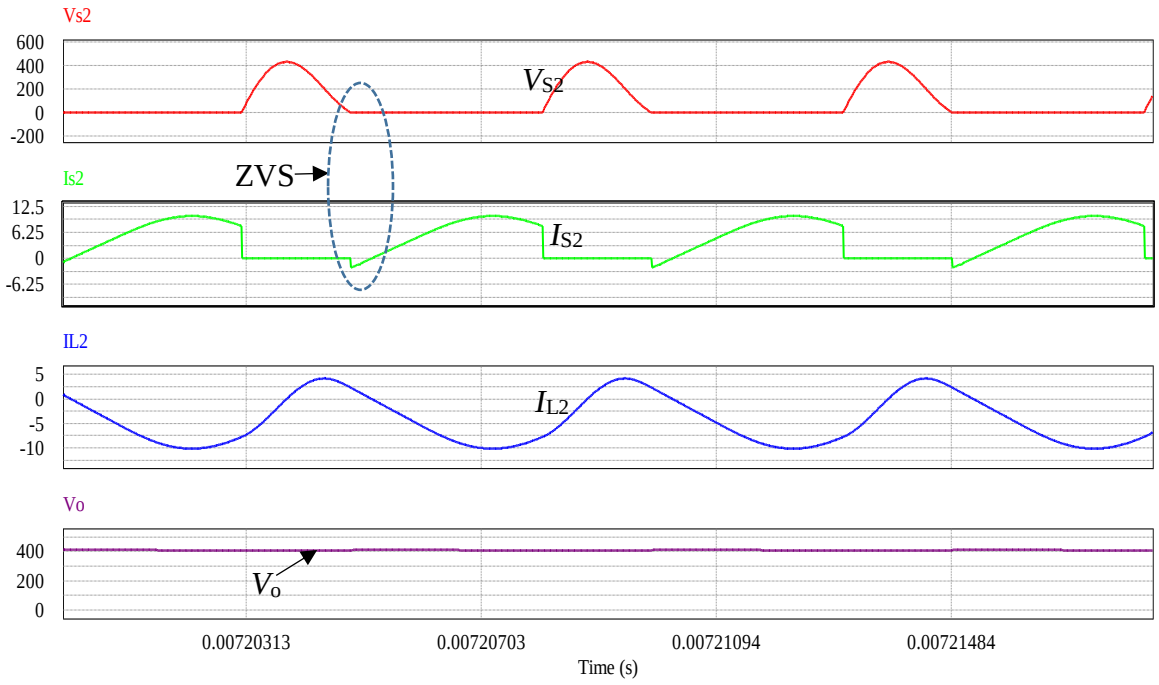

Figure 3-2 Simulation results for boost operating stage for 500 W, 200 kHz topology

Figure 3-2 shows the results obtained for the boost operating stage when the power rating is 500 W and the switching frequency is 200 kHz. The input voltage during this mode of operation was reversed. The output voltage of the buck operating stage, 96 V, now became the input voltage for the boost operating stage. Switch S_2, is turned on during the boost mode of operation and switch S_1 remains off. In Fig. 3-2, the voltage (V_{S2}) and current (I_{s2}) across the switch S_2 are presented. The curves show zero voltage switching during turn on and zero current switching during turn off. The resonant tank of for this switch consists of inductor L_2 and capacitor C_{S2}. The resonant inductor

current (I_{L2}) is shown in Fig. 3-2. The current is in continuous conduction mode as per requirement. The output voltage when the duty cycle was 0.61 is then 400 V. The output voltage level was selected to be 400 V as the standard voltage of the microgrid [60].

The efficiency of the proposed converter during the buck operating stage was determined to be 96.7%.

Owing to the soft-switching capability of the circuit, it has been found to be highly efficient.

3.3.2 Results of 500 W, 2 MHz simulation of proposed converter

Following the same procedures illustrated in the previous section for the 200 kHz design, the circuit parameters for a switching frequency of 2 MHz are obtained and listed in Table 3-3. Figure 3-3 shows the results obtained for the buck operating stage when the power is 500W and the switching frequency is 2 MHz.

Table 3-3 Circuit parameters for 500 W, 2 MHz simulation of proposed circuit

Circuit parameter	Value
Switch On-State Resistance	390 mΩ
Switch Diode Forward Voltage	0.8 V
Resonant Inductor (L_1)	10.48 μH
Resonant Capacitor (C_{S1})	0.5 nF
Resonant Inductor (L_2)	2.42 μH
Resonant Capacitor (C_{S2})	0.2 nF

Switch S_1, is turned on during the buck mode of operation and switch S_2 remains off. In Fig. 3-3, the voltage (V_{S1}) and current (I_{s1}) across the switch S_1 are presented. The curves show zero voltage switching during turn on and zero current switching during turn off. The resonant tank of for this switch consists of inductor L_1 and capacitor C_{S1}. The resonant inductor current (I_{L1}) is shown in Fig. 3-3. The current is in continuous conduction mode as per requirement [61]. The duty cycle was 0.33. The efficiency of the proposed converter during the buck operating mode was determined to be 96.3%.

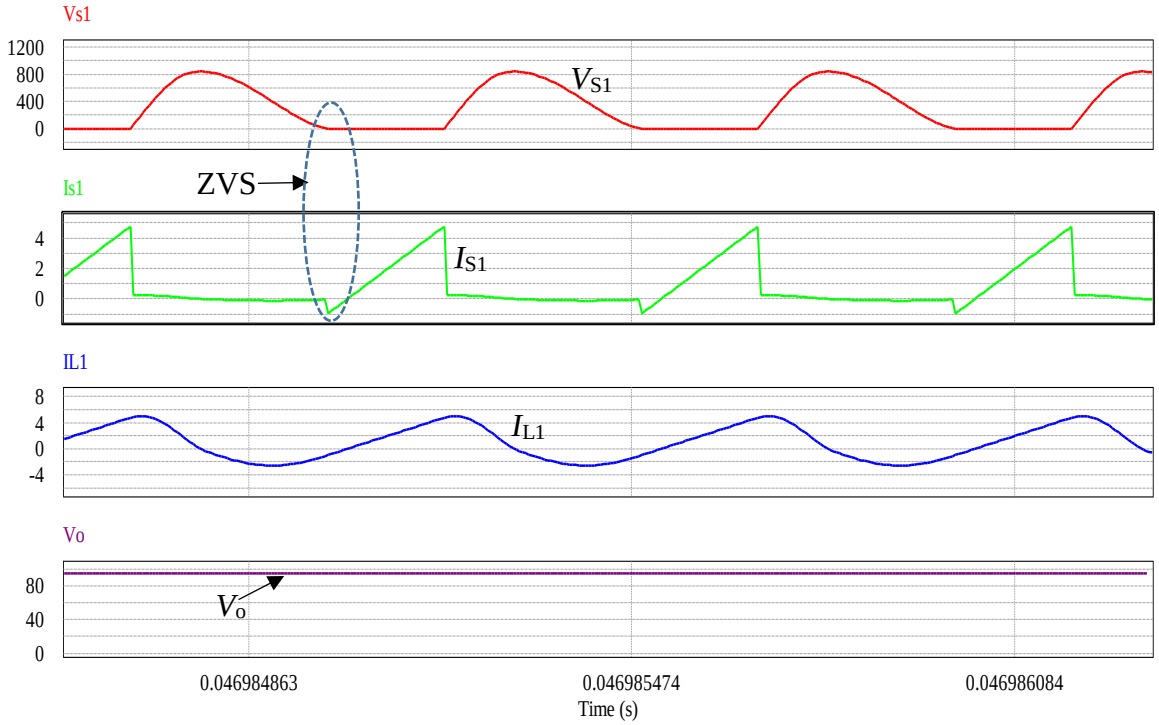

Figure 3-3 Simulation results for buck operating stage for 500 W, 2 MHz topology

Figure 3-4 shows the results obtained for the boost operating stage when the power rating is 500 W and the switching frequency is 2 MHz. Switch S_2, is turned on during the boost mode of operation.

In Fig. 3-4, the voltage (V_{s2}) and current (I_{s2}) across the switch S_2 are presented. The curves show zero voltage switching during turn on and zero current switching during turn off. The resonant tank of for this switch consists of inductor L_2 and capacitor C_{S2}. The resonant inductor current (I_{L2}) is shown in Fig. 3-4. The duty cycle was 0.65. The efficiency of the proposed converter during the buck operating stage was determined to be 96.5%.

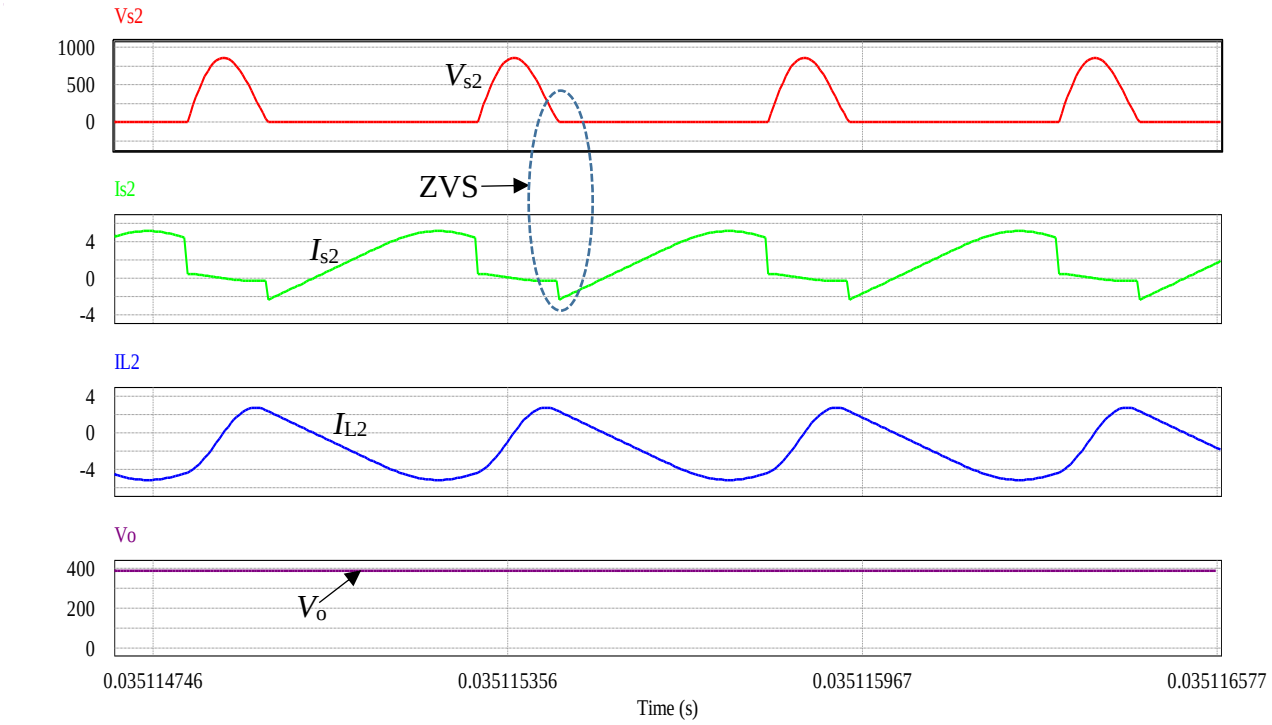

Figure 3-4 Simulation results for boost operating stage for 500 W, 2 MHz topology

3.3.3 Results for Conventional Buck-Boost Bidirectional Converter

The buck-boost bidirectional converter was also simulated. The power efficiency for the buck operating mode was found to be 89.3% for the buck operating stage and 89.7% for the boost

operating stage. Fig. 3-5 shows the results for the buck operating stage for conventional buck-boost bidirectional converter without a resonant tank.

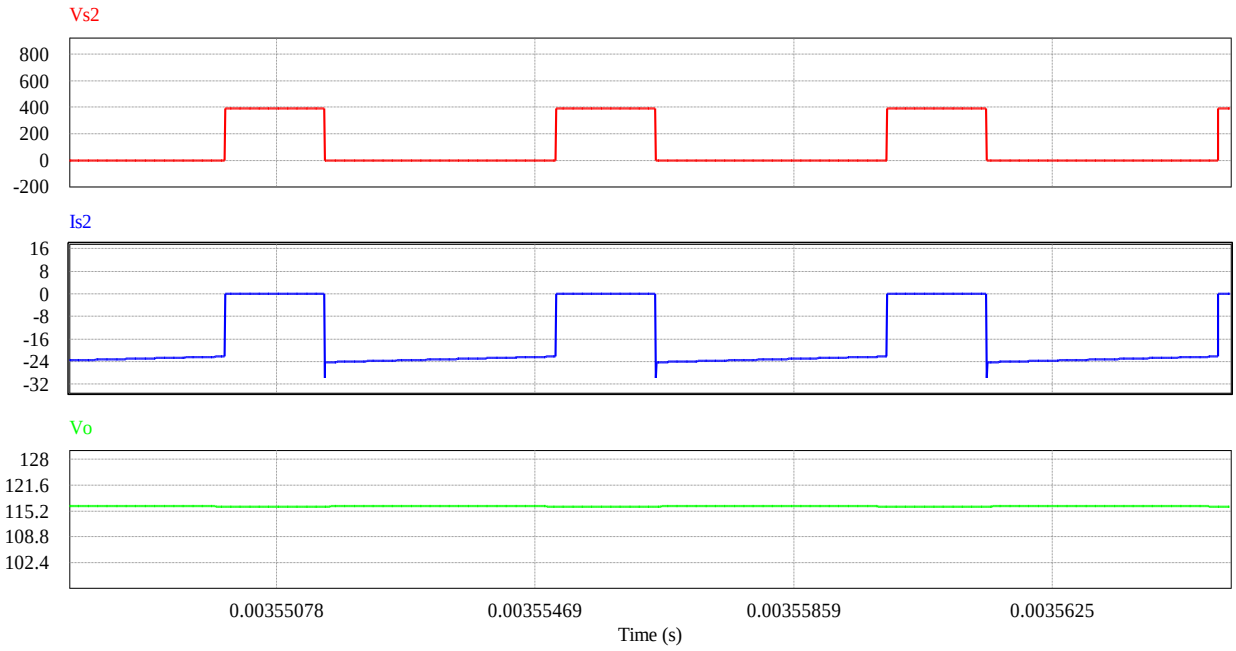

Figure 3-5 Simulation results for buck operating stage for buck-boost converter topology

Fig. 3-6 shows the results for the boost operating stage for conventional buck-boost bidirectional converter without a resonant tank.

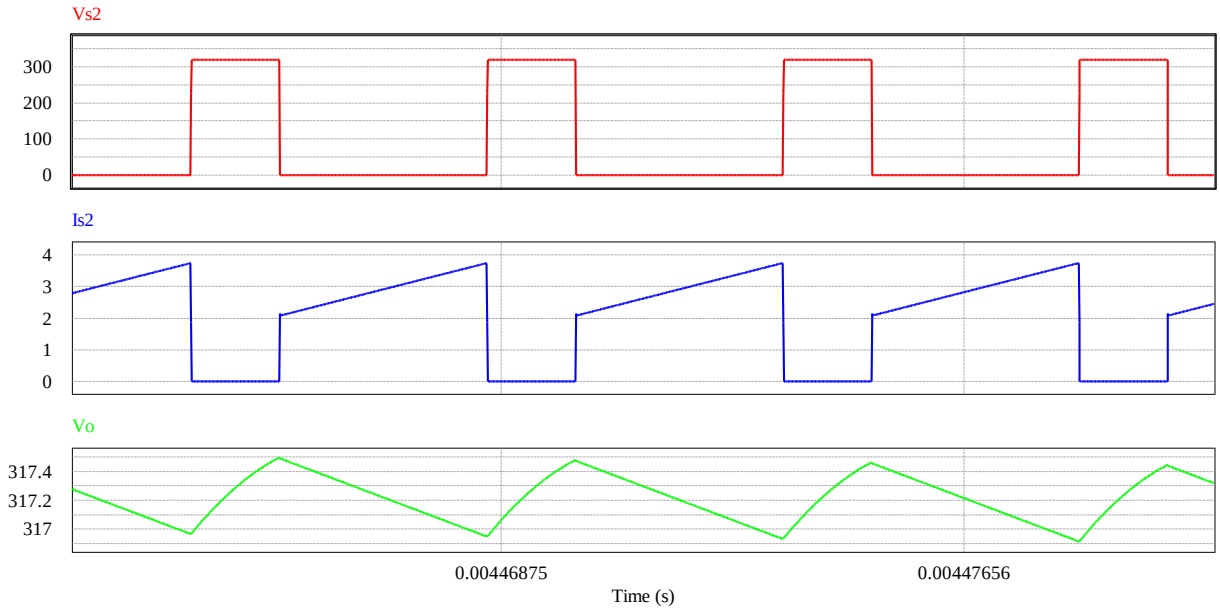

Figure 3-6 Simulation results for boost operating stage for the buck-boost converter topology

3.3.4 Results from Experimental Work

A hardware prototype of the proposed quasi-resonant bidirectional converter was devised. Table 3-4 lists the components used in the hardware prototype.

Table 3-4: List of components used in prototype

Component	Part name
MOSFET	CREE Silicon Carbide Power MOSFET (CRM0280090D)
Resonant Inductance (L_1)	Coilcraft Shielded Power Inductor (SER3018H-223KE)
Resonant Capacitance (C_1)	Murata Monolithic Chip Ceramic Capacitors (1210, 1206)
Resonant Inductance (L_2)	Coilcraft Shielded Power Inductor (SER1390-473ML)
Resonant Capacitance (C_2)	Murata Monolithic Chip Ceramic Capacitors (1210, 1206)

Table 3-5: Design Specifications used in prototype

	Buck Mode	**Boost Mode**
Input voltage	60 V	30 V
Output voltage	22.1 V	54.2 V

Switching frequency	100 kHz	100 kHz

Fig.3-7 shows the hardware prototype which has been devised to verify the results obtained from simulation.

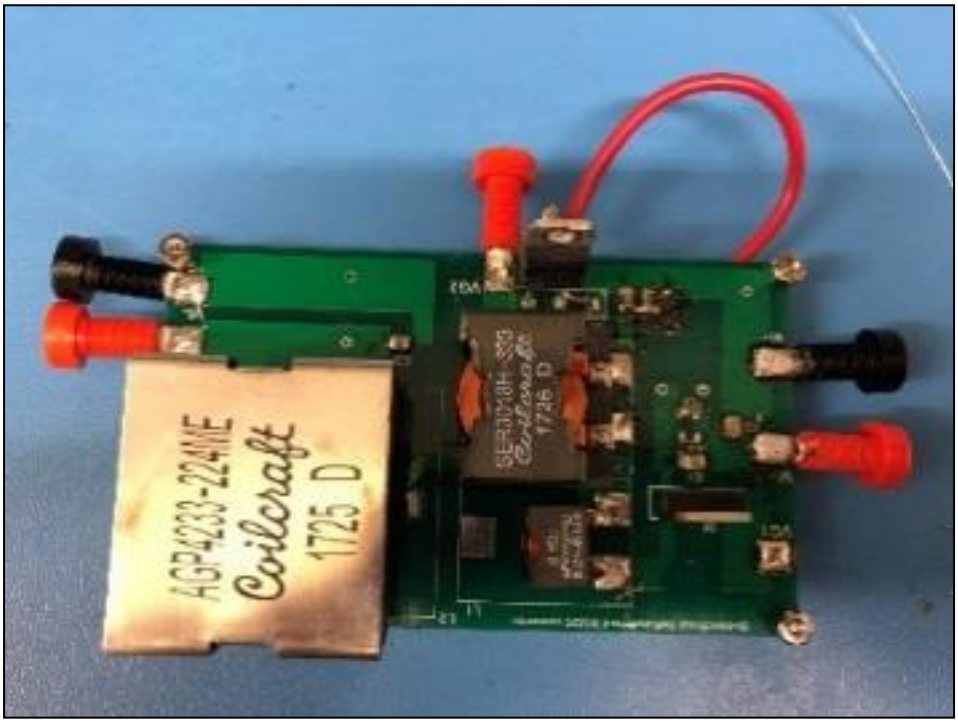

Figure 3-7 Picture of the proof-of-concept hardware prototype

Fig. 3-8 shows the results obtained from the buck mode of operation when the input voltage is $60\ V$, the switching frequency is $100\ kHz$ and the duty cycle is 50%.

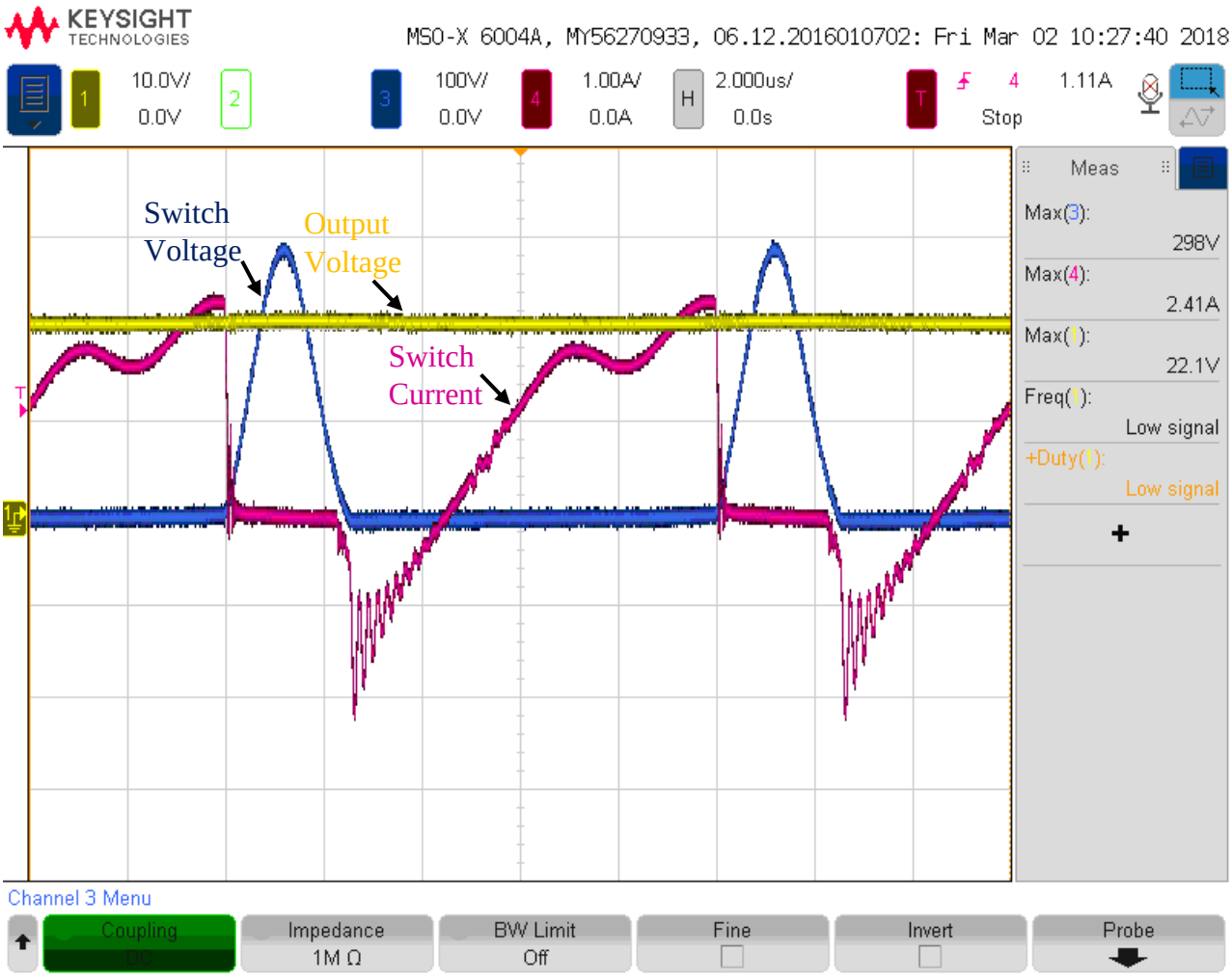

Figure 3-8 Results from prototype for buck operating stage

[Output Voltage: 10.0 V/div; Switch Voltage: 100 V/div; Switch Current: 1.0 A/div; Time: 2.0 µs/div]

As is evident from the results shown in Fig. 3-8, the proposed bidirectional converter topology achieves soft-switching operation in the buck operating stage. This has now been verified experimentally. The efficiency is determined to be ~95.5%.

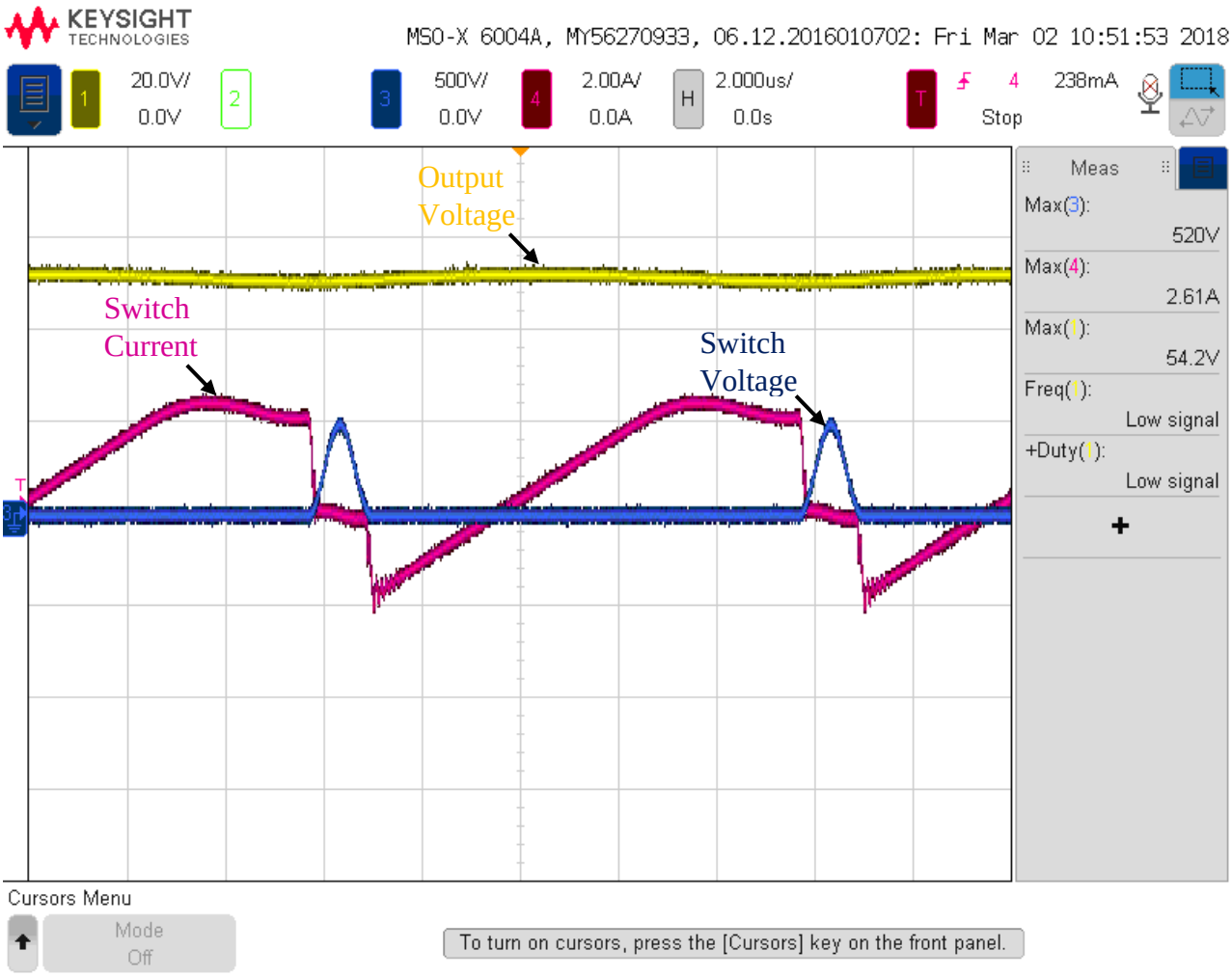

Figure 3-9 Results from prototype for boost operating stage

[Output Voltage: 20.0 V/div; Switch Voltage: 500 V/div; Switch Current: 2.0 A/div; Time: 2.0 µs/div]

Fig. 3-9 shows results from the hardware prototype during the boost operating stage. The input voltage is $30\,V$, the switching frequency is $100\,kHz$ and the duty cycle is 68%. In the boost operating mode as well, soft-switching has been achieved in the hardware prototype results. The efficiency was determined to be 96%.

3.4 Chapter Summary

This chapter presented the results and performance of the proposed bidirectional converter topology. Results have confirmed that the proposed converter has soft-switching capabilities in both buck and boost operating modes. The measured power efficiency is found to be above 96% in both operating conditions. Moreover, the efficiency performance comparison between the proposed topology and the conventional buck-boost bidirectional converter has also been presented. In addition, experimental results on a proof-of-concept prototype have also been provided. Final results confirmed the proposed bidirectional converter circuit is able to achieve ZVS turn-on and ZCS turn-off to significantly reduce the switching power losses of the converter.

Chapter 4

Modular Design Approach with the Proposed Bidirectional Converter

4.1 Introduction

The previous chapter presented an improved bidirectional converter that employs quasi-resonant power conversion with the use of only two switches. In order to much higher rated output power, an extension version of the proposed bidirectional topology is presented in this chapter, where a modular design approach with the proposed bidirectional converter with quasi-resonant soft-switching will be discussed. In literature, it is well-known that modular design approach is commonly used to allow the power converter to have much higher power handling capability [62]. Each module in the power converter will handle equal amount of power. This design approach is becoming increasingly popular due to the increased penetration of distributed energy sources which are connected to microgrids over very long distances. Owing to long distance power transmission, the DC voltage line is at medium voltage level. However, this inhibits the connection of low voltage level energy storage devices such as the batteries discussed in Chapter 1. To make converters which are necessary to ensure correctly matched voltage levels in the grid connected distributed generation system, the switching frequency level has to be made substantially higher and reduces the usage of high voltage semiconductor switches [63].

Modular design approach for power converters is a highly efficient way for the fore-mentioned application (i.e. high-power application) as the rated power of each module remains the same. Modular design structures can have four possible configurations:

1. Parallel Input Parallel Output configuration as shown in Fig. 4-1

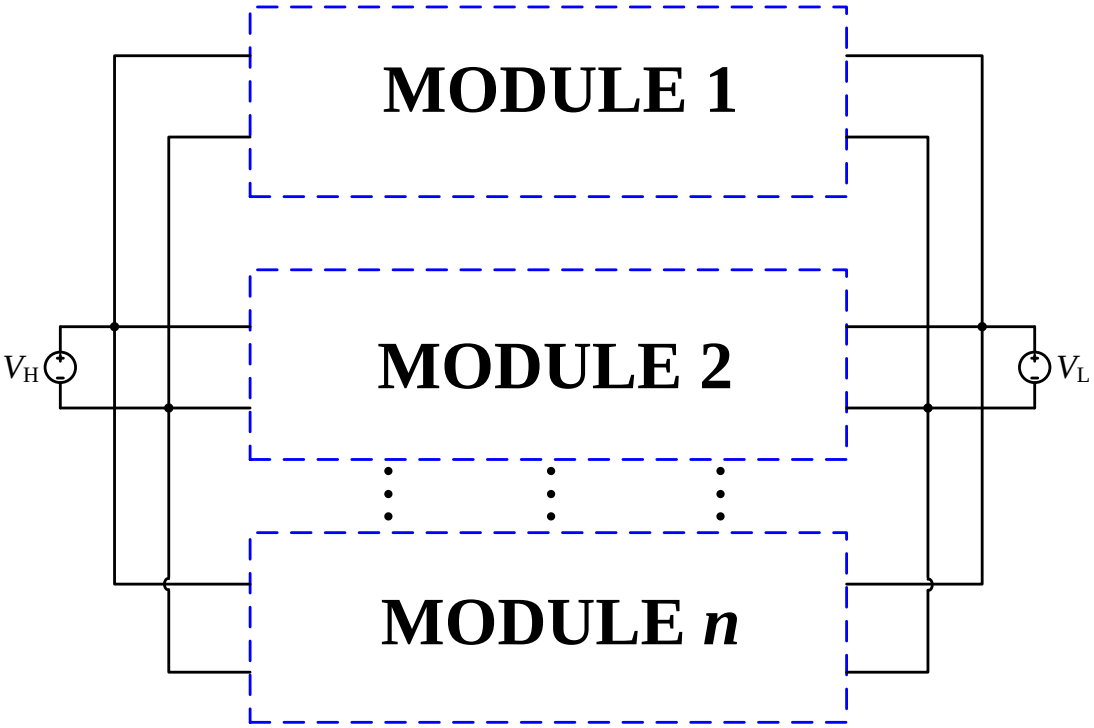

Figure 4-1 Parallel input parallel output configuration

2. Series Input Series Output Configuration as shown in Fig. 4-2

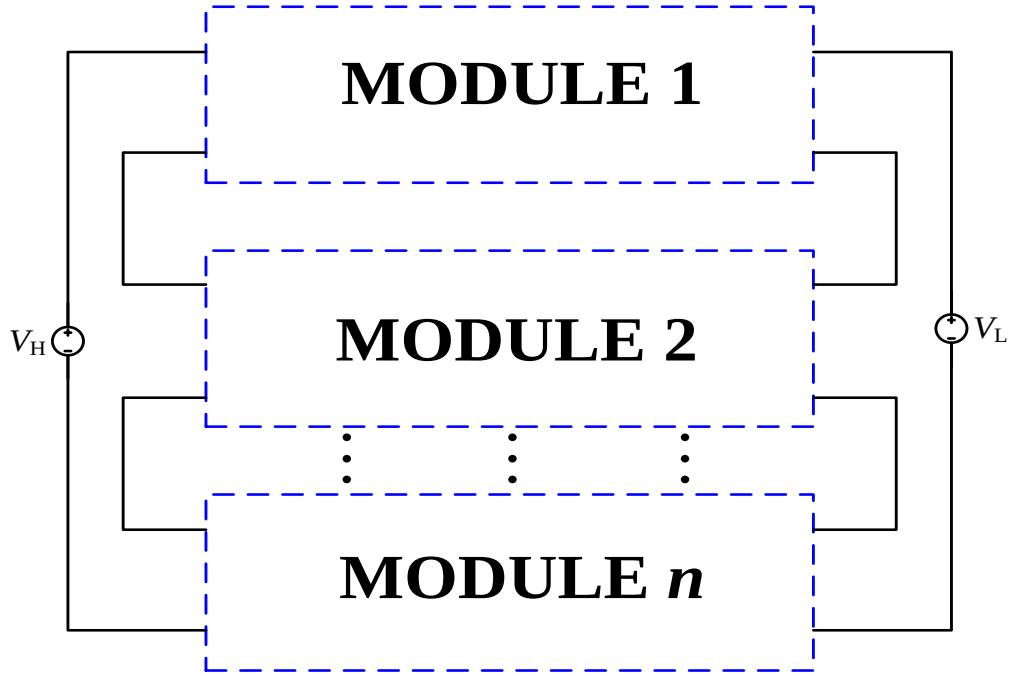

Figure 4-2 Series input series output configuration

3. Series Input Parallel Output Configuration as shown in Fig. 4-3

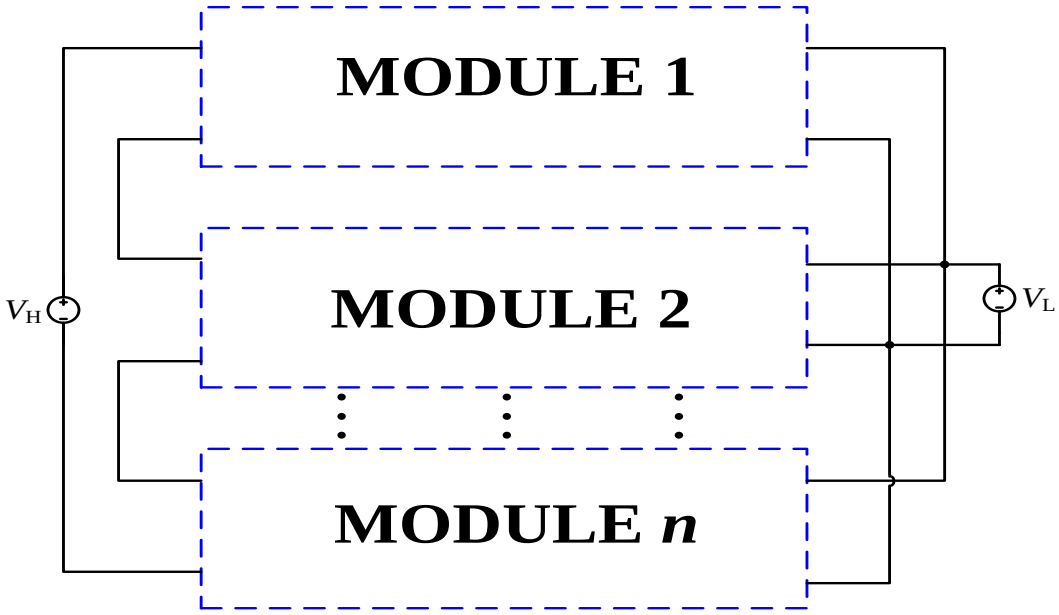

Figure 4-3 Series input parallel output configuration

4. Parallel Input Series Output Configuration as shown in Fig. 4-4

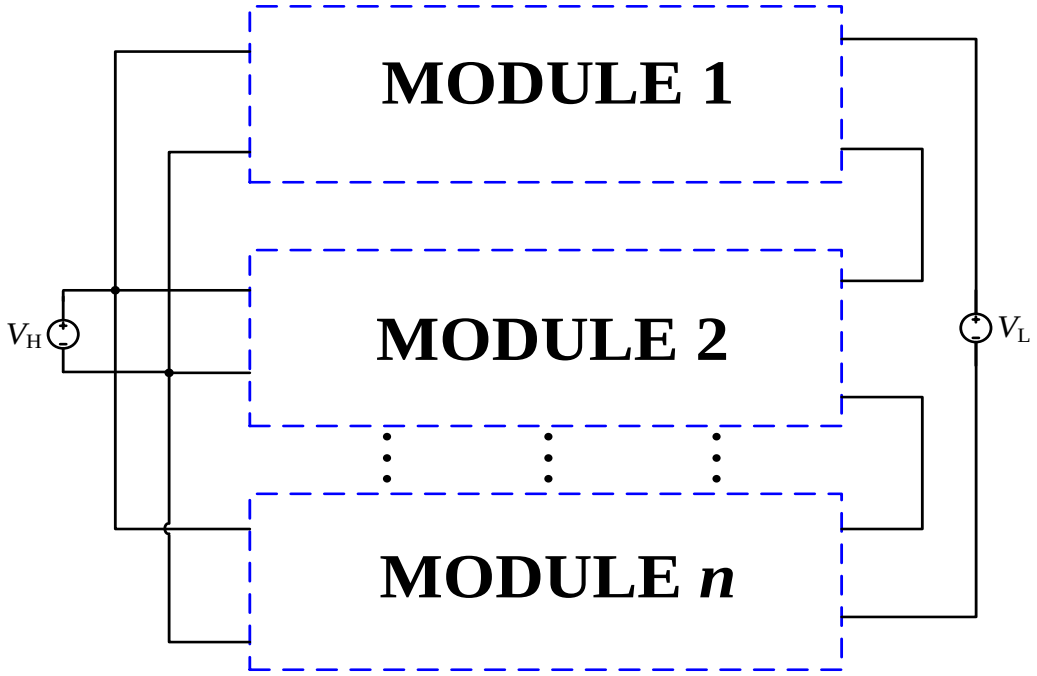

Figure 4-4 Parallel input series output configuration

4.2 Proposed Modular Bidirectional Converter Topology

Fig. 4-5 shows an example of the proposed bidirectional converter topology in a modular design approach, where a parallel-input, parallel-output configuration is presented. In this topology the input voltage to each of the modules is the same. The output voltage remains the same as that obtained for a single module. However, the power level of the circuit increases as multiple modules are added to the modular converter bidirectional converter topology. The soft-switching capability of the bidirectional converter is retained in the modular topology as well.

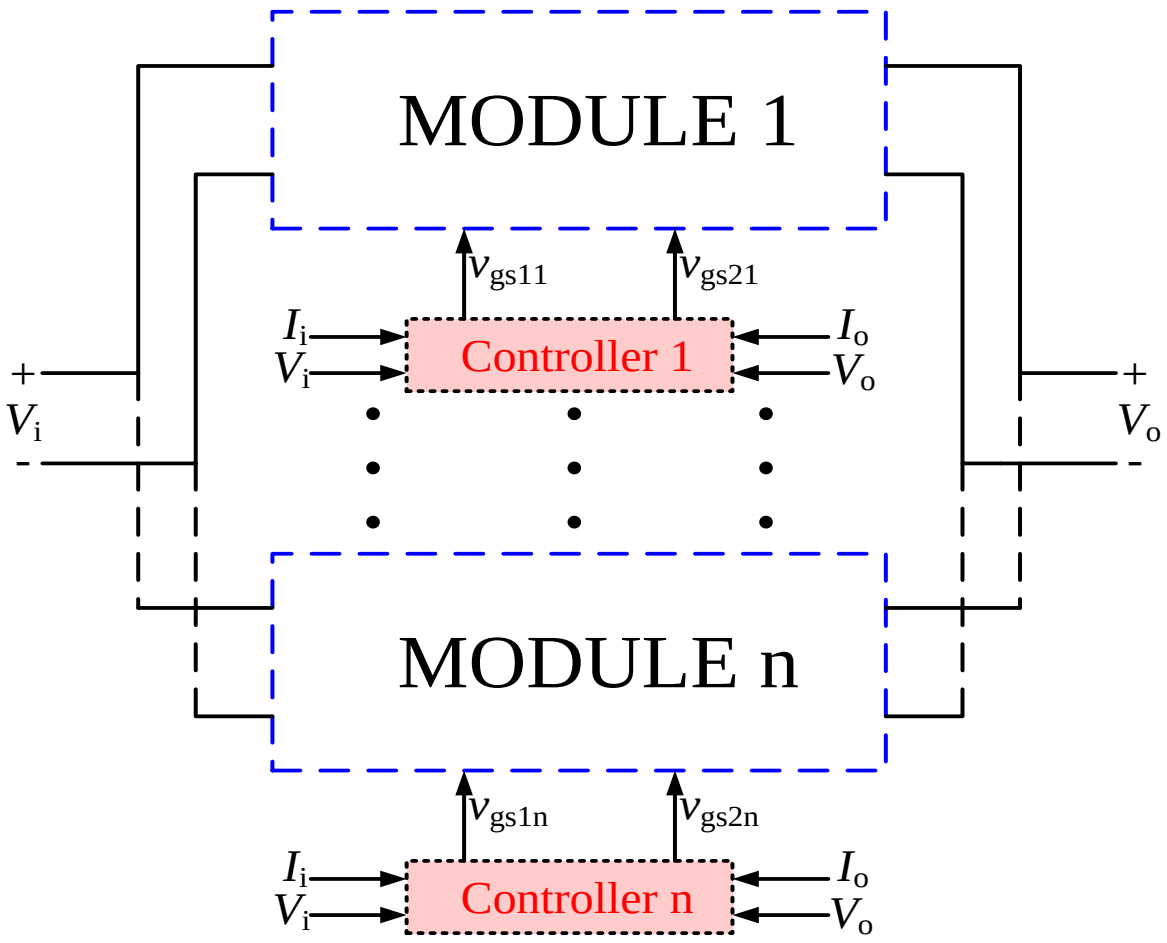

Figure 4-5 Modular design structure with the proposed bidirectional converter

4.3 Controller

Fig. 4-6 shows the controller designed for the modular bidirectional converter topology. The controller is based on a conventional PWM controller. It can turn switches on and off at the required switching frequency and duty cycle by providing gate voltage during the buck as well as the boost mode of operation. During the buck mode of operation switches $S_{11}, S_{21} \ldots S_{n1}$ are turned on. During the boost operating stage only the switches, $S_{12}, S_{22} \ldots S_{n2}$ are turned on.

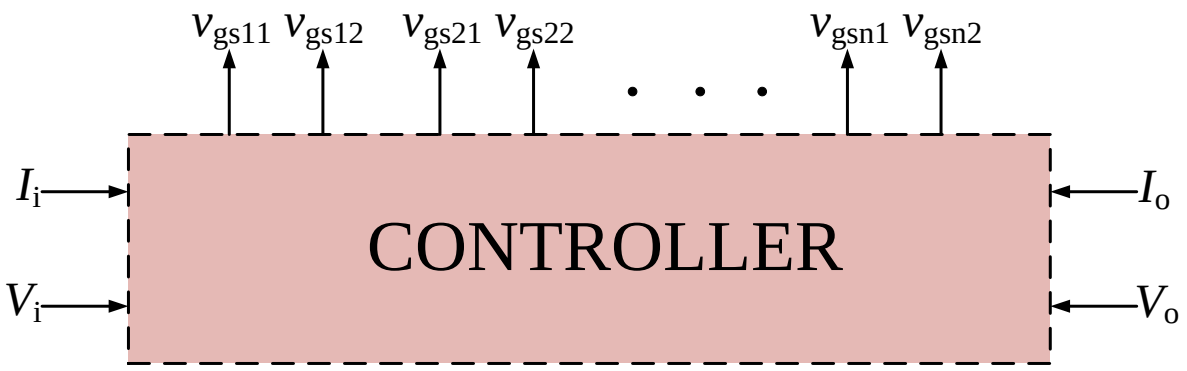

Figure 4-6 Controller for the modular topology

4.4 Results and Analysis

Table 4-1 shows the design specifications. Since the two modules are identical, the circuit component parameters are same too.

Table 4-1 Circuit parameters for 500 W, 200 kHz simulation of proposed modular topology

Circuit parameter	Value
Switching frequency	200 kHz
Rated power of each module	500 W
Switch On-State Resistance	390 mΩ
Switch Diode Forward Voltage	0.8 V
Resonant Inductor (L_1)	40.7 μH
Resonant Capacitor (C_{S1})	10.4 nF
Resonant Inductor (L_2)	20 μH
Resonant Capacitor (C_{S2})	7.4 nF

Fig. 4-7 shows the output voltage which is achieved when two 500 W bidirectional converter modules are connected together during buck operating stage. The input voltage is 400 V to each module and the frequency is 200 kHz. The output voltage using two modules remains 96 V since the configuration of the proposed modular bidirectional converter is Parallel Input – Parallel Output. Fig. 4.-8 shows the input and output power during the buck operating mode. The power level increases to 1000 W when two modules are connected as the input and output current level increases while the voltage levels remain the same. The efficiency of the circuit was calculated to be 97.3%. Fig. 4-9 shows that there is soft-switching in the switches $S_{1,1}$ which is turned on in buck operating stage in module 1 and $S_{1,2}$ which is turned on in buck operating stage in module 2.

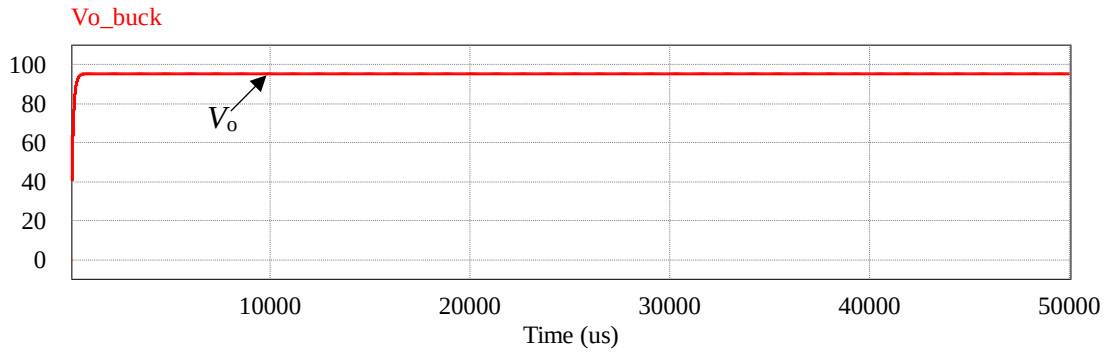

Figure 4-7 Output voltage in buck operating stage

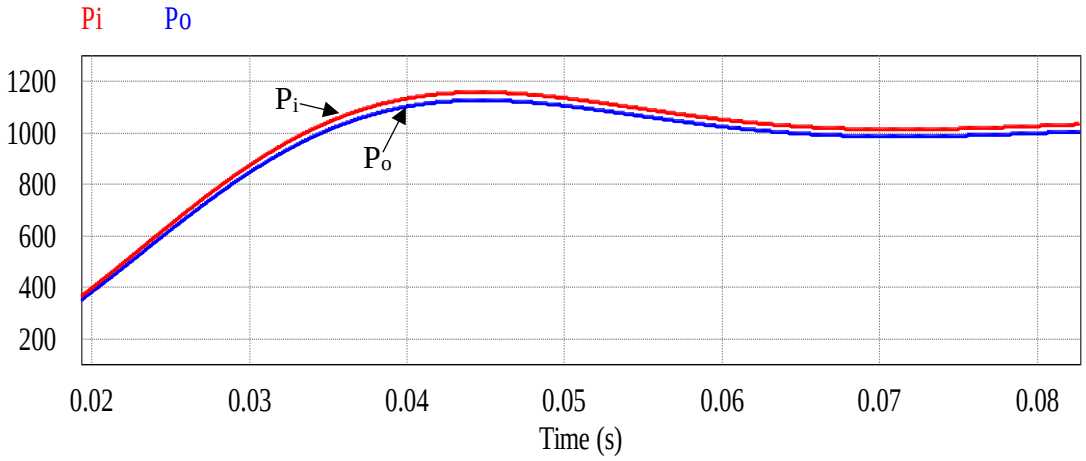

Figure 4-8 Input and output power in buck operating stage

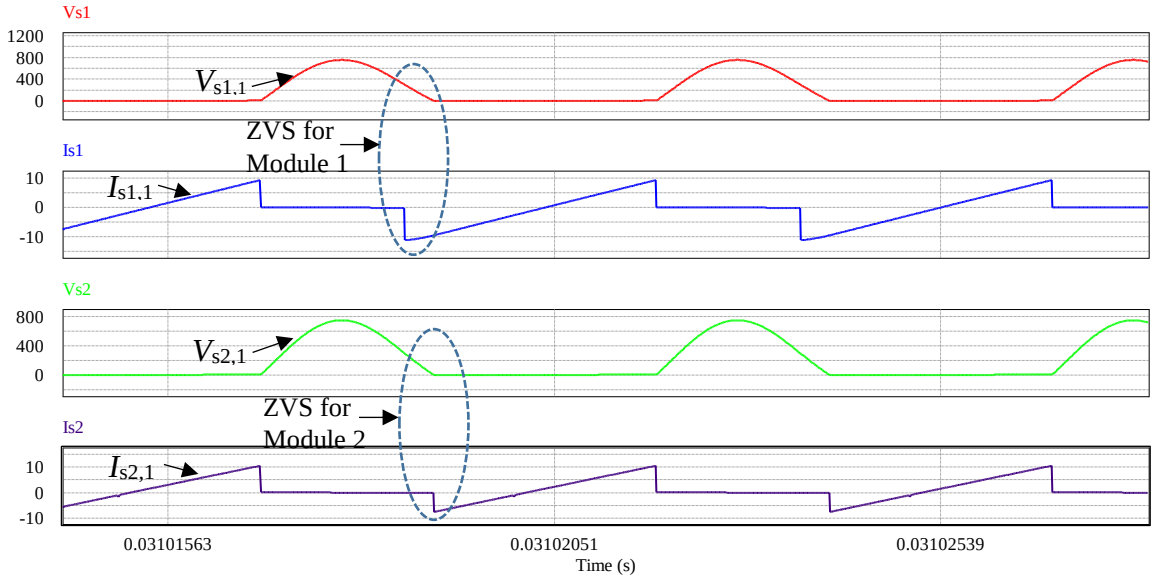

Figure 4-9 Soft-switching in buck operating stage

Fig. 4-10 shows the output voltage which is achieved when two 500 W bidirectional converter modules are connected together in a parallel input-parallel output configuration during boost operating stage. The input voltage is 96 V to each module and the frequency is 200 kHz. The output

voltage using two modules remains 400 V since the configuration of the proposed modular bidirectional converter is Parallel Input – Parallel Output. Fig. 4.-11 shows the input and output power during the buck operating mode. The power level increases as the input and output current level increases while the voltage levels remain the same. The efficiency of the circuit was calculated to be 96.2%. Fig. 4-12 shows that there is soft-switching in the switches $S_{2,1}$ which is turned on in buck operating stage in module 1 and $S_{2,2}$ which is turned on in buck operating stage in module 2.

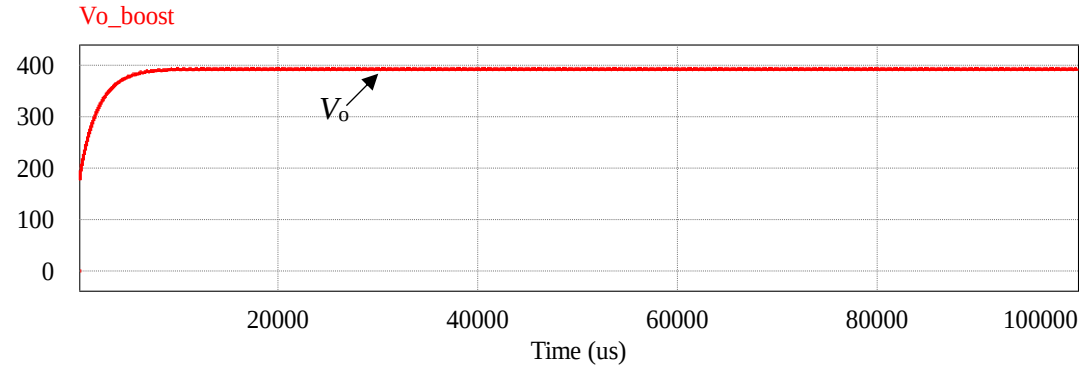

Figure 4-10 Output voltage in boost operating stage

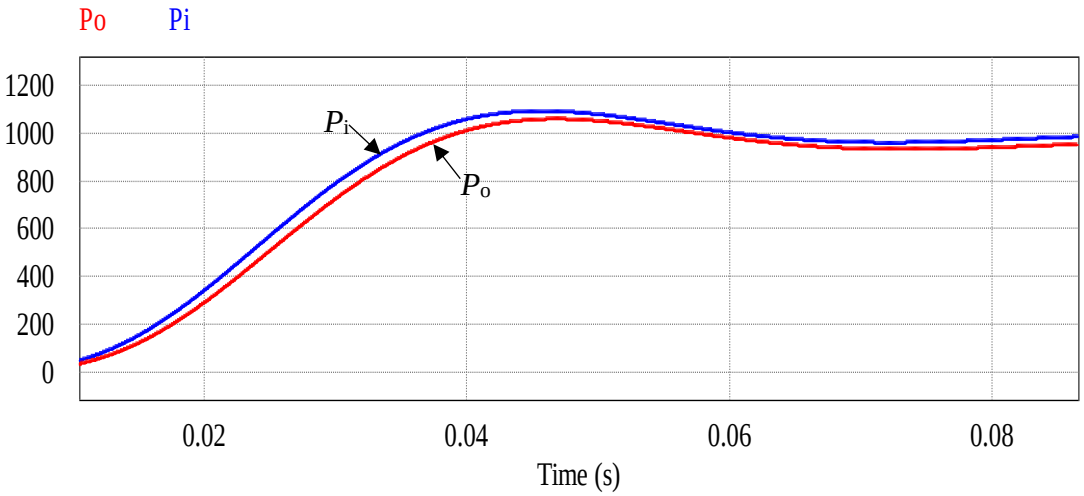

Figure 4-11 Input and output power in boost operating stage

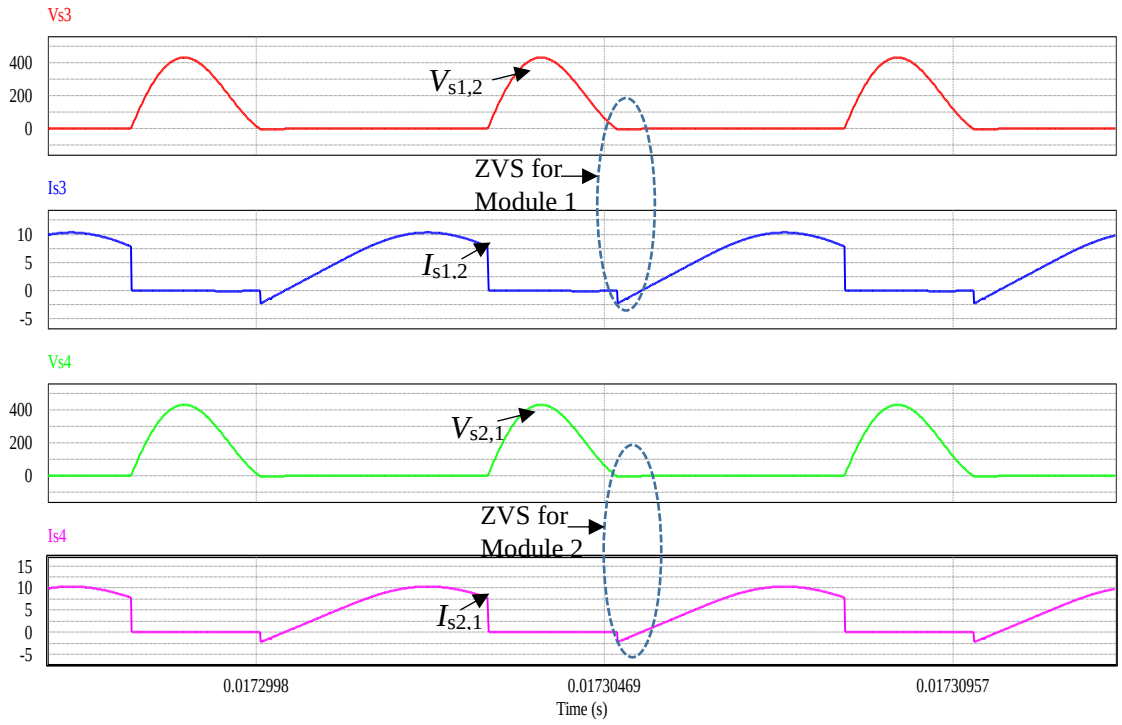

Figure 4-12 Soft-switching in boost operating stage

4.5 Chapter Summary

This chapter presented an extend version of the proposed bidirectional converter topology, where a modular design approach was presented. The proposed modular bidirectional converter topology can perform step-up or step-down voltage conversion at high power levels. Finally, results have been presented to demonstrate that soft-switching operations were achieved at higher power levels, with an efficiency of at least 96% is achieved at the rated power condition.

Chapter 5

Summary and Conclusions

5.1 Summary

The advent of renewable energy sources as well as growing energy needs across the world has made energy storage devices incredibly important. These energy storage systems can be deployed in any subsystem of the electric power system [64]-[65]. The subsystems are:

1. Generation
2. Transmission
3. Substations
4. Distribution
5. Final Consumer Stage

Electricity has the property that it cannot be stored directly. Therefore, there is a lot of wastage of electricity in the absence of energy storage devices. Adequate power has to be generated to meet peak demand, which lasts a short period of time and occurs infrequently. When demand is low and supply is high, there is often wastage.

To store electricity, it needs to be converted into a different form of energy. Common energy storage devices are batteries, in which electrical energy is converted to chemical energy, flywheels in which it is converted to kinetic energy, and pumped hydro which stores electrical power in the form of gravitational potential energy.

There are several reasons for the increase in interest in energy storage devices. They are:

1. Increase in the demand of power and the need to adapt to the changes in demand fast and efficiently.
2. To seamlessly incorporate distributed generation (renewable energy systems) into the existing power grid.
3. Increase in congestion of existing power grids.
4. To increase the stability, reliability and efficiency of the power grid by recognizing the ancillary services provided by energy storage devices.
5. To reduce fluctuations in the power grid.

In all these cases, a bidirectional converter is required as an intermediary between the power grid and the energy storage device. The energy storage devices act as a load when energy has to be stored and as a source when energy has to be supplied to the power grid. The bidirectional converter must be able to step up and step down the voltage to the required levels for both ends of the system. Hence, the bidirectional converter is essential to the deployment of energy storage devices in a renewable power system. The focus of this thesis was to develop a highly efficient, quasi-resonant bidirectional converter topology to ensure efficient power transfer between the energy storage device and the power grid.

5.2 Contributions

The contributions of this thesis are summarized below:

1. An improved bidirectional DC/DC converter circuit has been devised in this thesis. As the proposed circuit requires only two switches, compared to the conventional full-bridge based bidirectional DC/DC converters, the total number of active switching devices has been significantly reduced.
2. The presented bidirectional converter topology has shown to be able to achieve loss-less switching techniques with ZVS turn-on and ZCS turn-off, allowing high operating frequency to be utilized with almost zero-switching power losses.
3. Owing to very high frequency operation, the sizes of all the passive circuit components such as inductors and capacitors has been reduced in the devised converter, resulting in a truly compact bidirectional converter.
4. The operating stages and theoretical analysis of the proposed circuit has been presented in detail in this thesis. Especially, the step-up and step-down operating modes of the proposed converter and their operating waveforms have been discussed.
5. A modular circuit structure of the proposed bidirectional converter topology has been presented. The proposed modular bidirectional converter topology combines multiple modules in parallel input parallel output configuration to increase the power level while ensuring high efficiency and low power loss.
6. A proof-of-concept experimental prototype of the proposed circuit has been developed and tested to validate the results obtained from simulation proving the feasibility of the proposed topology.

5.3 Future Works

Regarding the research works conducted in this thesis, some possible future works are summarized below:

1. Design and implementation of an advanced and automated controller for the presented bidirectional converter. The implemented controller will be able to communicate with the proposed converter and inform the converter the proper operating modes depending on the loading power requirement.
2. Hardware implementation of the circuit prototype for higher input and output voltages. The design procedure will involve proper selection of the switching devices as well as the design of the magnetic components to achieve the required power level. All the other circuit parameters will then be designed and obtained according to the theoretical analysis illustrated in this thesis.

5.4 Conclusions

In conclusion, a quasi-resonant bidirectional converter for energy storage applications has been presented in this thesis. With soft-switching techniques, the presented converter has been designed to be highly efficient as has been validated by the results shown in this thesis. In addition, due to the significant reduction of the number of switches, the presented bidirectional converter provides a cost-effective and compact power solution, making it ideal for energy storage application in renewable energy systems. Finally, PSIM simulation results have been obtained to verify the performance of the proposed topology. Experimental results on a proof-of-concept hardware prototype have also been provided to further support the features of the proposed bidirectional converter circuit.

BIBLIOGRAPHY

[1] UN Environment (2017). *Renewable Energy.* Retrieved from http://www.unep.org/energy/what-we-do/renewable-energy

[2] Enerdata (2017). *Global Energy Statistical Yearbook 2017*. Retrieved from https://yearbook.enerdata.net/

[3] Ecotrocity (2017). *The End of Fossil Fuels*. Retrieved from https://www.ecotricity.co.uk/our-green-energy/energy-independence/the-end-of-fossil-fuels

[4] U.S. Energy Information Administration (2011). *Renewable Energy Shows a Strongest Growth in Global Electric Generating Capacity.* Retrieved from https://www.eia.gov/todayinenergy/detail.php?id=3270

[5] T. Mark (2016). *Energy Storage in Canada: Status and Outlook.* Retrieved from https://solarcanadaconference.ca/wp-content/uploads/2016/12/LP-Energy-Storage-in-Canada-Status-and-Outlook-Mark-Tinkler.pdf

[6] Y. Levron, J. M. Guerrero and Y. Beck, "Optimal Power Flow in Microgrids With Energy Storage," in *IEEE Transactions on Power Systems*, vol. 28, no. 3, pp. 3226-3234, Aug. 2013.

[7] I. Hadjipaschalis, A. Poullikkas, and V. Efthimiou, “Overview of current and future energy storage technologies for electric power applications,” *Renew. Sustain. Energy Rev.*, vol. 13, nos. 6-7, pp. 1513-1522, 2009.

[8] Peter J. Hall, Euan J. Bain, “Energy-storage technologies and electricity generation,” *In Energy Policy*, vol. 36, pp. 4352-4355, 2008.

[9] A. Oudalov, T. Buehler and D. Chartouni, "Utility Scale Applications of Energy Storage," *2008 IEEE Energy 2030 Conference*, Atlanta, GA, pp. 1-7, 2008.

[10] H. Qian, J. Zhang, J. S. Lai and W. Yu, "A high-efficiency grid-tie battery energy storage system," in *IEEE Transactions on Power Electronics*, vol. 26, no. 3, pp. 886-896, March 2011.

[11] M. Guarnieri, P. Mattavelli, G. Petrone and G. Spagnuolo, "Vanadium Redox Flow Batteries: Potentials and Challenges of an Emerging Storage Technology," in *IEEE Industrial Electronics Magazine*, vol. 10, no. 4, pp. 20-31, Dec. 2016.

[12] R. Sathishkumar, S. K. Kollimalla and M. K. Mishra, "Dynamic energy management of microgrids using battery super capacitor combined storage," *2012 Annual IEEE India Conference (INDICON)*, Kochi, pp. 1078-1083, 2012.

[13] J. S. Lai and M. W. Ellis, "Fuel Cell Power Systems and Applications," in *Proceedings of the IEEE*, vol. 105, no. 11, pp. 2166-2190, Nov. 2017.

[14] K. Zhang, C. Mao, J. Lu, D. Wang, X. Chen and J. Zhang, "Optimal control of state-of-charge of superconducting magnetic energy storage for wind power system," in *IET Renewable Power Generation*, vol. 8, no. 1, pp. 58-66, January 2014.

[15] G. Navarro, J. Torres, P. Moreno-Torres, M. Blanco and M. Lafoz, "Technology description and characterization of a low-cost flywheel for energy management in microgrids," *2015 17th European Conference on Power Electronics and Applications (EPE'15 ECCE-Europe)*, Geneva, pp. 1-10, 2015.

[16] D. Villela *et al*., "Compressed-air energy storage systems for stand-alone off-grid photovoltaic modules," *2010 35th IEEE Photovoltaic Specialists Conference*, Honolulu, HI, pp. 000962-000967, 2010.

[17] S. Ekoh, I. Unsal and A. Maheri, "Optimal sizing of wind-PV-pumped hydro energy storage systems," *2016 4th International Symposium on Environmental Friendly Energies and Applications (EFEA)*, Belgrade, pp. 1-6, 2016.

[18] A. Xiang, "Applications of BESS," *Narada*, *Slideshare*, slide 13, February 2017.

[19] D. Fiakas, "More in the Air than Spring," *Small Cap Strategist*, 2017, Retrieved from http://crystalequityresearch.blogspot.ca/2013/04/more-in-air-than-spring_2.html

[20] D. Miranda, C.M. Costa, S. Lanceros-Mendez, "Lithium ion rechargeable batteries: State of the art and future needs of microscopic theoretical models and simulations," *Journal of Electroanalytical Chemistry*, vol. 739, pp. 97-110, February 2015.

[21] H. Hinz, "Investigations on Lithium-Ion Batteries for Power Generation Applications," *2017 International Conference on Industrial Engineering, Management Science and Application (ICIMSA)*, Seoul, pp. 1-5, 2017.

[22] J. McDowall, "Nickel-cadmium batteries for energy storage applications," *Fourteenth Annual Battery Conference on Applications and Advances. Proceedings of the Conference (Cat. No.99TH8371)*, Long Beach, CA, pp. 303-308, 1999.

[23] Nirmal-Kumar C. Nair, Niraj Garimella, "Battery energy storage systems: Assessment for small-scale renewable energy integration," *In Energy and Buildings*, vol. 42, pp. 2124-2130, 2010.

[24] S. Yao, P. Liao, M Xiao, J. Cheng, K. He, “Equivalent circuit modeling and simulation of the zinc nickel single flow battery*,” AIP Advances 7*, May 2017.

[25] Y. X. Li *et al.*, "Modeling of novel single flow zinc-nickel battery for energy storage system," *2014 9th IEEE Conference on Industrial Electronics and Applications*, Hangzhou, pp. 1621-1626, 2014.

[26] GlobeTek, Inc., “Nickel Metal Hydride,” *NiMH Battery Safety Notes*, October 2017, Retrieved from https://en.globtek.com/nimh-battery-safety-notes/#

[27] J. Tarabay and N. Karami, "Nickel Metal Hydride battery: Structure, chemical reaction, and circuit model," *2015 Third International Conference on Technological Advances in Electrical, Electronics and Computer Engineering (TAEECE)*, Beirut, 2015, pp. 22-26.

[28] N. Bashir, H. S. Sardar, M. Nasir, N. U. Hassan and H. A. Khan, "Lifetime maximization of lead-acid batteries in small scale UPS and distributed generation systems," *2017 IEEE Manchester PowerTech*, Manchester, 2017, pp. 1-6.

[29] B. Zhao, X. Zhang, J. Chen, C. Wang and L. Guo, "Operation Optimization of Standalone Microgrids Considering Lifetime Characteristics of Battery Energy Storage System," in *IEEE Transactions on Sustainable Energy*, vol. 4, no. 4, pp. 934-943, Oct. 2013.

[30] R. Kaiser, “Optimized battery-management system to improve storage lifetime in renewable energy systems,” *In Journal of Power Sources*, vol. 168, Issue 1, 2007, pp. 58-65.

[31] M. J. Riezenman, "Metal fuel cells [Zn-air fuel cells]," in *IEEE Spectrum*, vol. 38, no. 6, pp. 55-59, Jun 2001.

[32] Y. Chen, W. Wei, F. Zhang, C. Liu and C. Meng, "Design of PV hybrid DC/AC microgrid for electric vehicle charging station," *2017 IEEE Transportation Electrification Conference and Expo, Asia-Pacific (ITEC Asia-Pacific)*, Harbin, China, 2017, pp. 1-6.

[33] B. M. Grainger, G. F. Reed, A. R. Sparacino and P. T. Lewis, "Power Electronics for Grid-Scale Energy Storage," *in Proceedings of the IEEE*, vol. 102, no. 6, pp. 1000-1013, June 2014.

[34] M. R. Mohammadi and H. Farzanehfard, "Family of Soft-Switching Bidirectional Converters With Extended ZVS Range," *in IEEE Transactions on Industrial Electronics*, vol. 64, no. 9, pp. 7000-7008, Sept. 2017.

[35] D. Han , J. Noppakunkajorn, and B. Sarlioglu, " Comprehensive efficiency, weight, and volume comparison of SiC and Si-based bidirectional dc–dc converters for hybrid electric vehicles*," IEEE Trans. Veh. Technol.*, vol. 63, no. 7, pp. 3001–3010, Sep. 2014.

[36] F. Akar , Y. Tavlasoglu, E. Ugur, B. Vural, and I. Aksoy , "A bidirectional non-isolated multi input DC-DC converter for hybrid energy storage systems in electric vehicles," *IEEE Trans. Veh. Technol.*, vol. 65, no. 10, pp. 7944–7955 , Oct. 2016.

[37] S.-T. Kim , S. Bae, Y. C. Kang, and J.-W. Park, "Energy management based on the photovoltaic HPCS with an energy storage device," *IEEE Trans. Ind. Electron*., vol. 62, no. 7, pp. 4608–4617 , Jul. 2015.

[38] M. A. Abusara , J. M. Guerrero, and S. M. Sharkh, " Line-interactive UPS for microgrids," *IEEE Trans. Ind. Electron*., vol. 61, no. 3, pp. 1292–1300, Mar. 2014.

[39] V. Yuhimenko , G. Geula, G. Agranovich, M. Averbukh, and A. Kuperman , "Average modeling and performance analysis of voltage sensorless active supercapacitor balancer with peak current protection," *IEEE Trans. Power Electron*., vol. 32, no. 2, pp. 1570– 1578, Feb. 2017.

[40] C. Nan and R. Ayyanar, “A 1 MHz bi-directional soft-switching DC-DC converter with planar coupled inductor for dual voltage automotive systems,” *in Proc. IEEE Appl. Power Electron. Conf. Expo.* , Long Beach, CA, USA, 2016, pp. 432– 439.

[41] H. Ardi, R. Reza Ahrabi and S. Najafi Ravadanegh, "Non-isolated bidirectional DC–DC converter analysis and implementation," in *IET Power Electronics*, vol. 7, no. 12, pp. 3033-3044, 12 2014.

[42] K. Venkatesan, "Current mode controlled bidirectional flyback converter," *20th Annual IEEE Power Electronics Specialists Conference*, Milwaukee, WI, 1989, pp. 835-842 vol.2.

[43] P. Thummala, Z. Zhang and M. A. E. Andersen, "High voltage Bi-directional flyback converter for capacitive actuator," *2013 15th European Conference on Power Electronics and Applications (EPE)*, Lille, 2013, pp. 1-10.

[44] L. Huber and M. H. Jovanovic, "Forward-flyback converter with current-doubler rectifier: analysis, design, and evaluation results," in *IEEE Transactions on Power Electronics*, vol. 14, no. 1, pp. 184-192, Jan 1999.

[45] O. A. Montes, S. Son, S. Kim, H. Seok, J. S. Lee and M. Kim, "Forward-flyback resonant converter for high-efficient medium-power photovoltaic applications," *2017 IEEE Applied Power Electronics Conference and Exposition (APEC)*, Tampa, FL, 2017, pp. 1223-1228.

[46] Gang Chen, Yim-Shu Lee, S. Y. R. Hui, Dehong Xu and Yousheng Wang, "Actively clamped bidirectional flyback converter," in *IEEE Transactions on Industrial Electronics*, vol. 47, no. 4, pp. 770-779, Aug 2000.

[47] G. Ma, W. Qu, G. Yu, Y. Liu, N. Liang and W. Li, "A Zero-Voltage-Switching Bidirectional DC–DC Converter With State Analysis and Soft-Switching-Oriented Design Consideration," in *IEEE Transactions on Industrial Electronics*, vol. 56, no. 6, pp. 2174-2184, June 2009.

[48] F. Z. Peng, Hui Li, Gui-Jia Su and J. S. Lawler, "A new ZVS bidirectional DC-DC converter for fuel cell and battery application," in *IEEE Transactions on Power Electronics*, vol. 19, no. 1, pp. 54-65, Jan. 2004.

[49] Yamamoto, K.; Hiraki, E.; Tanaka, T.; Nakaoka, M.; Mishima, T., "Bidirectional DC-DC converter with full-bridge/push-pull circuit for automobile electric power systems," In *Proceedings of the IEEE Power Electronics Specialists Conference*, Jeju, Korea, 18–22 June 2006; pp. 1–5.

[50] A. Bijani, M. R. Amini, H. Farzanehfard and E. Adib, "A zero voltage switching PWM bidirectional flyback converter with one auxiliary switch," *20th Iranian Conference on Electrical Engineering (ICEE2012)*, Tehran, 2012, pp. 398-403.

[51] Kumar, L., Jain, S.: 'Multiple-input DC/DC converter topology for hybrid energy system', *IET Power Electron*. 2013, 6, pp. 1483–1501

[52] Fang Zheng Peng, Fan Zhang and Zhaoming Qian, "A magnetic-less DC-DC converter for dual-voltage automotive systems," in *IEEE Transactions on Industry Applications*, vol. 39, no. 2, pp. 511-518, Mar/Apr 2003.

[53] I. D. Kim, S. H. Paeng, J. W. Ahn, E. C. Nho and J. S. Ko, "New Bidirectional ZVS PWM Sepic/Zeta DC-DC Converter," *2007 IEEE International Symposium on Industrial Electronics*, Vigo, 2007, pp. 555-560.

[54] K. T. Chau, T. W. Ching and C. C. Chan, "Bidirectional soft-switching converter-fed DC motor drives," *PESC 98 Record. 29th Annual IEEE Power Electronics Specialists Conference (Cat. No.98CH36196)*, Fukuoka, 1998, pp. 416-422 vol.1.

[55] P. Das, S. A. Mousavi and G. Moschopoulos, "Analysis and Design of a Nonisolated Bidirectional ZVS-PWM DC–DC Converter With Coupled Inductors," in *IEEE Transactions on Power Electronics*, vol. 25, no. 10, pp. 2630-2641, Oct. 2010.

[56] Dimna Denny C and Shahin M, "Analysis of bidirectional SEPIC/Zeta converter with coupled inductor," *2015 International Conference on Technological Advancements in Power and Energy (TAP Energy)*, Kollam, 2015, pp. 103-108.

[57] M. K. Kazimierczuk, "Steady-state analysis and design of a buck zero-current-switching resonant DC/DC converter," in *IEEE Transactions on Power Electronics*, vol. 3, no. 3, pp. 286-296, Jul 1988.

[58] M. K. Kazimierczuk, "Design-oriented analysis of boost zero-voltage-switching resonant DC/DC converter," in *IEEE Transactions on Power Electronics*, vol. 3, no. 2, pp. 126-136, April 1988.

[59] R. Carnegie, D. Gotham, D. Nderitu, P.V. Preckel, Utility Scale Energy Storage Systems: Benefits, Applications, and Technologies (2013)

[60] M. Noritake *et al*., "Experimental study of a 400 V class DC microgrid for commercial buildings," *2015 9th International Conference on Power Electronics and ECCE Asia (ICPE-ECCE Asia)*, Seoul, 2015, pp. 1730-1735.

[61] R. Sheehan, "Understanding and applying current-mode control theory," *Power Electronics Technology Exhibition and Conference (PES07)*, Oct 2007.

[62] P. Nuechteriein, "A modular approach to the design of high-power DC-DC converters," *1977 IEEE Power Electronics Specialists Conference*, Palo Alto, CA, USA, 1977, pp. 223-226.

[63] Steven Keeping, “Design Trade-offs when selecting a High-frequency switching regulator,” *2015 Digikey.*

[64] Haisheng Chen, Thang Ngoc Cong, Wei Yang, Chunqing Tan, Yongliang Li, Yulong Ding, *Progress in electrical energy storage system: A critical review, Progress in Natural Science*, Volume 19, Issue 3, 2009, Pages 291-312, ISSN 1002-0071.

[65] R. H. Byrne, T. A. Nguyen, D. A. Copp, B. R. Chalamala and I. Gyuk, "Energy Management and Optimization Methods for Grid Energy Storage Systems," in *IEEE Access*, vol. PP, no. 99, pp. 1-1.